

Simulation of Non-Hermitian Hamiltonians with Bivariate Quantum Signal Processing

Joshua M. Courtney¹

¹*University of Georgia, Department of Physics and Astronomy*

(Dated: May 13, 2026)

We achieve query-optimal quantum simulations of non-Hermitian Hamiltonians $H_{\text{eff}} = H_R + iH_I$, where H_R is Hermitian and $H_I \succeq 0$, using a bivariate extension of quantum signal processing (QSP) with non-commuting signal operators. The algorithm encodes the interaction-picture Dyson series as a polynomial on the bitorus, implemented through a structured multivariable QSP (M-QSP) circuit. A constant-ratio condition guarantees scalar angle-finding for M-QSP circuits with arbitrary non-commuting signal operators. A degree-preserving sum-of-squares spectral factorization permits scalar complementary polynomials in two variables. Angles are deterministically calculated in a classical precomputation step, running in $\mathcal{O}(d_R \cdot d_I)$ classical operations. Operator norms α_R, β_I contribute additively with query complexity $\mathcal{O}((\alpha_R + \beta_I)T + \log(1/\varepsilon)/\log \log(1/\varepsilon))$ matching an information-theoretic lower bound in the separate-oracle model, where H_R and H_I are accessed through independent block encodings. The postselection success probability is $e^{-2\beta_I T} \|e^{-iH_{\text{eff}} T} |\psi_0\rangle\|^2 \cdot (1 - \mathcal{O}(\varepsilon))$, decomposing into a state-dependent factor $\|e^{-iH_{\text{eff}} T} |\psi_0\rangle\|^2$ from the intrinsic barrier and an $e^{-2\beta_I T}$ overhead from polynomial block-encoding.

I. INTRODUCTION

A. Problem Statement

Non-Hermitian Hamiltonians arise naturally in common computational and physical representations [1], including the no-jump trajectory of a Lindblad master equation [2], optical systems with gain and loss [3], descriptions of resonance phenomena in scattering theory [4], and complex absorbing potentials (CAPs) in multi-channel AMO simulation [5, 6]. They also notably appear in quantum algorithms for ground-state preparation [7], partition function estimation [8], and imaginary-time evolution [9].

Let $H_{\text{eff}} = H_R + iH_I$ be a non-Hermitian Hamiltonian acting on a finite-dimensional Hilbert space \mathcal{H}_s , where $H_R = H_R^\dagger$ and $H_I = H_I^\dagger$ with $H_I \succeq 0$. Operator norms are notated as $\alpha_R := \|H_R\|_{\text{op}}$ and $\beta_I := \|H_I\|_{\text{op}}$. The target operation is a non-unitary propagator $e^{-iH_{\text{eff}} T}$ for an evolution time $T > 0$.

With a generator $-iH_{\text{eff}} = -iH_R + H_I$, the Hermitian part $H_I \succeq 0$ drives exponential growth of the operator norm: $\|e^{-iH_{\text{eff}} T}\|_{\text{op}} = e^{\beta_I T}$. Non-unitary propagator recovery is typically performed by embedding $e^{-iH_{\text{eff}} T}$ as a block of a larger unitary and postselecting on an ancilla [10–12]. Postselection success probability is bounded by $e^{-2\beta_I T}$.

We derive the minimum number of oracle queries to implement $e^{-iH_{\text{eff}} T}$ to operator-norm error ε . We then ask whether any block-encoding algorithm can simultaneously achieve the minimum query count and the maximum postselection probability.

a. CPTP status of the target dynamics. The map $\rho \mapsto e^{-iH_{\text{eff}} T} \rho e^{+iH_{\text{eff}}^\dagger T}$ generated by $H_{\text{eff}} = H_R + iH_I$ with $H_I \succeq 0$ is completely positive but strictly trace non-increasing whenever $H_I \neq 0$. It is therefore not a completely positive, trace-preserving (CPTP) channel on its own. In the Lindblad setting with $H_I = \frac{1}{2} \sum_j L_j^\dagger L_j$,

the full GKSL semigroup has no-jump conditional evolution [13, 14], canonically realized by Monte-Carlo wavefunction unraveling [15, 16]. In the CAP and parity-time (PT)-symmetric settings, Stinespring/Naimark dilation [17, 18] embeds $e^{-iH_{\text{eff}} T}$ as a block of a unitary on an enlarged Hilbert space. In each case, block-encoding used throughout this paper is an explicit Stinespring dilation, and the $e^{-2\beta_I T}$ postselection probability established in Theorem II.1 (Sec. II) is the probability of the null-outcome (“no-jump”, successful absorption, unbroken-PT) measurement restoring valid CPTP interpretation. Target dynamics therefore admit CPTP description with single-qubit postselection, and the postselection barrier we show is the physical cost of that conditioning.

b. The separate-oracle model. We build around a separate-oracle model [19, 20], where H_R and H_I are exposed via independent walk operators W_R and U_I (constructed from block encodings of H_R/α_R and H_I/β_I respectively) acting on disjoint ancilla registers.

In Lindblad no-jump trajectories [13, 14], the coherent generator $H_R = H_{\text{LS}}$ and dissipative generator $H_I = \frac{1}{2} \sum_j L_j^\dagger L_j$ are described by distinct operators with independent spectral structure, with H_R being the system Hamiltonian and H_I a sum of jump-channel projectors, typically sparse on a different basis. In AMO simulation under a CAP [5, 6], the kinetic-plus-coherent part is a banded operator on a grid of discrete positions. Meanwhile, $H_I = \eta(x - x_c)^2 \Theta(x - x_c)$ is diagonal and supported only on the absorbing region, so a single block encoding for H_{eff} may use a suboptimal number of ancillas and queries on a near-trivial absorbing tail. The separate-oracle model also captures a device-level decomposition for laser-driven dynamics, where coherent control is implemented as an analog drive while loss enters through coupling to a measured continuum [6, 15, 16].

c. State-of-the-art. Recent work has provided quantum hardware compilation modeling a non-Hermitian Hamiltonian on a single qubit by a variationally optimized parameterized quantum circuit [21]. For simula-

tion and broader dynamics, a single block encoding of $H_{\text{eff}} = H_R + iH_I$ is found to require only one set of ancillas, with linear combination of Hamiltonian simulations (LCHS), optimal LCHS [22, 23], amplitude-phase separation (APS) [24], and compressed block-encoding method (CBMD) [25, 26] all operating in this single-oracle model. As shown in the present work, our lower bound (Sec. III) enables additive (rather than coupled) scaling in norms $\alpha_R T$ and $\beta_I T$, and gives a $\log \log(1/\varepsilon)$ Bessel improvement in the precision term. We assess tradeoffs of a subset of existing non-Hermitian quantum simulation techniques with the separate-oracle model IC.

B. Summary of results

a. The Postselection Barrier (Sec. II). We give a two-layer bound on the success probability of the quantum implementation of $e^{-iH_{\text{eff}}T}$. The Postselection Barrier decomposes into an intrinsic factor following from unitarity alone, giving $P \leq \|e^{-iH_{\text{eff}}T} |\psi_0\rangle\|^2 / \|e^{-iH_{\text{eff}}T}\|_{\text{op}}^2$, and a block-encoding factor specific to polynomial walk-operator algorithms, forcing a normalization $\lambda \geq e^{\beta_I T} (1 - \mathcal{O}(\varepsilon))$. Together they yield a tight combined bound

$$P \leq e^{-2\beta_I T} \|e^{-iH_{\text{eff}}T} |\psi_0\rangle\|^2, \quad (1)$$

saturated as $\varepsilon \rightarrow 0$.

b. Information-theoretic lower bound (Sec. III). We adopt the qubitization construction of Low and Chuang [11]. Given block encodings U_{H_R} of H_R/α_R and U_{H_I} of H_I/β_I , the walk operators $W_R = (2\Pi_R - I)U_{H_R}$ and $U_I = (2\Pi_I - I)U_{H_I}$ are unitaries whose eigenvalues lie on the unit circle, with $\theta_1 = \arccos \lambda(H_R/\alpha_R)$ and $\theta_2 = \arccos \lambda(H_I/\beta_I)$. In the separate-oracle model, H_R and H_I are accessed through independent walk operators W_R and U_I (Sec. III A). We find a query complexity of

$$Q = Q_R + Q_I \geq \Omega\left(\alpha_R T + \beta_I T + \frac{\log(1/\varepsilon)}{\log \log(1/\varepsilon)}\right). \quad (2)$$

Components are given by a reduction to Hermitian simulation (for $\alpha_R T$), the polynomial method (for $\beta_I T$), and Chebyshev/Bessel analysis showing that $\log(1/\varepsilon)/\log \log(1/\varepsilon)$ bounds polynomial approximation to $e^{c(x-1)}$ (Sec. III F). Additivity follows from oracle independence on disjoint ancilla registers.

c. Prerequisite results (Secs. VI–VIII). The M-QSP algorithm requires a *degree-preserving sum-of-squares* (SOS) *spectral factorization* for bivariate trigonometric polynomials on the torus \mathbb{T}^2 , avoiding algebraic obstruction to scalar complementary polynomials in two variables (Sec. VI). We show $L = 2$ for the Dyson polynomial, where the SOS rank is 2, yielding a constant ancilla overhead of $a_{\text{SOS}} = 2$ qubits, independent of (d_R, d_I) . A *constant-ratio condition* (CRC) giving recursive angle-finding yields well-defined scalar angles for

M-QSP circuits with arbitrary non-commuting signal operators [19] (Sec. VII). We compose a *constructive angle-finding algorithm* to compute M-QSP rotation angles in $\mathcal{O}(d_R \cdot d_I)$ classical operations via CRC-exploiting block peeling (Sec. VIII).

d. Three progressively optimal algorithms (Secs. IX–XI). We present three algorithms for simulating $e^{-iH_{\text{eff}}T}$ in the separate-oracle model, each improving on the previous:

- **Lorentzian interaction picture (LIP)** (Sec. IX): a post-Trotter split-operator method using a Lorentzian ancilla register to implement the non-unitary factor segment by segment. Query complexity is $\mathcal{O}(T^{1+1/(2p)} \varepsilon^{-1/(2p)} (\alpha_R T + \log(1/\varepsilon)))$ for p -th order operator splitting, requiring intermediate postselections.
- **Dyson LCU** (Sec. X): packages a segmented Taylor expansion into a single linear combination of unitaries (LCU) with a single postselection, achieving $\mathcal{O}((\alpha_R + \beta_I)T + \beta_I T \log(1/\varepsilon))$ queries.
- **Bivariate M-QSP** (Sec. XI): implements the interaction-picture Dyson polynomial as a single bivariate QSP circuit, with query complexity

$$Q = \mathcal{O}\left((\alpha_R + \beta_I)T + \frac{\log(1/\varepsilon)}{\log \log(1/\varepsilon)}\right) \quad (3)$$

and a single postselection on one ancilla qubit achieving success probability (1) up to $1 - \mathcal{O}(\varepsilon)$. This matches the lower bound (2) exactly, with Theorem III.4 giving $\Omega(\log(1/\varepsilon)/\log \log(1/\varepsilon))$ for the ε -dependent term, closing a $(\log \log)$ gap left by the Stirling-form bound of Lemma III.3.

e. Overview. Section II develops the two-layer barrier (intrinsic + block-encoding) and its saturation. Section III recovers the matching query lower bound. Subsequent sections develop the bivariate M-QSP construction, its circuit-level realization, and a small-scale numerical demonstration. Open problems appear in Sec. XIV D, including barrier-hierarchy refinement treated in the companion paper [27].

C. Comparison with prior work

a. LCHS. The linear combination of Hamiltonian simulations (LCHS) represents the non-unitary propagator $e^{-iH_{\text{eff}}T}$ as an integral over purely Hermitian evolution kernels [22, 23].

$$e^{-iH_{\text{eff}}T} = \int_{\mathbb{R}} K(y) e^{-i(H_R + yH_I)T} dy, \quad (4)$$

where K is a kernel function derived from the Hubbard–Stratonovich transformation or the Bromwich

integral, concentrating around $y = 0$ [28, 29]. The integral discretizes by quadrature into a finite linear combination of Hermitian simulations, implemented by block-encoding.

As a single oracle model, LCHS block-encodes and queries the full Hamiltonian $H_R + yH_I$. Postselection follows via multiple ancilla registers, with one register for the LCU selection register (of dimension equal to the number of quadrature points, scaling as $\mathcal{O}(\log(\beta_I T/\varepsilon))$) and one for each block-encoding. Success probability is the product of individual postselection probabilities.

Total query complexity inherits a union-bound penalty (an additional log factor), achieving $\mathcal{O}((\alpha + \beta)T \text{polylog}(1/\varepsilon))$ queries in the single-oracle model, with polylog overhead from quadrature discretization and per-segment simulation [23].

Aside from quadrature weights ($\mathcal{O}(\text{polylog}(\beta_I T/\varepsilon))$), the LCHS protocol requires no classical preprocessing, making it an attractive technique for non-Hermitian quantum simulation.

b. APS. Amplitude-Phase Separation (APS) [24] extracts the non-unitary component of H_{eff} by eigenvalue transformation with a polynomial or rational approximation to $e^{-\beta t}$ applied to anti-Hermitian eigenvalues.

With a single oracle, APS achieves query complexity $\mathcal{O}((\alpha + \beta)T + \log(1/\varepsilon))$, provably optimal in the single-oracle model. A distinct advantage of the APS method occurs when the initial state has support concentrated on eigenspaces of H_I , allowing for $\sqrt{\beta_I}$ -fast-forwarding when eigenvalues are much smaller than β_I .

c. Schrödingerization. Schrödingerization [3] embeds non-Hermitian dynamics into a unitary evolution on an extended Hilbert space, introducing a continuous ancilla variable p (the “warped phase space”). The non-Hermitian Schrödinger equation $i\partial_t |\psi\rangle = H_{\text{eff}} |\psi\rangle$ maps to a Hermitian Schrödinger equation on $\mathcal{H} \otimes L^2(\mathbb{R})$, where the physical state is recovered by measuring the ancilla. Postselection is avoided, replaced by a dilational embedding. An ancilla register is instantiated with $\mathcal{O}(\log(\beta_I T/\varepsilon))$ scaling. Query complexity becomes $\mathcal{O}((\alpha + \beta)T \text{polylog}(\beta_I T/\varepsilon))$, with polylog overhead arising from warped phase space discretization and Trotterization.

d. Lindbladian simulation. Non-Hermitian dynamics is often viewed as an open quantum system, simulating the Lindblad master equation and extracting the non-Hermitian propagator as the no-jump trajectory [2]. No-jump evolution with a single jump operator L and jump rate γ is governed by the effective Hamiltonian $H_{\text{eff}} = H - i(\gamma/2)L^\dagger L$ [13, 14]. Simulating the Lindbladian conditioned on zero jumps yields $e^{-iH_{\text{eff}}T}$.

Postselection is on the absence of quantum jumps and constitutes a multi-time-step conditioning rather than a single-shot measurement. Query complexity depends on Lindbladian parameters and the jump rate, not directly comparable to block-encoding-based methods.

e. CBMD. The compressed block-encoding method [25, 26] block-encodes $H_{\text{eff}} = H_R + iH_I$ in

a single unitary $U_{H_{\text{eff}}}$, implementing a polynomial approximation to $e^{-iH_{\text{eff}}T}$ via a compressed Chebyshev LCU. The compression reduces standard LCU’s per-term ancilla overhead, with query complexity

$$Q_{\text{CBMD}} = \mathcal{O}((\alpha + \beta)T \cdot \text{polylog}(1/\varepsilon)) \quad (5)$$

in the single-oracle model, with α, β denoting Hermitian and anti-Hermitian operator-norm contributions of the joint block encoding. Postselection requires multiple ancilla registers (one for the LCU selection register and one for the joint block encoding), with success probability decomposed as a product of register-wise contributions.

CBMD is the closest single-oracle analog of M-QSP, being polynomial methods rather than integral decompositions (LCHS, optimal LCHS) or Lindbladian simulators, and both CBMD and M-QSP achieve scaling that is linear in T up to logarithmic factors in $1/\varepsilon$. CBMD’s polylog($1/\varepsilon$) overhead may be improved in a separate-oracle handling of the Hamiltonian, closing a small gap in the error bound. Joint encoding of H_{eff} in CBMD couples α and β through the joint operator norm, whereas the separate-oracle model permits additive scaling. If α_R/β_I is large, this can lead to a constant-factor improvement in the leading T -dependent term, being more significant in the weak-dissipation regime relevant to AMO simulation (Sec. XIII).

CBMD requires $\mathcal{O}(\log(\beta_I T/\varepsilon))$ ancilla qubits for the compressed LCU register, compared to the $\max(a_R, a_I) + 3$ ancilla cost of M-QSP (Proposition XI.1), with M-QSP overhead exceeding CBMD log-scaling when $a_R, a_I \gg 1$. We expect CBMD to be preferable in the regime $\beta_I \sim \alpha_R$ with single-oracle access, and M-QSP when $\beta_I \ll \alpha_R$ with physically separated coherent and dissipative components. A quantitative benchmark is deferred to Appendix A and the companion paper [27].

f. Interaction-picture simulation (Low-Wiebe). The interaction-picture algorithm [30] inspires the present construction. Low and Wiebe showed that an interaction-picture propagator $V(T)$ cast as a Dyson series can be truncated and implemented via a product of generalized quantum signal processing (GQSP) circuits and block-encoding queries, achieving query complexity $\mathcal{O}(\alpha_R T + \beta_I T \log(\beta_I T/\varepsilon))$ for Hermitian Hamiltonians $H = H_A + H_B$ with $\|H_A\| = \alpha_R$ and $\|H_B\| = \beta_I$.

The interaction-picture decomposition generalizes to $H_{\text{eff}} = H_R + iH_I$ with $H_I \succeq 0$, promoting the Dyson polynomial to a bivariate polynomial (in the walk-operator variable of H_R and the block-encoding variable of H_I). A sequence of independent circuits is replaced by a bivariate M-QSP circuit, saving a factor of $\log(\beta_I T/\varepsilon)$. The M-QSP construction presented here achieves optimal query complexity in the separate-oracle model, single-qubit postselection matching the information-theoretic barrier, and non-split-operator circuit structure. Each property has been achieved individually by other methods, combined in the present architecture (Secs. VI–VIII). A summary of this comparison is given in Table I.

Throughout this paper we adopt the convention $H_{\text{eff}} =$

Method	Query complexity	Oracle model	# postselections	ε scaling	Ancilla qubits
LCHS [22]	$\mathcal{O}(\alpha t \cdot \text{polylog}(1/\varepsilon))$	Single A	$\mathcal{O}(\log(\beta_I T))$ registers	polylog	$\mathcal{O}(\log(\beta_I T)) + a$
Optimal LCHS [23]	$\mathcal{O}((\alpha_R + \beta_I)T + \log(1/\varepsilon))$	Single A	multi-register	polylog	$\mathcal{O}(\log(1/\varepsilon)) + a$
APS [24]	$\mathcal{O}((\alpha + \beta)T + \log(1/\varepsilon))$	Single A	multi-register	log	$a + 1$
Schrödingerization [3]	$\mathcal{O}(\alpha t \cdot \text{polylog}(1/\varepsilon))$	Embedding	implicit	polylog	$\mathcal{O}(\log T) + 1$
Lindbladian [2]	$\mathcal{O}((\alpha_R + \beta_I)T \cdot \text{polylog}(1/\varepsilon))$	Lindblad	implicit	polylog	implicit
(M-QSP)	$\mathcal{O}((\alpha_R + \beta_I)T + \log(1/\varepsilon))^a$	W_R, U_I separate	1 qubit	\log^a	$\max(a_R, a_I) + 3$

TABLE I. Comparison of approaches to non-Hermitian Hamiltonian simulation. The first four entries operate in the single-oracle model (one block encoding of H_{eff}). M-QSP operates in the separate-oracle model (independent block encodings of H_R/α_R and H_I/β_I on disjoint ancilla registers). The two models are not directly comparable on a per-query basis (see the introduction and Sec. III A). Here α and β denote the norms of the Hermitian and anti-Hermitian parts respectively. For single-oracle methods, these refer to corresponding components of the joint block encoding. ^aSuppressing a $\log \log(1/\varepsilon)$ factor in the ε -dependent term. See Theorem XI.1 for the precise expression.

$H_R + iH_I$ with $H_I \succeq 0$, so the propagator $e^{-iH_{\text{eff}}T}$ has operator norm $\|e^{-iH_{\text{eff}}T}\|_{\text{op}} = e^{\beta_I T}$. The convention matches the semigroup notation, where $H_I \succeq 0$ drives exponential growth of $\|e^{-iH_{\text{eff}}T}\|_{\text{op}}$, absorbed by block-encoding normalization $\lambda \geq e^{\beta_I T}$.

Lindblad mapping. In the Lindblad quantum-jump formalism, the effective Hamiltonian in the no-jump trajectory picture takes the form

$$H_{\text{eff}}^{\text{Lindblad}} = H_{\text{LS}} - \frac{i}{2} \sum_j L_j^\dagger L_j, \quad (6)$$

where H_{LS} is the Liouvillian-Schrodinger Hamiltonian and L_j are Lindblad operators. We identify $H_R = H_{\text{LS}}$ (Hermitian) and $H_I^{\text{raw}} = -(1/2) \sum_j L_j^\dagger L_j \preceq 0$ (negative semidefinite). The spectral shift $H_I \rightarrow H_I^{\text{raw}} + \beta_I I$ with $\beta_I = \|(1/2) \sum_j L_j^\dagger L_j\|$ recovers $H_I \succeq 0$. The global phase $e^{-i\beta_I T}$ introduced by the shift represents the no-jump survival probability in the original trajectory formalism, cancelling from all physical observables.

II. THE POSTSELECTION BARRIER

We first establish a constraint on quantum implementations for non-Hermitian time evolution. The result follows from unitarity and polynomial block encoding structure. Unitary block contraction, numerical abscissa bound on semigroup norms [31–33], and polynomial structure of block-encoding algorithms [10, 34] are already well-established. We focus on providing a decomposition into two independent layers (intrinsic and block-encoding), with a tightness proof showing that the combined bound is a more general limit for non-Hermitian simulation protocols.

A. The necessity of postselection

The target operation $e^{-iH_{\text{eff}}T}$ is non-unitary when $H_I \neq 0$. Any quantum circuit implements a unitary U on a composite system $\mathcal{H}_a \otimes \mathcal{H}_s$. The non-unitary map

is recovered by projecting the ancilla onto a designated state $|0\rangle_a$:

$$(\langle 0|_a \otimes I_s) U (|0\rangle_a \otimes |\psi_0\rangle) = \frac{1}{\lambda} e^{-iH_{\text{eff}}T} |\psi_0\rangle, \quad (7)$$

where $\lambda > 0$ is the block-encoding normalization. Success probability of ancilla measurement is

$$P = \frac{\|e^{-iH_{\text{eff}}T} |\psi_0\rangle\|^2}{\lambda^2}. \quad (8)$$

We focus on the minimum possible λ , and hence the maximum achievable P .

B. The intrinsic factor

The first constraint follows from unitarity.

Theorem II.1 (Intrinsic factor). *For a quantum implementation of the form (7),*

$$P \leq \frac{\|e^{-iH_{\text{eff}}T} |\psi_0\rangle\|^2}{\|e^{-iH_{\text{eff}}T}\|_{\text{op}}^2}. \quad (9)$$

Proof. Since U is unitary, its $(0,0)$ -block $A := (\langle 0|_a \otimes I_s) U (|0\rangle_a \otimes I_s)$ is a contraction: $\|A\|_{\text{op}} \leq 1$. By (7), $A = e^{-iH_{\text{eff}}T}/\lambda$, so the contraction condition requires $\lambda \geq \|e^{-iH_{\text{eff}}T}\|_{\text{op}}$. Substituting into (8) gives (9).

Remark II.1 (Semigroup bound on operator norm). The operator norm of $e^{-iH_{\text{eff}}T}$ is controlled by the numerical abscissa. Since $-iH_{\text{eff}} = -iH_R + H_I$, the numerical abscissa is $\omega(-iH_{\text{eff}}) = \sup_{\|v\|=1} \text{Re} \langle v | -iH_R + H_I | v \rangle = \sup_{\|v\|=1} \langle v | H_I | v \rangle = \beta_I$. The spectral abscissa $\omega_{\text{spec}}(H_{\text{eff}}) := \max\{\text{Im}(\lambda) : \lambda \in \text{spec}(H_{\text{eff}})\}$ satisfies $\omega_{\text{spec}}(H_{\text{eff}}) \leq \beta_I$, with equality if and only if $[H_R, H_I] = 0$. The gap $\beta_I - \omega_{\text{spec}}(H_{\text{eff}})$ is controlled by the commutator norm $\|\text{ad}_{H_R}(H_I)\|$; see the companion paper [27] for a quantitative statement. Throughout this paper we use the symbol $\omega := \omega_{\text{spec}}(H_{\text{eff}})$, distinct from the numerical abscissa β_I , and we never use ω to denote β_I . The Hille–Yosida bound [31–33] then gives $\|e^{-iH_{\text{eff}}T}\|_{\text{op}} \leq e^{\beta_I T}$,

with equality holding when H_I achieves its norm on an eigenspace in the support of $|\psi_0\rangle$.

Substituting into (9) yields the explicit bound

$$P \leq e^{-2\beta_I T} \|e^{-iH_{\text{eff}}T} |\psi_0\rangle\|^2. \quad (10)$$

The state-dependent factor $\|e^{-iH_{\text{eff}}T} |\psi_0\rangle\|^2 / \|e^{-iH_{\text{eff}}T}\|_{\text{op}}^2$ in (9) is the ratio of propagator action on $|\psi_0\rangle$ to the worst-case action. Initial states aligned with the top eigenspace of H_I saturate this ratio at 1; states orthogonal to it experience additional exponential suppression.

C. Layer 2: The block-encoding factor

A second constraint specifies algorithms based on polynomial block encodings, including the known approaches to Hamiltonian simulation with polylogarithmic error dependence [10, 12, 34].

Theorem II.2 (Block-encoding factor). *Let $P_\delta(e^{i\theta_1}, e^{i\theta_2})$ be a bivariate polynomial of bidegree (d_R, d_I) that ε -approximates the normalized propagator $V(T; \theta_1, \theta_2)/\lambda$ on the physical eigenvalue region. If P_δ is implemented as a block of a unitary circuit that queries walk operators W_R and U_I (encoding H_R/α_R and H_I/β_I), then the polynomial bound $|P_\delta(e^{i\theta_1}, e^{i\theta_2})| \leq 1$ must hold for all $(\theta_1, \theta_2) \in \mathbb{T}^2$, including eigenvalues outside the physical spectrum. This forces*

$$\lambda \geq e^{\beta_I T} (1 - O(\varepsilon)). \quad (11)$$

Proof. P_δ is the $(0,0)$ -block of a unitary \mathcal{G} , so $|P_\delta(e^{i\theta_1}, e^{i\theta_2})| \leq 1$ for all $(\theta_1, \theta_2) \in \mathbb{T}^2$. With a restriction to $\theta_1 = 0$:

$$|P_\delta(1, e^{i\theta_2})| \leq 1, \quad \forall \theta_2 \in [0, 2\pi). \quad (12)$$

This must hold for all θ_2 , including those outside the physical spectrum of H_I . The walk operator U_I encodes H_I/β_I via $U_I = e^{i \arccos(H_I/\beta_I)}$, with eigenvalues $e^{i\theta_2}$ ranging over the full unit circle \mathbb{T} , even though the physical spectrum of H_I/β_I lies in $[-1, 1]$.

At $\theta_2 = 0$, the interaction-picture propagator evaluates to $V(T; \theta_1, 0) = e^{+\beta_I T}$ for all θ_1 (Proposition V.2), so the normalized polynomial satisfies

$$|P_\delta(e^{i\theta_1}, 1)| = \frac{e^{\beta_I T}}{\lambda} (1 + O(\varepsilon)). \quad (13)$$

The constraint $|P_\delta| \leq 1$ forces $\lambda \geq e^{\beta_I T} (1 - O(\varepsilon))$. The same conclusion follows from a fixed θ_1 , since every univariate slice $\{e^{i\theta_1}\} \times \mathbb{T}$ contains a maximizing point $\theta_2 = 0$.

Remark II.2 (Scope). Theorem II.2 applies to all algorithms that implement $e^{-iH_{\text{eff}}T}/\lambda$ as a polynomial in block-encoding eigenvalues. It does not apply to methods that avoid the polynomial framework entirely. The intrinsic barrier (Theorem II.1) does not have this constrained applicability.

Remark II.3 (Function-class universality of the barrier). Theorem II.2 holds for $e^{-iH_{\text{eff}}T}$ polynomial block-encodings, but the barrier $\lambda \geq e^{\beta_I T}$ is not restricted to function class for the walk-operator oracle model. Any block of a unitary \mathcal{G} satisfies $|f(z_1, z_2)| \leq 1$ on \mathbb{T}^2 , and the spectral point $z_2 = 1$ forces $|f(e^{i\theta_1}, 1)| = e^{\beta_I T}/\lambda$ for all θ_1 , giving $\lambda \geq e^{\beta_I T}$ unconditionally. The walk-operator-class extension theorem in the companion paper [27] states this formally. One open question, also addressed there, is whether direct-access constructions that bypass the walk-operator framework could achieve $\lambda = e^{\omega T} (1 + o(1))$ for the spectral abscissa $\omega < \beta_I$, beating the barrier.

D. The Postselection Barrier (combined bound)

Corollary II.1 (The Postselection Barrier). *For a polynomial block-encoding algorithm:*

$$P \leq e^{-2\beta_I T} \|e^{-iH_{\text{eff}}T} |\psi_0\rangle\|^2. \quad (14)$$

This is a product of two independent factors:

$$\underbrace{e^{-2\beta_I T}}_{\text{block-encoding cost}} \times \underbrace{\|e^{-iH_{\text{eff}}T} |\psi_0\rangle\|^2}_{\text{state-dependent factor}}. \quad (15)$$

The first factor is the cost from encoding a non-unitary operator in a unitary circuit with polynomial structure. The second is the survival probability of the initial state under non-Hermitian evolution.

Proof. Combine $\lambda \geq e^{\beta_I T} (1 - O(\varepsilon))$ from Theorem II.2 with (8). In the limit $\varepsilon \rightarrow 0$, this gives (14).

E. Tightness

The bound (14) is the tight limit. Iterated postselection neither helps nor hurts.

Lemma II.1 (Telescoping identity). *Let M be a contraction ($\|M\|_{\text{op}} \leq 1$), applied K times with normalization after each step: $|\psi_{k+1}\rangle = M |\psi_k\rangle / \|M |\psi_k\rangle\|$. The total success probability satisfies*

$$P_{\text{total}} = \prod_{k=0}^{K-1} \|M |\psi_k\rangle\|^2 = \|M^K |\psi_0\rangle\|^2. \quad (16)$$

Proof. By strong induction. The base case $K = 1$ is immediate. For the inductive step, suppose $P_n = \|M^n |\psi_0\rangle\|^2$. Then

$$\begin{aligned} P_{n+1} &= P_n \cdot \|M |\psi_n\rangle\|^2 \\ &= \|M^n |\psi_0\rangle\|^2 \cdot \frac{\|M^{n+1} |\psi_0\rangle\|^2}{\|M^n |\psi_0\rangle\|^2} \\ &= \|M^{n+1} |\psi_0\rangle\|^2. \end{aligned} \quad (17)$$

Theorem II.3 (Achievability of the barrier). *In the continuum limit ($K \rightarrow \infty$, $\sum_k \Delta t_k = T$), a quantum implementation of $e^{-iH_{\text{eff}}T}$ via K iterated non-unitary steps with per-step operator $M_k \approx e^{-iH_{\text{eff}}\Delta t_k} / \|e^{-iH_{\text{eff}}\Delta t_k}\|_{\text{op}}$ yields a total success probability*

$$P_{\text{total}} \rightarrow e^{-2\beta_I T} \|e^{-iH_{\text{eff}}T} |\psi_0\rangle\|^2. \quad (18)$$

Proof. Each M_k has unit operator norm by construction. By Lemma II.1,

$$P_{\text{total}} = \frac{\|e^{-iH_{\text{eff}}T} |\psi_0\rangle\|^2}{\prod_{k=1}^K \|e^{-iH_{\text{eff}}\Delta t_k}\|_{\text{op}}^2}. \quad (19)$$

The numerical abscissa bound gives $(\ln \|e^{-iH_{\text{eff}}\Delta t}\|_{\text{op}}) / \Delta t \rightarrow \omega(-iH_{\text{eff}}) = \beta_I$ as $\Delta t \rightarrow 0$, so

$$\prod_{k=1}^K \|e^{-iH_{\text{eff}}\Delta t_k}\|_{\text{op}}^2 \rightarrow e^{2\beta_I T}, \quad (20)$$

yielding (18).

Remark II.4 (Algorithm independence). Theorem II.3 applies to quantum algorithms implementing $e^{-iH_{\text{eff}}T}$ with vanishing error. Postselection cost is determined by the Hamiltonian and the initial state.

F. Physical interpretation

The postselection barrier separates physical cost from algorithmic cost for non-Hermitian simulation. In the block-encoding oracle model, postselection is required whenever $H_I \neq 0$, and success probability cannot exceed $e^{-2\beta_I T} \|e^{-iH_{\text{eff}}T} |\psi_0\rangle\|^2$. Dilational methods (Schrödingerization) avoid postselection but pay an equivalent exponential cost in ancilla resources (details in Sec. XIV B). Amplitude amplification reduces repetition cost from $O(e^{2\beta_I T})$ to $O(e^{\beta_I T})$ [35]. Our methods optimize algorithmic cost, manifesting in oracle queries per run, number of postselection events, and whether query complexity is additive or multiplicative in $\alpha_R T$ and $\beta_I T$.

As established in the Lindblad mapping (Sec. IA), non-Hermitian evolution $e^{-iH_{\text{eff}}T} |\psi_0\rangle$ describes the conditional state given no quantum jump over $[0, T]$, and ancilla postselection mimics this conditioning. The cost $e^{-2\beta_I T}$ reflects an event whose probability is exponentially small in $\beta_I T$.

Theorem II.1 follows from linearity and unitarity, while Theorem II.2 is a tighter, model-specific refinement within the polynomial block-encoding framework. This barrier includes dilational embeddings (Schrödingerization [3]) that avoid postselection at the cost of a continuous ancilla register. The combined bound applies to polynomial block-encoding [10, 12, 34]. We do not presently consider whether equivalent overhead is unavoidable across oracle models, or whether dilational methods escape it rather than redistributing it into ancilla resources (Sec. XIV B).

III. LOWER BOUNDS

Here we show that a quantum algorithm simulating $e^{-iH_{\text{eff}}T}$ in the separate-oracle model requires $\Omega((\alpha_R + \beta_I)T + \log(1/\varepsilon) / \log \log(1/\varepsilon))$ total queries. Components are proved independently, with $\Omega(\alpha_R T)$ established by reduction to Hermitian simulation, $\Omega(\beta_I T)$ by the polynomial method, and $\Omega(\log(1/\varepsilon) / \log \log(1/\varepsilon))$ by polynomial approximation. Bounds are additive, as block-encoding oracles for H_R and H_I act on disjoint ancilla registers. We also prove a joint query-normalization bound coupling query count to block-encoding normalization.

All three component bounds use standard techniques [10, 12, 36]. We contribute an assembly of such techniques in the separate-oracle model, where additivity yields a stronger composite bound than is available in the single-oracle setting.

A. The oracle model

Access H_R and H_I through block-encoding unitaries:

$$U_R \in \mathcal{U}(\mathcal{H}_s \otimes \mathcal{H}_{a_R}), \quad (\langle 0|_{a_R} \otimes I_s) U_R (|0\rangle_{a_R} \otimes I_s) = H_R / \alpha_R. \quad (21)$$

Analogously, U_I encodes H_I / β_I on $\mathcal{H}_s \otimes \mathcal{H}_{a_I}$. U_R and U_I act on disjoint ancilla registers \mathcal{H}_{a_R} and \mathcal{H}_{a_I} .

An algorithm makes Q_R queries to U_R (or U_R^\dagger) and Q_I queries to U_I (or U_I^\dagger), interleaved with unitaries on $\mathcal{H}_s \otimes \mathcal{H}_{a_R} \otimes \mathcal{H}_{a_I} \otimes \mathcal{H}_{\text{work}}$ that do not depend on H_R or H_I . Total query count is $Q = Q_R + Q_I$.

B. Main result

Theorem III.1 (Additive query lower bound). *For all valid $(H_R, H_I, |\psi_0\rangle)$ with $\|H_R\|_{\text{op}} \leq \alpha_R$ and $\|H_I\|_{\text{op}} \leq \beta_I$, a quantum algorithm that produces a state ε -close in operator norm to $e^{-iH_{\text{eff}}T} |\psi_0\rangle / \|e^{-iH_{\text{eff}}T} |\psi_0\rangle\|$, must make at least*

$$Q = Q_R + Q_I \geq \Omega\left(\alpha_R T + \beta_I T + \frac{\log(1/\varepsilon)}{\log \log(1/\varepsilon)}\right) \quad (22)$$

queries to the block-encoding oracles, for $\varepsilon \leq 1/36$.

We show this by assembling component bounds (Sec. III C) and demonstrating additivity (Sec. III D). A complementary joint query-normalization bound is given in Sec. III E.

C. Component bounds

1. The Hermitian component: $\Omega(\alpha_R T)$

Lemma III.1. $Q_R \geq \Omega(\alpha_R T)$, even when H_I is known.

Proof. Set $H_I = 0$. $H_{\text{eff}} = H_R$ is Hermitian and the non-Hermitian simulation problem reduces to Hermitian Hamiltonian simulation. The no-fast-forwarding theorem [37] gives $Q_R \geq \Omega(\alpha_R T)$. Since $H_I = 0$ is known, all U_I queries are uninformative and the full cost falls on Q_R .

2. *The anti-Hermitian component:* $\Omega(\beta_I T)$

Lemma III.2. $Q_I \geq \Omega(\beta_I T)$, even when H_R is known.

Proof. Set $H_R = 0$, so that $e^{-iH_{\text{eff}}T} = e^{H_I T}$. The task reduces to implementing $e^{H_I T}$ using queries to the block encoding of H_I . We use the polynomial method of Beals et al. [36] applied to a one-parameter family of Hamiltonians.

a. *One parameter family.* Let $|\phi\rangle$ be a fixed known state. Consider the family

$$H_I(\eta) = \eta |\phi\rangle\langle\phi|, \quad \eta \in [0, \beta_I]. \quad (23)$$

The target evolution on input $|\phi\rangle$ is $e^{H_I(\eta)T} |\phi\rangle = e^{\eta T} |\phi\rangle$. After normalization by $e^{\beta_I T}$, the algorithm produces a state whose overlap with $|\phi\rangle$ encodes the ratio $e^{(\eta - \beta_I)T}$, ranging from $e^{-\beta_I T}$ (at $\eta = 0$) to 1 (at $\eta = \beta_I$).

b. *Acceptance probability is a polynomial.* The block encoding acts on the $|\phi\rangle$ eigenspace as $\langle 0|_\ell U_I(\eta) |0\rangle_\ell |_{|\phi\rangle} = x := \eta/\beta_I$. By the polynomial method [36], a quantum circuit making Q queries to $U_I(\eta)$ and $U_I(\eta)^\dagger$ produces a final state whose amplitudes are polynomials of degree at most Q in x . Each oracle call introduces one power of x from the block-encoded eigenvalue on the $|\phi\rangle$ eigenspace; all other operations act on registers not touched by the oracle, being η -independent by definition of the query model (see [36] and [10] for the formal statement). More precisely, Q queries produce a Laurent polynomial of degree Q in $e^{i\theta_2}$, where $\cos\theta_2 = \eta/\beta_I = x$; since acceptance probability \mathcal{P} is real and symmetric under $\theta_2 \rightarrow -\theta_2$ (by Hermiticity of H_I), \mathcal{P} depends on θ_2 only through $\cos\theta_2 = x$ via $T_k(\cos\theta) = \cos(k\theta)$, and is therefore a polynomial of degree at most Q in x . Probability of a specific measurement outcome (acceptance probability) is therefore

$$\mathcal{P}(x) = |\langle m | \Psi_{\text{final}}(x) \rangle|^2, \quad (24)$$

a polynomial of degree at most $2Q$ in x . Polynomial structure relies on the black-box oracle assumption that the algorithm's dependence on η enters only through oracle calls.

c. *Approximation-theoretic lower bound.* If the algorithm correctly simulates $e^{H_I(\eta)T}$ to constant precision $\varepsilon_0 < 1/4$ for all $\eta \in [0, \beta_I]$, then $\mathcal{P}(x)$ must ε_0 -approximate the target function

$$f(x) = e^{2\beta_I T(x-1)}, \quad x \in [0, 1]. \quad (25)$$

The best polynomial approximation error for e^{at} on $[-1, 1]$ follows [38], satisfying

$$E_n(e^{a \cdot})_{\infty, [-1, 1]} \geq c \frac{a^{n+1}}{(n+1)! e^a} \quad (26)$$

for a constant $c > 0$. Setting this $\leq \varepsilon_0$ and inverting via Stirling's formula gives $n \geq \Omega(a)$ when $a = \beta_I T$. Since $\mathcal{P}(x)$ is a degree- $2Q$ polynomial that ε_0 -approximates f on $[0, 1]$, we conclude $2Q \geq \Omega(\beta_I T)$, giving $Q_I \geq \Omega(\beta_I T)$.

Remark III.1 (Black-box assumption). The result is founded on an exactness of polynomial structure, where $\mathcal{P}(x)$ is a polynomial of degree exactly $2Q$. If the algorithm can exploit internal structure of $U_I(\eta)$ beyond the oracle, acceptance probability can depend on η non-polynomially.

3. *The precision component:* $\Omega(\log(1/\varepsilon))$ (Stirling form; tightened to $\log/\log\log$ in Sec. III F)

Lemma III.3. $Q \geq \Omega(\log(1/\varepsilon))$, including for $\alpha_R T = O(1)$ and $\beta_I T = O(1)$. The tighter bound $Q \geq \Omega(\log(1/\varepsilon)/\log\log(1/\varepsilon))$ is established in Theorem III.4.

Proof. Set $\alpha_R = \beta_I = 1$, $T = 1$, $H_R = Z$, and $H_I = \eta Z$ for $\eta \in [0, 1]$. Then $e^{-iH_{\text{eff}}T} = e^{(-i+\eta)Z}$. By the polynomial method, acceptance probability after Q queries is a degree- $2Q$ polynomial in η . To achieve ε -precision, this polynomial must approximate $e^{2\eta}$ on $[0, 1]$ to error ε .

The best degree- d polynomial approximation to $e^{2\eta}$ on $[0, 1]$ has error $\Theta(2^d/d!)$ from the Taylor remainder [38]. Setting $2^d/d! \leq \varepsilon$ and inverting via Stirling gives $d \geq \Omega(\log(1/\varepsilon)/\log\log(1/\varepsilon))$. The sharper bound $d \geq \Omega(\log(1/\varepsilon))$ follows from degree lower bounds for e^{cz} in the complex plane (see [38] for the classical result). We state the lower bound as $Q \geq \Omega(\log(1/\varepsilon))$ throughout.

Remark III.2 (log vs. $\log/\log\log$). The Stirling-based argument yields $\Omega(\log(1/\varepsilon)/\log\log(1/\varepsilon))$. $\Omega(\log(1/\varepsilon))$ requires the full complex-valued propagator rather than just acceptance probability. The gap between this lower bound and the best known upper bound of $O(\log(1/\varepsilon)/\log\log(1/\varepsilon))$ in the d_I degree is discussed in Sec. XII.

D. Additivity

Component bounds must be shown to be additive $Q \geq \Omega(\alpha_R T + \beta_I T + \log(1/\varepsilon))$ [36].

Theorem III.2 (Additivity). *In the separate-oracle model,*

$$Q = Q_R + Q_I \geq \Omega(\alpha_R T) + \Omega(\beta_I T) + \Omega\left(\frac{\log(1/\varepsilon)}{\log\log(1/\varepsilon)}\right). \quad (27)$$

Proof.

a. Oracle independence. U_R and U_I act on disjoint ancilla registers, so a query to U_R acts as the identity on \mathcal{H}_{a_I} and carries no information about H_I , and vice versa. An adversary choosing H_R and H_I independently forces $Q_R \geq \Omega(\alpha_R T)$ (by Lemma III.1) and $Q_I \geq \Omega(\beta_I T)$ (by Lemma III.2) simultaneously. Every query is either to U_R or to U_I , so $Q = Q_R + Q_I \geq \Omega(\alpha_R T) + \Omega(\beta_I T)$.

Disjoint-register structure ensures each query contributes to the polynomial degree in one variable (θ_1 for U_R , θ_2 for U_I), so the implementable polynomial's bidegree (Q_R, Q_I) is bounded by the number of queries to each oracle, precluding any benefit from interleaving U_R and U_I queries.

b. Adding the ε -dependent term. The $\Omega(\log(1/\varepsilon)/\log \log(1/\varepsilon))$ bound (Lemma III.3) applies to the total query count $Q = Q_R + Q_I$. We show additivity with $\alpha_R T$ and $\beta_I T$ terms by considering a single adversarial instance where all three constraints apply simultaneously.

Consider $\alpha_R T = \Theta(n)$, $\beta_I T = \Theta(n)$, and $\varepsilon = e^{-\Theta(n)}$ for $n \rightarrow \infty$. By oracle independence (Part 1), bounds $Q_R \geq \Omega(\alpha_R T)$ (Lemma III.1) and $Q_I \geq \Omega(\beta_I T)$ (Lemma III.2) apply simultaneously to the same fixed circuit, because U_R and U_I act on disjoint ancilla registers. Additionally, the adversary can set the precision requirement to $\varepsilon = e^{-\Theta(n)}$, forcing $Q = Q_R + Q_I \geq \Omega(\log(1/\varepsilon)/\log \log(1/\varepsilon)) = \Omega(n/\log n)$ by Lemma III.3.

Since the fixed circuit must simultaneously satisfy:

1. $Q_R \geq \Omega(\alpha_R T) = \Omega(n)$,
2. $Q_I \geq \Omega(\beta_I T) = \Omega(n)$,
3. $Q = Q_R + Q_I \geq \Omega(\log(1/\varepsilon)/\log \log(1/\varepsilon)) = \Omega(n/\log n)$,

the total query count satisfies

$$Q \geq \Omega(\alpha_R T) + \Omega(\beta_I T) + \Omega\left(\frac{\log(1/\varepsilon)}{\log \log(1/\varepsilon)}\right). \quad (28)$$

The ε -dependent term is additive when $\log(1/\varepsilon) \gg (\alpha_R + \beta_I)T$ (the precision requirement dominates) and is dominated otherwise. Since all three bounds hold simultaneously on the single instance, they sum unconditionally.

A separate-oracle bidegree lower bound $d_I \geq \Omega(\beta_I T)$ (proved in the companion paper [27]) shows that the additivity of Theorem III.2 cannot be circumvented by a polynomial of small d_I .

E. Joint query–normalization bound

The following result couples query count to block-encoding normalization, providing a complementary perspective on the lower bound.

Theorem III.3 (Joint query–normalization bound). *Let an algorithm make Q total queries and implement $e^{-iH_{\text{eff}}T}/\lambda$ as the $(0,0)$ -block of a unitary, with operator-norm error at most ε for $\varepsilon \leq 1/36$. Then*

$$Q \cdot \log(\lambda e^{-\beta_I T}) \geq \Omega(\beta_I T). \quad (29)$$

If $\lambda = e^{\beta_I T}$ (minimal normalization), then $Q \geq \Omega(\beta_I T)$ with no logarithmic gain. If $\lambda = e^{(1+\eta)\beta_I T}$ for some $\eta > 0$ (over-normalized), then $Q \geq \Omega(1/\eta)$.

Proof. Consider $H_I(\delta) = (\beta_I + \delta)|\phi\rangle\langle\phi|$ for a fixed state $|\phi\rangle$, with $H_R = 0$ and $\delta \in [0, \beta_I]$.

Step 1 (Sensitivity). On the $|\phi\rangle$ eigenspace, acceptance probability $P(\delta) = e^{2(\beta_I + \delta)T}/\lambda^2$, with derivative $P'(0) = 2T e^{2\beta_I T}/\lambda^2$.

Step 2 (Polynomial constraint). After Q queries, P is a polynomial of degree at most $2Q$ in δ/β_I . By the Markov inequality [39], a polynomial p of degree d satisfying $0 \leq p(x) \leq 1$ on an interval of length L has $|p'(x)| \leq 2d^2/L$. Applied with $d = 2Q$ and $L = \beta_I$:

$$P'(0) \leq \frac{8Q^2}{\beta_I}. \quad (30)$$

Step 3 (Combining). Equating: $2T e^{2\beta_I T}/\lambda^2 \leq 8Q^2/\beta_I$, giving $Q^2 \geq (\beta_I T/4) \cdot e^{2\beta_I T}/\lambda^2$. If $\lambda = e^{\beta_I T}$, this yields $Q \geq \sqrt{\beta_I T}/2$, which is the suboptimal Markov bound.

Step 4 (Upgrade via transfer). Choose $\delta_0 = 2\sqrt{\varepsilon}/T$. For $\varepsilon \leq 1/36$ (i.e., $6\sqrt{\varepsilon} \leq 1$; see Remark III.3), the algorithm must distinguish $\delta = 0$ from $\delta = \delta_0$ to precision ε . With the choice $\delta_0 = 2\sqrt{\varepsilon}/T$, we have $\delta_0 T = 2\sqrt{\varepsilon}$, so output states for $\delta = 0$ and $\delta = \delta_0$ differ in operator-norm bias by

$$\begin{aligned} \frac{e^{\beta_I T}(e^{\delta_0 T} - 1)}{\lambda} &= \frac{e^{\beta_I T}(e^{2\sqrt{\varepsilon}} - 1)}{\lambda} \\ &\geq \frac{2\sqrt{\varepsilon} \cdot e^{\beta_I T}}{\lambda}, \end{aligned}$$

where the inequality uses $e^x - 1 \geq x$ for $x \geq 0$ applied at $x = 2\sqrt{\varepsilon}$.

The acceptance-probability polynomial $\mathcal{P}(x) = P(x\beta_I)$ has degree at most $2Q$ on $[0, 1]$ (rescaling $\delta \mapsto x = \delta/\beta_I$), with $0 \leq \mathcal{P}(x) \leq 1$. On the sub-interval $[0, \delta_0/\beta_I]$ of length $\ell = 2\sqrt{\varepsilon}/(\beta_I T)$, \mathcal{P} achieves a variation $\Delta \geq 2\sqrt{\varepsilon} \cdot e^{\beta_I T}/\lambda$. By the Chebyshev node bound for bounded polynomials on an interval of length ℓ , a variation of Δ requires degree $d \geq \Omega(\Delta/\ell)$. Substituting: $2Q \geq \Omega(\beta_I T \cdot e^{\beta_I T}/\lambda)$.

Upgrade via polynomial approximation. We extract a degree lower bound using classical approximation theory. Define $\mathcal{P}(x) := P(x\beta_I)$ on $[0, 1]$ (i.e., $x = \delta/\beta_I$). Then $\deg(\mathcal{P}) \leq 2Q$ and $\mathcal{P}(x) \in [0, 1]$ for all $x \in [0, 1]$. Rescaling to the canonical interval $[-1, 1]$ by setting $y = 2x - 1$:

$$\tilde{\mathcal{P}}(y) := \mathcal{P}\left(\frac{y+1}{2}\right). \quad (31)$$

Then $\tilde{\mathcal{P}}$ has degree $\leq 2Q$ with $|\tilde{\mathcal{P}}(y)| \leq 1$ on $[-1, 1]$. By proof of Step 3, $\tilde{\mathcal{P}}(-1) \approx 1$ and $\tilde{\mathcal{P}}(1) \approx e^{-2\beta_I T}/\lambda^2$. For the polynomial to realize this decay while remaining bounded in magnitude, it must approximate an exponential profile of effective rate $c = \beta_I T + \log \lambda$ over $[-1, 1]$.

The best polynomial approximation of degree d to e^{cx} on $[-1, 1]$ has error at least $(c/2)^{d+1}/(d+1)!$ (Bernstein's approximation theorem [40, 41]); for this to be $\leq \varepsilon$, one needs $d \geq \Omega(c)$. Applying this to $\tilde{\mathcal{P}}$:

$$2Q \geq \deg(\tilde{\mathcal{P}}) = \Omega(\beta_I T + \log \lambda). \quad (32)$$

When $\lambda = e^{\beta_I T}$ (minimal normalization), $\beta_I T + \log \lambda = 2\beta_I T$, giving $Q = \Omega(\beta_I T)$. For general λ , the constraint becomes

$$Q \cdot \log(\lambda e^{-\beta_I T}) \geq \Omega(\beta_I T). \quad (33)$$

When $\lambda = e^{\beta_I T}$, this yields $Q \geq \Omega(\beta_I T)$ with no logarithmic factor.

Remark III.3 (The constraint $\varepsilon \leq 1/36$). The threshold $\varepsilon \leq 1/36$ in Step 4 arises from the Chebyshev transfer argument: $\delta_0 = 2\sqrt{\varepsilon}/T$ requires the variation $e^{\delta_0 T} - 1 \geq 2\sqrt{\varepsilon}$ to exceed the algorithm's distinguishing resolution, holding if $6\sqrt{\varepsilon} \leq 1$. The factor of 6 combines error from normalization, approximation, and rounding, each contributing a factor of ~ 2 . This constraint is pragmatically hollow, since simulation targets $\varepsilon \ll 1/36$ in practice. Whether the constant can be reduced (e.g., to 4, giving $\varepsilon \leq 1/16$) is an question about the proof technique.

Remark III.4 (Interpretation). Theorem III.3 quantifies a tradeoff of over-normalizing the block encoding (choosing $\lambda \gg e^{\beta_I T}$) to reduce per-query difficulty, increasing postselection cost. The product $Q \cdot \log(\lambda e^{-\beta_I T})$ is bounded below by $\Omega(\beta_I T)$ regardless of normalization strategy.

F. Lower bound for the anti-Hermitian degree

The $\log \log(1/\varepsilon)$ factor in the d_I component comes from bounded polynomial approximation.

Theorem III.4 (log/log log scaling). *Let $c > 0$ and $\varepsilon \in (0, 1/2)$. Define $d^*(c, \varepsilon)$ as the minimum degree of a polynomial p satisfying $|p(x)| \leq 1$ on $[-1, 1]$ and $\|p - e^{c(x-1)}\|_{\infty, [0, 1]} \leq \varepsilon$. Then*

$$d^*(c, \varepsilon) = \frac{\log(1/\varepsilon)}{\log \log(1/\varepsilon)} (1 + o(1)) \quad \text{as } \varepsilon \rightarrow 0. \quad (34)$$

Proof. The Chebyshev–Bessel–Lambert- W analysis appears in full in the companion paper [27] (log/log log lower bound theorem). We reproduce only the Bessel-positivity step needed to guarantee $|S_d(x)| \leq 1$ on $[-1, 1]$: The function $e^{c(x-1)}$ is bounded by 1 on $[-1, 1]$ and its Chebyshev coefficients $b_k = 2e^{-c/2} I_k(c/2)$ are all non-negative, where I_k is the modified Bessel function. For

a polynomial with non-negative Chebyshev coefficients, the Chebyshev partial sums $S_d(x) = \sum_{k=0}^d b_k T_k(x)$ satisfy $S_d(x) \leq S_d(1) = \sum_{k=0}^d b_k = e^{c(1-1)} = 1$ for all $x \in [-1, 1]$ (since $T_k(1) = 1$ and $|T_k(x)| \leq 1$ on $[-1, 1]$). The constraint $|p| \leq 1$ is automatically satisfied at the optimal degree. Inversion via Lambert- W exists in the companion paper [27].

Remark III.5 (Implications for the M-QSP lower bound). Theorem III.4 upgrades the lower bound on the anti-Hermitian query count from $Q_I \geq \Omega(\beta_I T + \log(1/\varepsilon))$ to $Q_I \geq \Omega(\beta_I T + \log(1/\varepsilon)/\log \log(1/\varepsilon))$. The d_R component achieves $\Theta(\log(1/\varepsilon))$ via Bessel tails (Jacobi–Anger expansion), so the overall lower bound becomes

$$Q \geq \Omega\left((\alpha_R + \beta_I)T + \frac{\log(1/\varepsilon)}{\log \log(1/\varepsilon)}\right). \quad (35)$$

We will see that M-QSP algorithm achieves this bound exactly.

IV. THE INTERACTION-PICTURE FRAMEWORK

The interaction-picture approach to Hamiltonian simulation was introduced by Low and Wiebe [30] for Hermitian Hamiltonians $H = A + B$, where query complexity scales with interaction strength $\|B\|$ rather than total energy $\|A + B\|$. We adapt this to the non-Hermitian setting $H_{\text{eff}} = H_R + iH_I$ with $H_I \geq 0$.

Factorization and Dyson series are textbook constructions from time-dependent perturbation theory, making adaptation straightforward. Non-Hermiticity of H_{eff} introduces a nonunitarity in the interaction-picture propagator $V(T)$, with an operator norm growing as $e^{\beta_I T}$, requiring an imposed postselection barrier in block-encoding normalization approaches (Sec. II). Positive semidefiniteness of H_I (and hence $\tilde{H}(s)$) constrains the spectrum of $V(T)$ to the positive real axis, creating a zero-locus obstruction analyzed in Sec. V.

A. Interaction-picture propagator

Proposition IV.1 (Exact interaction-picture factorization). *Define the interaction-picture propagator*

$$V(t) := e^{iH_R t} e^{-iH_{\text{eff}} t} = e^{iH_R t} e^{(-iH_R + H_I) t}. \quad (36)$$

Then V satisfies the initial-value problem

$$\frac{dV}{dt}(t) = \tilde{H}(t) V(t), \quad V(0) = I, \quad (37)$$

where the interaction-picture Hamiltonian is

$$\tilde{H}(t) := e^{iH_R t} H_I e^{-iH_R t}. \quad (38)$$

The unique solution is the time-ordered (Dyson) exponential

$$V(T) = \mathcal{T}_> \exp\left(\int_0^T \tilde{H}(s) ds\right), \quad (39)$$

and the full non-Hermitian evolution factors as

$$e^{-iH_{\text{eff}}T} = e^{-iH_R T} \cdot V(T). \quad (40)$$

Proof. Differentiate $V(t) = e^{iH_R t} e^{(-iH_R + H_I)t}$. The $e^{iH_R t}$ factor contributes iH_R ; the $e^{(-iH_R + H_I)t}$ factor contributes $(-iH_R + H_I)$. Using $[e^{iH_R t}, H_R] = 0$:

$$\begin{aligned} \frac{dV}{dt} &= e^{iH_R t} [iH_R + (-iH_R + H_I)] e^{(-iH_R + H_I)t} \\ &= e^{iH_R t} H_I e^{(-iH_R + H_I)t}. \end{aligned} \quad (41)$$

Substituting $e^{(-iH_R + H_I)t} = e^{-iH_R t} V(t)$ from (36) gives $dV/dt = \tilde{H}(t)V(t)$ as claimed. The initial condition $V(0) = I$ is immediate, and rearranging (36) gives the factorization (40).

B. Properties of $\tilde{H}(s)$

The following properties are consequent to unitary conjugation $X \mapsto e^{iH_R s} X e^{-iH_R s}$, preserving the adjoint, spectrum, and operator norm.

Lemma IV.1 (Properties of $\tilde{H}(s)$). *For all $s \geq 0$:*

1. $\tilde{H}(s)$ is Hermitian.
2. $\tilde{H}(s) \succeq 0$ (positive semidefinite, since $H_I \succeq 0$).
3. $\|\tilde{H}(s)\| = \|H_I\| = \beta_I$.
4. $\text{spec}(\tilde{H}(s)) = \text{spec}(H_I)$.
5. $\|d^n \tilde{H}/ds^n\| \leq (2\alpha_R)^n \beta_I$ for all integers $n \geq 1$.

Proof. Properties (1)–(4) follow directly from unitary conjugation: $\tilde{H}(s) = UH_IU^\dagger$ with $U = e^{iH_R s}$ unitary, so the adjoint, positive semidefiniteness, norm, and spectrum of H_I are preserved.

For (5), differentiate using the adjoint action: $d\tilde{H}/ds = i[H_R, \tilde{H}(s)] = i\text{ad}_{H_R}(\tilde{H}(s))$. By induction, $d^n \tilde{H}/ds^n = (i)^n \text{ad}_{H_R}^n(\tilde{H}(s))$. Submultiplicativity of the commutator gives $\|\text{ad}_{H_R}(X)\| = \|[H_R, X]\| \leq 2\|H_R\| \|X\| \leq 2\alpha_R \|X\|$, so by induction $\|d^n \tilde{H}/ds^n\| \leq (2\alpha_R)^n \beta_I$.

Remark IV.1 (Role of positive semidefiniteness). Property (2) follows from the convention $H_I \succeq 0$ and ensures that $V(T)$ is expansive ($\|V(T)\|_{\text{op}} = e^{\beta_I T}$) rather than contractive. The Lindblad spectral shift (as mentioned in Sec. IA) reduces the $H_I \leq 0$ case to this convention.

C. Norm bound on $V(T)$

Proposition IV.2 (Operator-norm bound). $\|V(T)\|_{\text{op}} \leq e^{\beta_I T}$. Consequently, $|P(z_1, z_2)| \leq 1$ on \mathbb{T}^2 for the normalized polynomial $P = V(T)/e^{\beta_I T}$.

Proof. The Grönwall bound applied to $V' = \tilde{H}V$, $V(0) = I$, with $\|\tilde{H}(s)\| = \beta_I$ gives $\|V(t)\| \leq e^{\beta_I t}$.

D. The Dyson series

The time-ordered exponential (39) admits the convergent Dyson series:

$$\begin{aligned} V(T) &= \sum_{n=0}^{\infty} \int_{0 \leq s_1 \leq \dots \leq s_n \leq T} \tilde{H}(s_n) \\ &\quad \dots \tilde{H}(s_1) ds_1 \dots ds_n. \end{aligned} \quad (42)$$

The n -th term has norm at most $\beta_I^n T^n/n!$ (by $\|\tilde{H}\| = \beta_I$ and the volume of the n -simplex), confirming convergence with $\|V(T)\| \leq \sum_n \beta_I^n T^n/n! = e^{\beta_I T}$.

The factorization (40) converts non-Hermitian simulation into logically independent tasks: the Hermitian simulation of H_R (the unitary factor $e^{-iH_R T}$, implementable optimally by GQSP at cost $O(\alpha_R T + \log(1/\varepsilon))$ queries [10]), and non-unitary implementation of $V(T)$ (a contraction after normalization by $e^{\beta_I T}$, requiring block encoding and postselection).

E. Segmented Taylor expansion

Dyson series truncation to a form suitable for quantum implementation follows Low and Wiebe [30], adapted to non-Hermitian systems where $\tilde{H}(s) \succeq 0$ and $\|V(T)\|_{\text{op}} = e^{\beta_I T}$.

Divide $[0, T]$ into r segments of width $\Delta = T/r$ with midpoints $\tau_j = (j - \frac{1}{2})\Delta$, $j = 1, \dots, r$. On each segment, replace $\tilde{H}(s)$ by its midpoint value $\tilde{H}(\tau_j)$, giving the midpoint-approximated propagator:

$$V_r(T) = \prod_{j=r}^1 e^{\tilde{H}(\tau_j) \Delta}. \quad (43)$$

Theorem IV.1 (Quadrature error bound). *The midpoint approximation satisfies*

$$\begin{aligned} \|V(T) - V_r(T)\| &\leq \frac{C_2 T^3}{r^2} e^{\beta_I T}, \\ C_2 &= O(\beta_I^2 \alpha_R^2 + \beta_I^2 \alpha_R). \end{aligned} \quad (44)$$

p -th order Magnus-based quadrature gives

$$\|V(T) - V_r^{(p)}(T)\| \leq C_p T^{2p+1} r^{-2p} e^{\beta_I T}. \quad (45)$$

Proof. On each segment $[\tau_j - \Delta/2, \tau_j + \Delta/2]$, expand $\tilde{H}(s) = \tilde{H}(\tau_j) + (s - \tau_j)\tilde{H}'(\tau_j) + \frac{1}{2}(s - \tau_j)^2\tilde{H}''(\tau_j) + O(\Delta^3)$. The midpoint integral satisfies

$$\int_{\tau_j - \Delta/2}^{\tau_j + \Delta/2} \tilde{H}(s) ds = \tilde{H}(\tau_j)\Delta + \frac{\Delta^3}{24}\tilde{H}''(\tau_j) + O(\Delta^5), \quad (46)$$

where the linear term vanishes by midpoint symmetry. Leading error is the second-order Magnus term. By Lemma IV.1(v), $\|\tilde{H}''\| \leq (2\alpha_R)^2\beta_I$, so per-segment error from the midpoint approximation to the Magnus exponent is $O(\Delta^3\alpha_R^2\beta_I)$.

Propagator error on segment j satisfies

$$\|e^{\int \tilde{H} ds} - e^{\tilde{H}(\tau_j)\Delta}\| \leq O(\Delta^3\alpha_R^2\beta_I)e^{\beta_I\Delta}, \quad (47)$$

where the exponential prefactor arises from matrix exponential perturbation bound applied to a generator of norm $\beta_I\Delta$. The second-order Magnus commutator $[\tilde{H}(\tau_j), \int (s - \tau_j)\tilde{H}'(s) ds]$ contributes an additional $O(\Delta^3\beta_I^2\alpha_R)$ term (from $\|\tilde{H}\| \cdot \|\tilde{H}'\| = \beta_I \cdot 2\alpha_R\beta_I$), giving a combined constant $C'_2 = O(\beta_I^2\alpha_R^2 + \beta_I^2\alpha_R)$ per segment.

To pass from per-segment to global error, write $V(T) = \prod_{j=r}^1 V_j$ where $V_j = \mathcal{T}_> \exp(\int_{\text{seg}_j} \tilde{H} ds)$, and $V_r(T) = \prod_{j=r}^1 e^{\tilde{H}(\tau_j)\Delta}$. The telescoping identity for products of bounded operators gives

$$\|V(T) - V_r(T)\| \leq \sum_{j=1}^r \|V_j - e^{\tilde{H}(\tau_j)\Delta}\| \prod_{k \neq j} e^{\beta_I\Delta}, \quad (48)$$

where operator norms of remaining factors are bounded by $e^{\beta_I\Delta}$ via the Grönwall estimate (Proposition IV.2). Since the product of $r - 1$ such factors is at most $e^{\beta_I(T-\Delta)} \leq e^{\beta_I T}$, and each per-segment error is $O(\Delta^3 C'_2)$, the sum yields

$$\begin{aligned} \|V(T) - V_r(T)\| &\leq r \cdot O(\Delta^3 C'_2) \cdot e^{\beta_I T} \\ &= O\left(\frac{T^3}{r^2}\right) C'_2 e^{\beta_I T}, \end{aligned} \quad (49)$$

using $r\Delta^3 = T^3/r^2$. Identifying $C_2 = C'_2$ recovers the theorem statement (44) with

$$C_2 = O(\beta_I^2\alpha_R^2 + \beta_I^2\alpha_R) = O(\beta_I^2\alpha_R^2) \quad \text{for } \alpha_R \geq 1,$$

where the simplified form relevant in the simulation regime $\alpha_R T \gg 1$. Contributions arise from the second-order Magnus quadrature ($\beta_I^2\alpha_R^2$) and the commutator $[\tilde{H}, \int (s - \tau)\tilde{H}' ds]$ ($\beta_I^2\alpha_R$).

For (45): replace midpoint integration with p -th order Gauss–Legendre quadrature, eliminating error terms through $O(\Delta^{2p-1})$ per segment by quadrature node symmetry. Per-segment error becomes $O(\Delta^{2p+1} C'_p)$, and the same telescoping argument gives $r \cdot O(\Delta^{2p+1}) \cdot e^{\beta_I T} = O(T^{2p+1} r^{-2p}) e^{\beta_I T}$. Cost of p -th order quadrature is $O(p)$ evaluation points per segment, each requiring one frame rotation and one H_I application.

Quadrature of a smooth integrand (smoothness guaranteed by Lemma IV.1(v): $\|d^n \tilde{H}/ds^n\| \leq (2\alpha_R)^n \beta_I$) gains $2p$ orders per refinement via midpoint symmetry, doubling the exponent as opposed to the symmetric Trotter expansion, which gains only p orders from the BCH expansion. Per-order cost is polynomial ($O(p)$) for Gauss–Legendre versus superpolynomial ($O(5^{p/2})$) for Suzuki decompositions [42]. Quadratic improvement in the exponent propagates into the total query complexity of all three simulation methods (Secs. IX–XI).

Each factor $e^{\tilde{H}(\tau_j)\Delta}$ is truncated to Taylor order M :

$$e^{\tilde{H}(\tau_j)\Delta} = \sum_{m=0}^M \frac{(\tilde{H}(\tau_j)\Delta)^m}{m!} + O\left(\frac{(\beta_I\Delta)^{M+1}}{(M+1)!}\right). \quad (50)$$

Setting $M = O(\beta_I\Delta + \log(1/\varepsilon))$ makes the Taylor truncation error exponentially small. The full truncated propagator is:

$$\hat{V}_{r,M}(T) = \prod_{j=r}^1 \left[\sum_{m_j=0}^M \frac{(\tilde{H}(\tau_j)\Delta)^{m_j}}{m_j!} \right], \quad (51)$$

a sum over $(M+1)^r$ terms forming a linear combination of unitaries.

F. The zero-cost unitary factor

The following observation follows from Low and Wiebe [30]

Theorem IV.2 (Zero-cost Hermitian evolution). *The GQSP frame rotations implementing each segment's interaction-picture transformation $e^{iH_R\tau_j}(\cdot)e^{-iH_R\tau_j}$ cumulatively advance the frame by $e^{-iH_R\Delta} = e^{-iH_R T}$. The full circuit output is*

$$e^{-iH_R T} \cdot \frac{\hat{V}_{r,M}(T)}{\lambda} |\psi_0\rangle \approx \frac{e^{-iH_{\text{eff}} T}}{\lambda} |\psi_0\rangle. \quad (52)$$

No additional circuit is needed for the unitary factor $e^{-iH_R T}$.

Proof. After r SELECT steps, the total frame rotation is $\prod_{j=1}^r e^{-iH_R\Delta} = e^{-iH_R T}$. By factorization (40), net circuit output is $e^{-iH_R T} \hat{V}_{r,M}(T)/\lambda \approx e^{-iH_{\text{eff}} T}/\lambda$.

G. Error analysis and query complexity

Theorem IV.3 (Total approximation error).

$$\begin{aligned} \|V(T) - \hat{V}_{r,M}(T)\| &\leq \underbrace{C_{\text{Mag}} \frac{\alpha_R \beta_I^2 T^3}{r^2}}_{\text{Magnus quadrature}} \\ &\quad + r \underbrace{\frac{(\beta_I\Delta)^{M+1}}{(M+1)!}}_{\text{Taylor truncation}} e^{\beta_I T}. \end{aligned} \quad (53)$$

With $\beta_I \Delta = c$ (constant), $r = O(\beta_I T)$, and $M = O(\beta_I T + \log(1/\varepsilon))$: both terms are bounded by $\varepsilon/2$, giving total error $\leq \varepsilon$.

Complexity consequences for Dyson LCU are given in Section XD. See Appendix B for the detailed error budget.

V. THE DYSON POLYNOMIAL AND ITS ZERO LOCUS

The interaction-picture framework (Sec. IV) reduces non-Hermitian simulation to the application of the propagator $V(T)$ as a block of a unitary circuit. After qubitization, walk operators W_R and U_I act on eigenspaces labeled by phases θ_1 and θ_2 , and the propagator becomes a bivariate polynomial on the bitorus $\mathbb{T}^2 = \mathbb{T} \times \mathbb{T}$. In this section we define this polynomial, establish its bidegree, and analyze a structural property of its zero locus, motivating spectral factorization machinery of Sec. VI.

A. Polynomial spaces on \mathbb{T}^2

Definition V.1 (Polynomial spaces).

1. $\mathcal{P}_{d_1, d_2}^+ := \left\{ P(z_1, z_2) = \sum_{n_1=0}^{d_1} \sum_{n_2=0}^{d_2} a_{n_1 n_2} z_1^{n_1} z_2^{n_2} : a_{n_1 n_2} \in \mathbb{C} \right\}$ is the space of analytic polynomials of bidegree at most (d_1, d_2) .
2. \mathcal{T}_{d_1, d_2} is the space of real trigonometric polynomials of bidegree (d_1, d_2) : functions $T(\theta_1, \theta_2) = \sum_{|n_1| \leq d_1} \sum_{|n_2| \leq d_2} c_{n_1 n_2} e^{i(n_1 \theta_1 + n_2 \theta_2)}$ with $T = \bar{T}$.
3. For $P \in \mathcal{P}_{d_1, d_2}^+$, the restriction $|P|^2|_{\mathbb{T}^2}$ lies in \mathcal{T}_{d_1, d_2} (and is non-negative, though \mathcal{T}_{d_1, d_2} itself contains all real trigonometric polynomials of the given bidegree).

B. Eigenvalue parameterization

The circuit achieves eigenvalue parameterization by implementing the propagator using walk operators encoding H_R and H_I . Specifically, W_R encodes H_R/α_R with eigenphases $\theta_1 \in [0, 2\pi)$ related to eigenvalues $\lambda_R(\theta_1) = \alpha_R \cos \theta_1$. The walk operator U_I encodes H_I/β_I with eigenphases $\theta_2 \in [0, 2\pi)$ related to eigenvalues $\mu_I(\theta_2) = \beta_I \cos \theta_2$.

On the tensor-product eigenspace of $W_R \otimes U_I$ (acting on the composite Hilbert space $\mathcal{H}_s \otimes \mathcal{H}_{a_R} \otimes \mathcal{H}_{a_I}$) where W_R has eigenphase θ_1 and U_I has eigenphase θ_2 , the interaction-picture Hamiltonian evaluates to $\tilde{H}(s)|_{(\theta_1, \theta_2)} = e^{i\lambda_R s} \mu_I e^{-i\lambda_R s} = \mu_I$, and the propagator becomes

$$V(T; \theta_1, \theta_2) = \exp(\mu_I(\theta_2) T) = e^{\beta_I T \cos \theta_2}. \quad (54)$$

The normalized propagator becomes

$$P(e^{i\theta_1}, e^{i\theta_2}) := \frac{V(T; \theta_1, \theta_2)}{e^{\beta_I T}} = e^{\beta_I T (\cos \theta_2 - 1)}. \quad (55)$$

P must be evaluated for all pairs $(\theta_1, \theta_2) \in \mathbb{T}^2$, not just those corresponding to simultaneous eigenvalues of H_R and H_I on the physical Hilbert space. Since H_R and H_I generically do not commute ($[H_R, H_I] \neq 0$), joint eigenspaces of H_R and H_I do not exist on the physical system. However, W_R and U_I act on independent ancilla registers and generate their eigenphases independently, bounding the polynomial $P(e^{i\theta_1}, e^{i\theta_2})$ on all of \mathbb{T}^2 . This includes the ‘‘unphysical’’ region where (θ_1, θ_2) do not arise from a simultaneous diagonalization of H_R and H_I . This sources a global constraint on \mathbb{T}^2 in the block encoding model.

Remark V.1 (Independence of θ_1 and the necessity of bivariate implementation). The target normalized propagator (55) on the tensor product eigenspace depends only on θ_2 . The circuit must implement $P(e^{i\theta_1}, e^{i\theta_2})$ as a bivariate polynomial for two reasons: (i) the walk operator W_R does not preserve eigenspaces of H_I (frame rotations $e^{\pm i H_R s}$ do not commute with H_I), and (ii) the Jacobi–Anger expansion of these frame rotations distributes θ_2 -dependence across multiple z_1 -Fourier modes.

C. Dyson polynomial and its bidegree

The truncated Dyson series of Sec. IVE yields a bivariate polynomial in two signal operators when compiled into walk-operator queries via the Jacobi–Anger expansion [10, 11],

Proposition V.1 (Dyson polynomial encoding). *Implementing the truncated Dyson series $\hat{V}_{r, M}(T)$ (Eq. (51)) with d_R queries to the walk operator W_R and d_I queries to the walk operator U_I , yields a bivariate Laurent polynomial $P_{\text{Dyson}}(z_1, z_2) \in \mathcal{P}_{d_R, d_I}^+$ with bidegree*

$$\begin{aligned} d_R &= \mathcal{O}(\alpha_R T + \log(1/\varepsilon)), \\ d_I &= \mathcal{O}(\beta_I T + \log(1/\varepsilon)/\log \log(1/\varepsilon)), \end{aligned} \quad (56)$$

satisfying $|P_{\text{Dyson}}(e^{i\theta_1}, e^{i\theta_2})| \leq 1$ for all $(\theta_1, \theta_2) \in [0, 2\pi)^2$.

Proof. Dyson series structure. Each factor $\tilde{H}(s_k) = e^{i H_R s_k} H_I e^{-i H_R s_k}$ in the Dyson series involves a unitary conjugation by $e^{i H_R s_k}$ (requiring queries to W_R) sandwiching H_I (requiring one query to U_I). The n -th Dyson term contributes degree n in the eigenphases of U_I .

Jacobi–Anger encoding. Each Hermitian propagator $e^{-i H_R s_k}$ is approximated by a Laurent polynomial in $z_1 = e^{i\theta_1}$ of degree $\mathcal{O}(\alpha_R s_k + \log(N/\varepsilon))$ via the Jacobi–Anger expansion [11]. Summing over segments yields total degree $d_R = \mathcal{O}(\alpha_R T + \log(1/\varepsilon))$ in z_1 .

Block-encoding polynomial structure. Each appearance of H_I contributes degree 1 in $z_2 = e^{i\theta_2}$. The Taylor truncation at order M per segment, with $r = O(\beta_I T)$ segments, gives total degree $d_I = r \cdot M/r = M = \mathcal{O}(\beta_I T + \log(1/\varepsilon)/\log \log(1/\varepsilon))$ in z_2 . The log log denominator arises from the Stirling bound on the Taylor remainder $(\beta_I \Delta)^{M+1}/(M+1)!$.

Boundedness. $|P_{\text{Dyson}}| \leq 1$ on \mathbb{T}^2 , since it is the $(0, 0)$ -block of a product of unitary operators.

D. Zero-locus obstruction

The M-QSP circuit requires a complementary polynomial R satisfying $|P|^2 + |R|^2 = 1$ on \mathbb{T}^2 , amounting to a factoring of the non-negative trigonometric polynomial $H := 1 - |P|^2$ as a Hermitian square. *Notation convention (used throughout the construction, circuit, and main-theorem sections below, and in Appendices E–I).* We write the complementary polynomial interchangeably as R or Q : we use Q as it appears in algorithmic pseudocode and classical M-QSP recurrences [19] to denote the $(1, 0)$ -block of the $\text{SU}(2)$ -valued transfer matrix, while symbol Q in Section III denotes the total query count. We disambiguate by context (algorithmic block vs. complexity-theoretic counting), with the complementary-polynomial Q explicitly annotated as “the complementary polynomial Q ” when necessary. This is always possible by the Fejér–Riesz theorem in one variable, but can fail in two variables as we present in the Dyson polynomial.

Proposition V.2 (Zero-locus obstruction). *For the normalized Dyson propagator P ,*

$$P(e^{i\theta_1}, 1) = 1 \quad \text{for all } \theta_1 \in [0, 2\pi). \quad (57)$$

Hence $H(\theta_1, \theta_2) = 1 - |P|^2$ vanishes on $\gamma := \mathbb{T} \times \{1\} \subset \mathbb{T}^2$, a closed curve that is homologically nontrivial.

Proof. At $\theta_2 = 0$ (i.e., $z_2 = 1$), the block-encoding eigenvalue is $\mu_I = \beta_I \cos 0 = \beta_I$. The interaction-picture Hamiltonian evaluates to

$$\tilde{H}(s)|_{\theta_2=0} = e^{i\lambda_R(\theta_1)s} (\beta_I) e^{-i\lambda_R(\theta_1)s} = \beta_I, \quad (58)$$

since β_I is a scalar eigenvalue and commutes with the frame rotation. The time-ordered exponential reduces to

$$V(T; \theta_1, 0) = \exp\left(\int_0^T \beta_I ds\right) = e^{\beta_I T} \text{ for all } \theta_1. \quad (59)$$

Therefore $P(e^{i\theta_1}, 1) = e^{\beta_I T}/e^{\beta_I T} = 1$.

The zero set $\mathcal{Z} = \{H = 0\} = \{|P| = 1\}$ contains the full circle $\gamma = \mathbb{T} \times \{1\}$, a codimension-1 curve in \mathbb{T}^2 . Since γ generates the first factor of $H_1(\mathbb{T}^2, \mathbb{Z}) \cong \mathbb{Z}^2$, it is homologically nontrivial.

Corollary V.1 (Failure of scalar complementation). *The non-negative trigonometric polynomial $H = 1 - |P|^2$ does not admit a scalar factorization $H = |R|^2$ with $R \in \mathcal{P}_{d_R, d_I}^+$.*

Proof sketch. If R existed with $|R|^2 = 1 - |P|^2$, then R would vanish on $\gamma = \mathbb{T} \times \{1\}$, forcing $(z_2 - 1) \mid R$ by the identity theorem. Writing $R = (z_2 - 1)S$ gives $1 - |P|^2 = |z_2 - 1|^2 |S|^2 = (2 - 2\cos\theta_2) |S|^2$. This constrains H to factor as $(2 - 2\cos\theta_2) \times (\text{Hermitian square})$ on all of \mathbb{T}^2 . The moment-matrix rank criterion (Proposition VI.1) or the codimension argument of Appendix H, Proposition H.4 verifies that the quotient $H/(2 - 2\cos\theta_2)$ is not a Hermitian square at the reduced bidegree $(d_R, d_I - 1)$, verified via the moment-matrix rank criterion. The SOS resolution (Theorem VI.2) makes the scalar obstruction moot, where the algorithm does not require a single complementary polynomial.

Remark V.2 (Obstructions). Failure of scalar complementation arises from a local (point-zero) obstruction, where autocorrelation structure of H at isolated points prevents root pairing, as well as a global (curve-zero) obstruction, where the zero set \mathcal{Z} contains a homologically nontrivial curve. The Dyson polynomial encounters the latter. Both mechanisms are absent in one variable, where the Fejér–Riesz theorem always applies (Sec. VI).

Remark V.3 (Algebraic vs. topological framing). The obstruction in the bivariate Fejér–Riesz problem is sometimes described topologically, in terms of winding numbers or first Chern classes of line bundles attached to the zero set of $1 - |P|^2$ [43, 44]. We identify the Dyson polynomial obstruction algebraically, where matching Fourier coefficients between $|Q|^2$ and H gives a system with $(2d_R+1)(2d_I+1)$ real constraints against $2(d_R+1)(d_I+1) - 1$ effective real unknowns (see Proposition H.4 in Appendix H for the codimension argument).

E. Effect of truncation

The above analysis applies to the exact normalized propagator. For the truncated Dyson polynomial P_M (Taylor order M, r segments), the curve γ is not in the zero set:

$$|P_M(z_1, 1)| = 1 - O((\beta_I \Delta)^{M+1}/(M+1)!) < 1. \quad (60)$$

The finite Taylor truncation introduces a deficit of order ε , providing “natural regularization.” This deficit is not uniform across \mathbb{T}^2 and does not suffice for a controlled factorization. δ -regularization of Sec. VI makes this uniform and controllable, restoring SOS spectral factorization (Theorem VI.2).

VI. BIVARIATE SPECTRAL FACTORIZATION

The M-QSP circuit implements a bivariate polynomial P as the $(0, 0)$ -block of a unitary. Unitarity requires a complementary polynomial Q satisfying $|P|^2 + |Q|^2 = 1$ on \mathbb{T}^2 (or a sum-of-squares generalization). The Fejér–Riesz theorem guarantees this in one dimension.

Main result. We derive a circuit-level guarantee (Theorem VI.6 and Corollary VI.2) for M-QSP circuits: the M-QSP circuit is unitary by construction (pre-postselection), so the complement exists automatically as the $(1,0)$ -block, and the 2×2 ancilla forces $L = 2$ independent of d_R, d_I (Theorem VI.7). The circuit bypasses factorization, with inductive degree reduction with a constant-ratio condition (Sec. VII) achieving this guarantee.

We present different resolutions with trade-offs: δ -regularization (Resolution I, Sec. VID), Dritschel–Woerdeman SOS theory (Resolution II, Sec. VIE), and circuit-level unitarity (Resolution III, Sec. VIF), with full derivations in Appendix H.

The SOS rank hierarchy. We give successively tighter bounds on the number L of sum-of-squares terms needed to represent the complement $H = 1 - |P|^2$:

1. *Worst case (Dritschel–Woerdeman).* $L \leq (d_R+1)(d_I+1)$ for any $P \in \mathcal{P}_{d_R, d_I}^+$ with $|P|^2 \leq 1$ on \mathbb{T}^2 (Theorem VI.3).
2. *Symmetric reorganization.* $L \leq \min(d_R+1, d_I+1)$ when $H > 0$ uniformly on \mathbb{T}^2 , achieved by reorganizing H in the variable with the smaller degree before applying the operator Fejér–Riesz theorem (Theorem VI.2; details in Appendix H).
3. *Exact for M-QSP circuits.* $L = 2$ for any polynomial achievable as the $(0,0)$ -block of an M-QSP circuit, including the regularized Dyson polynomial (Theorem VI.7). The two $SU(2)$ branches of the QSP ancilla force the rank to two without regard of (d_R, d_I) .

The third bound is the operative one for the algorithm. The first two are stated for completeness and are also of independent interest as bounds on a generic bivariate Fejér–Riesz substitute.

A. The complementary polynomial problem

Definition VI.1 (Scalar and SOS complements). Let $P \in \mathcal{P}_{d_1, d_2}^+$ with $|P|^2 \leq 1$ on \mathbb{T}^2 , and set $H := 1 - |P|^2 \geq 0$.

1. A scalar complement is a polynomial $R \in \mathcal{P}_{d_1, d_2}^+$ with $H = |R|^2$ on \mathbb{T}^2 .
2. An *SOS complement* is a collection $\{R_1, \dots, R_L\} \subset \mathcal{P}_{d_1, d_2}^+$ with $H = \sum_{\ell=1}^L |R_\ell|^2$ on \mathbb{T}^2 .

Both require expressing the non-negative trigonometric polynomial H as a (sum of) Hermitian square(s) of analytic polynomials of the same bidegree.

B. Univariate Fejér–Riesz theorem

The Fejér–Riesz theorem [45, 46] is given as:

Theorem VI.1. Let $H \in \mathcal{T}_d$ satisfy $H(\theta) \geq 0$ for all θ . Then there exists $Q \in \mathcal{P}_d^+$ with $H(\theta) = |Q(e^{i\theta})|^2$.

A classical proof factors the self-reciprocal Laurent polynomial $\hat{H}(z) = z^d H(\theta)$ into its $2d$ roots, partitioning into conjugate-reciprocal pairs. Non-negativity forces every root on \mathbb{T} to have even multiplicity, and the off- \mathbb{T} roots pair as $(w, 1/\bar{w})$. Assigning one partner from each pair to Q yields $H = |Q|^2$. This argument uses three features specific to one complex variable: the zero set of H on \mathbb{T} is a finite set of points; each zero has a well-defined integer multiplicity; and non-negativity forces even multiplicity. All three can fail in two variables.

C. Bivariate obstruction

1. Algebraic mechanism: isolated zeros

We demonstrate that the univariate factorization theorem has no bivariate analog (even with a single isolated zero), given by counterexample.

Example VI.1 (Canonical algebraic obstruction). Define $H_{\text{can}}(\theta_1, \theta_2) = 4 \sin^2(\theta_1/2) + 4 \sin^2(\theta_2/2) = 4 - 2 \cos \theta_1 - 2 \cos \theta_2 \in \mathcal{T}_{1,1}$. Then $H_{\text{can}} \geq 0$ with a single zero at $(\theta_1, \theta_2) = (0, 0)$, but no $Q \in \mathcal{P}_{1,1}^+$ satisfies $H_{\text{can}} = |Q|^2$.

Proof. Write $Q(z_1, z_2) = a + bz_1 + cz_2 + dz_1 z_2$ and expand $|Q|^2$ on \mathbb{T}^2 . Matching mixed Fourier modes $e^{i(\theta_1+\theta_2)}$ and $e^{i(\theta_2-\theta_1)}$ against zero gives $\bar{a}d = 0$ and $\bar{b}c = 0$, while the pure modes require $\bar{a}b + \bar{c}d = -1$ and $\bar{a}c + \bar{b}d = -1$. A case analysis over the four branches of $\{\bar{a}d = 0\} \cap \{\bar{b}c = 0\}$ produces a contradiction in each case (see Appendix F).

2. Topological mechanism: curve zeros

The Dyson polynomial encounters a different obstruction. By Proposition V.2, $|P(e^{i\theta_1}, 1)| = 1$ for all θ_1 , so $H = 1 - |P|^2$ vanishes on the homologically nontrivial curve $\gamma = \mathbb{T} \times \{1\} \subset \mathbb{T}^2$. An analytic Q with $|Q|^2 = H$ would vanish on γ , forcing $(z_2 - 1) \mid Q$ and constraining H to factor as $(2 - 2 \cos \theta_2) |R|^2$. This is a separability condition that generically fails (Corollary V.1).

3. Discriminant source

Both mechanisms emerge by the same algebraic invariant.

Proposition VI.1 (Obstruction characterization). Let $H \in \mathcal{T}_{d_1, d_2}$ with $H \geq 0$ on \mathbb{T}^2 . Define the moment matrix $\mathbf{M} \in \mathbb{C}^{N \times N}$, $N = (d_1+1)(d_2+1)$, by $\mathbf{M}_{(m,n), (m',n')} = \hat{H}_{m-m', n-n'}$. Then $H = |R|^2$ for a single $R \in \mathcal{P}_{d_1, d_2}^+$ if and only if $\text{rank}(\mathbf{M}) = 1$.

Proof. Since $H \geq 0$, the Herglotz–Bochner characterization gives $\mathbf{M} \succeq 0$: for $\mathbf{v} = (v_{mn})$, define the analytic polynomial $f = \sum_{m,n} v_{mn} e^{i(m\theta_1+n\theta_2)}$; then $\mathbf{v}^\dagger \mathbf{M} \mathbf{v} = (2\pi)^{-2} \int_{\mathbb{T}^2} H |f|^2 d\theta_1 d\theta_2 \geq 0$. The spectral decomposition $\mathbf{M} = \sum_\ell \lambda_\ell \mathbf{u}_\ell \mathbf{u}_\ell^\dagger$ yields $H = \sum_\ell |R_\ell|^2$ where $R_\ell(z_1, z_2) = \sum_{m,n} (\sqrt{\lambda_\ell} u_\ell)_{mn} z_1^m z_2^n$. This sum reduces to a single term iff $\text{rank}(\mathbf{M}) = 1$.

Remark VI.1 (Contrast with one variable). In one variable, $\text{rank}(\mathbf{M}) = 1$ always holds: root-pairing succeeds because the zero set is discrete with even multiplicities and the univariate autocorrelation system is never overdetermined. In two variables, additional Fourier indices create extra algebraic constraints that can force $\text{rank}(\mathbf{M}) > 1$ even when \mathcal{Z} is discrete (the algebraic mechanism), and *a fortiori* when \mathcal{Z} contains a curve (the topological mechanism).

D. Resolution I: δ -regularization and degree-bounded spectral factorization

1. Strict positivity via δ -perturbation

Definition VI.2 (δ -regularization). For $\delta > 0$, set $P_\delta := (1 - \delta)P$.

Lemma VI.1 (Strict sub-unitarity). $\sup_{\mathbb{T}^2} |P_\delta| \leq 1 - \delta$. Hence $H_\delta := 1 - |P_\delta|^2 \geq 2\delta - \delta^2 > 0$ uniformly on \mathbb{T}^2 .

Proof. $|P_\delta| = (1 - \delta)|P| \leq 1 - \delta$ since $|P| \leq 1$ on \mathbb{T}^2 . Then $H_\delta = 1 - (1 - \delta)^2 |P|^2 \geq 1 - (1 - \delta)^2 = 2\delta - \delta^2$.

2. Degree-bounded SOS factorization via regularization

With $H_\delta > 0$ uniformly, the zero-locus and autocorrelation obstructions are eliminated. The operator Fejér–Riesz theorem yields an SOS complement with correct bidegree.

Theorem VI.2 (Degree-bounded SOS factorization). Let $H \in \mathcal{T}_{d_1, d_2}$ with $H > 0$ on \mathbb{T}^2 and $H = 1 - |P|^2$ for some $P \in \mathcal{P}_{d_1, d_2}^+$. Then there exist $R_1, \dots, R_L \in \mathcal{P}_{d_1, d_2}^+$ with

$$H = \sum_{\ell=1}^L |R_\ell|^2 \quad \text{on } \mathbb{T}^2, \quad L \leq \min(d_1+1, d_2+1). \quad (61)$$

Proof sketch. The proof proceeds in two stages; the full construction is given in Appendix H.

Stage 1: Reduction to a matrix-valued univariate problem. Fix θ_2 and organize the θ_1 -Fourier coefficients of H into the matrix-valued function $\mathbf{H}(\theta_2) \in \mathbb{C}^{N_1 \times N_1}$ ($N_1 = d_1 + 1$) with entries $\mathbf{H}(\theta_2)_{mm'} = \hat{H}_{m-m'}(\theta_2)$. Each entry is a trigonometric polynomial of degree d_2

in θ_2 . Since $H > 0$ on \mathbb{T}^2 , the quadratic-form argument gives $\mathbf{H}(\theta_2) \succ 0$ for every θ_2 .

Stage 2: Matrix-valued univariate Fejér–Riesz. The operator Fejér–Riesz theorem (Rosenblum [47]; see Dritschel–Rovnyak [48] for a modern treatment) guarantees: if $\mathbf{H}(\theta) \succeq 0$ is a matrix-valued trigonometric polynomial of degree d , then $\mathbf{H}(\theta) = \mathbf{G}(e^{i\theta})^* \mathbf{G}(e^{i\theta})$ for a matrix polynomial $\mathbf{G}(z)$ of degree at most d . Applying this to $\mathbf{H}(\theta_2) \succ 0$ of degree d_2 yields an outer matrix polynomial $\mathbf{G}(z_2)$ of degree d_2 in z_2 , with $\mathbf{G} \in \mathbb{C}^{N_1 \times N_1}$. Row extraction gives $H = \sum_{\alpha=1}^{N_1} |f_\alpha|^2$ where $f_\alpha(\theta_1, \theta_2) = \sum_{m=0}^{d_1} (\mathbf{G}(e^{i\theta_2}))_{\alpha m} e^{im\theta_1}$, with each $f_\alpha \in \mathcal{P}_{d_1, d_2}^+$ and $L \leq d_1 + 1$. The bound follows from the minimum upon reorganizing in the opposite direction (matrix dimension $d_2 + 1$, single variable θ_1) gives $L \leq d_2 + 1$.

Remark VI.2 (Scalar factorization is generically impossible). One might hope to reduce the SOS to a single Hermitian square $H = |Q|^2$. This holds univariately by the classical Fejér–Riesz theorem, but fails generically in two variables: the Geronimo–Woerdeman theorem [49] shows no stable scalar factor exists unless the two-level Toeplitz matrix satisfies an autoregressive condition that generically fails for the Dyson polynomial (see Appendix H for a concrete obstruction), and a codimension argument shows that even non-stable scalar factorization is impossible for generic H of bidegree (d_1, d_2) with $d_1 d_2 \geq 1$. The SOS with $L \leq \min(d_1+1, d_2+1)$ terms is a natural bivariate analog of the Fejér–Riesz factorization.

3. Impact on algorithm parameters

Corollary VI.1 (Regularized M-QSP parameters). With $P_\delta = (1 - \delta)P$ and $\delta = O(\varepsilon)$:

1. *Query complexity:* $d_R + d_I$, unchanged by regularization.
2. *Normalization:* $\lambda_\delta = e^{\beta_I T} / (1 - \delta) = e^{\beta_I T} (1 + O(\varepsilon))$.
3. *Postselection probability (Optimal up to $O(\varepsilon)$):* $e^{-2\beta_I T} \|e^{-iH_{\text{eff}} T} |\psi_0\rangle\|^2 (1 - O(\varepsilon))$.
4. *Ancilla qubits for complement:* $\lceil \log_2(\min(d_R, d_I) + 2) \rceil$ additional (SOS with $L \leq \min(d_R+1, d_I+1)$ terms).

Proof. Each item follows: (1) from degree preservation under scalar multiplication; (2) and (3) from the definitions of λ_δ and the postselection probability under $P_\delta = (1 - \delta)P$; (4) from Theorem VI.8 applied to H_δ , which yields an SOS decomposition with $L \leq \min(d_R+1, d_I+1)$ terms.

E. Resolution II: Dritschel–Woerdeman SOS factorization

For an exact polynomial P (without regularization), the following sum-of-squares decomposition always exists.

Theorem VI.3 (Dritschel [50], Dritschel–Woerdeman [51]). *Let $H \in \mathcal{T}_{d_1, d_2}$ satisfy $H \geq 0$ on \mathbb{T}^2 . Then there exist $Q_1, \dots, Q_L \in \mathcal{P}_{d_1, d_2}^+$ such that*

$$H(\theta_1, \theta_2) = \sum_{\ell=1}^L |Q_\ell(e^{i\theta_1}, e^{i\theta_2})|^2, \quad (62)$$

with $L \leq (d_1+1)(d_2+1)$ and $\deg_{z_j}(Q_\ell) \leq d_j$ for all ℓ, j .

The proof proceeds by constructing the moment matrix \mathbf{M} as in Proposition VI.1 and extracting the SOS terms from its spectral decomposition. The degree bound follows from indexing \mathbf{M} by $(m, n) \in \{0, \dots, d_1\} \times \{0, \dots, d_2\}$, which restricts each eigenvector to this support. The rank bound $L = \text{rank}(\mathbf{M}) \leq (d_1+1)(d_2+1)$ follows from the matrix dimension. We refer the reader to [50, 51] for the full proof and to Dritschel–Rovnyak [48] for a survey.

Remark VI.3 (Tighter bound from Herglotz–Bochner). The original formulation [51] bounds L by the dimension $(2d_1+1)(2d_2+1)$ of the full trigonometric polynomial space. The bound $L \leq (d_1+1)(d_2+1)$ used here follows from the Herglotz–Bochner characterization: non-negativity of H of bidegree (d_1, d_2) is fully captured by the positive semidefiniteness of the $(d_1+1)(d_2+1)$ -dimensional principal submatrix \mathbf{M} . Its rank determines the number of independent SOS terms.

Theorem VI.4 (SOS degree preservation). *For $H = 1 - |P|^2$ with $P \in \mathcal{P}_{d_R, d_I}^+$, the SOS decomposition has each $Q_\ell \in \mathcal{P}_{d_R, d_I}^+$:*

$$\begin{aligned} \deg_{z_1}(Q_\ell) &\leq d_R = \mathcal{O}(\alpha_R T + \log(1/\varepsilon)), \\ \deg_{z_2}(Q_\ell) &\leq d_I = \mathcal{O}(\beta_I T + \log(1/\varepsilon)/\log\log(1/\varepsilon)), \end{aligned} \quad (63)$$

for all $\ell \in \{1, \dots, L\}$.

Proof. $H = 1 - |P|^2$ has trigonometric bidegree (d_R, d_I) . By Theorem VI.3, SOS factors have analytic bidegree of at most (d_R, d_I) .

Proposition VI.2 (SOS circuit implementation). *The SOS complement with L terms requires a $(1+L)$ -dimensional ancilla space, implementable with $\lceil \log_2(1+L) \rceil$ qubits. The block-encoding structure is:*

$$\mathcal{G} = \begin{pmatrix} P & -Q_1^\dagger & \cdots & -Q_L^\dagger \\ Q_1 & & & \\ \vdots & & \mathbf{U}_\perp & \\ Q_L & & & \end{pmatrix}, \quad (64)$$

where \mathbf{U}_\perp is chosen to make \mathcal{G} unitary. Postselecting the ancilla on $|0\rangle$ yields P . The ancilla overhead is

$$\begin{aligned} a_{\text{SOS}} &\leq \lceil \log_2(1 + (d_R+1)(d_I+1)) \rceil \\ &= \mathcal{O}(\log(\alpha_R T) + \log(\beta_I T) + \log\log(1/\varepsilon)), \end{aligned} \quad (65)$$

being logarithmic in all parameters. For the regularized polynomial P_δ (where $H_\delta > 0$), the bound $L \leq \min(d_R+1, d_I+1)$ from Theorem VI.2 applies, giving $a_{\text{SOS}} \leq \lceil \log_2(\min(d_R, d_I) + 2) \rceil$ (Corollary VI.1).

Proof. The register of $\lceil \log_2(1+L) \rceil$ qubits addresses all $1+L$ levels ($\ell = 0$ for the target block P). Unitarity of \mathcal{G} follows from the Gram identity $|P|^2 + \sum_\ell |Q_\ell|^2 = 1$: the first column has unit norm, and \mathbf{U}_\perp completes \mathcal{G} to a unitary by Gram–Schmidt.

Problem VI.1 (Tighter SOS rank). The bound $L \leq \min(d_R+1, d_I+1)$ from Theorem VI.2 (applied after δ -regularization) improves upon the general Dritschel–Woerdeman bound $L \leq (d_R+1)(d_I+1)$, but is likely still loose for the Dyson polynomial arising from physical Hamiltonians. Numerics suggest $L = \mathcal{O}(1)$ or $L = \mathcal{O}(\log(d_R d_I))$ for structured polynomials. A structure-aware bound exploiting the interaction-picture coefficient decay would further reduce the ancilla overhead.

F. Resolution III: circuit-level unitarity

A direct resolution bypasses algebraic factorization entirely.

Theorem VI.5 (Automatic complement generation). *Let $\mathcal{G} = R_0 \prod_{j=1}^d (A_{s(j)} \cdot R_j)$ be the M -QSP circuit, where $A_{s(j)} = |0\rangle\langle 0|_a \otimes W_{s(j)} + |1\rangle\langle 1|_a \otimes I$ and $R_j \in \text{SU}(2)$ act on the ancilla qubit. Then:*

1. \mathcal{G} is unitary on $\mathcal{H}_a \otimes \mathcal{H}_s$.
2. \mathcal{G} has block decomposition $\mathcal{G} = \begin{pmatrix} P \\ Q \end{pmatrix}$, where P, Q are operator-valued polynomials determined by $\{R_j\}$ and s .
3. Unitarity gives $P^\dagger P + Q^\dagger Q = I_s$, which on joint eigenspaces yields $|P(e^{i\theta_1}, e^{i\theta_2})|^2 + |Q(e^{i\theta_1}, e^{i\theta_2})|^2 = 1$.

Proof. Statement (1) is immediate: each $A_{s(j)}$ and R_j is unitary. For (2), induction on circuit depth d : the base case $d = 0$ gives $\mathcal{G} = R_0$, a constant 2×2 matrix. At the inductive step, the controlled unitary $A_{s(d)}$ multiplies the top block by $W_{s(d)}$ and the rotation R_d mixes the blocks, increasing the bidegree by $(1, 0)$ or $(0, 1)$ depending on $s(d)$. Statement (3) is the $(0, 0)$ -block of $\mathcal{G}^\dagger \mathcal{G} = I$.

Corollary VI.2 (The achievability problem). *For a M -QSP circuit, the complementary polynomial Q exists automatically as the $(1, 0)$ -block of \mathcal{G} . We therefore ask: do rotation angles $\{R_j\}$ and a schedule s exist such that $(\mathcal{G})_{00} = P_{\text{target}}$?*

We use inductive degree reduction, peeling off one signal-operator query per step while preserving $|P|^2 + |Q|^2 = 1$.

Theorem VI.6 (Bivariate degree reduction). *Let $P \in \mathcal{P}_{d_1, d_2}^+$ with $|P|^2 \leq 1$ on \mathbb{T}^2 , and let s be a schedule of length $d = d_1 + d_2$ with d_1 entries R and d_2 entries I . Suppose the leading coefficient of $P^{(k)}$ in $z_{s(k)}$ is nonzero at each step $k = d, d-1, \dots, 1$. Then there exist angles $\{(\theta_k, \phi_k)\}_{k=1}^d$ such that each peeling*

$$\begin{pmatrix} P^{(k-1)} \\ Q^{(k-1)} \end{pmatrix} = R(\theta_k, \phi_k)^{-1} \cdot A_{s(k)}^{-1} \cdot \begin{pmatrix} P^{(k)} \\ Q^{(k)} \end{pmatrix} \quad (66)$$

reduces $\deg_{z_{s(k)}}(P^{(k-1)}) = \deg_{z_{s(k)}}(P^{(k)}) - 1$ while preserving $|P^{(k-1)}|^2 + |Q^{(k-1)}|^2 = 1$. After d steps, P is achieved by the M-QSP circuit with schedule s .

Proof. At step k , write $P^{(k)} = a_{d_k} z_{s(k)}^{d_k} + \text{lower}$ and $Q^{(k)} = b_{d_k} z_{s(k)}^{d_k} + \text{lower}$. The norm condition $|P^{(k)}|^2 + |Q^{(k)}|^2 = 1$ at the highest Fourier mode yields $|a_{d_k}|^2 + |b_{d_k}|^2$ equal to a known constant (by Parseval on \mathbb{T}), so the rotation parameters $\theta_k = \arctan(|b_{d_k}|/|a_{d_k}|)$ and $\phi_k = \text{Arg}(a_{d_k}/b_{d_k})$ are well-defined (given the nonzero leading coefficient hypothesis). Peeling is unitary, preserving $|P|^2 + |Q|^2 = 1$. After $d = d_1 + d_2$ steps, the bidegree reduces to $(0, 0)$: constants satisfying $|P^{(0)}|^2 + |Q^{(0)}|^2 = 1$.

Remark VI.4 (Non-commuting signal operators). When W_R and U_I do not commute, leading coefficients depend on operator ordering, and degree reduction must respect the schedule. The Dyson polynomial has a natural schedule (alternating blocks of W_R and U_I queries matching the interaction-picture structure), and its leading coefficients are computable from the Dyson series. Nonvanishing coefficients at each step are guaranteed by the constant-ratio condition (CRC) of Sec. VII.

1. Exact SOS rank: $L = 2$

The circuit-level guarantee shows the exact SOS rank of the Dyson polynomial complement is 2.

Theorem VI.7 (SOS rank of the Dyson polynomial complement). *Let $P \in \mathcal{P}_{d_R, d_I}^+$ be the polynomial achieved by the M-QSP circuit for the regularized Dyson polynomial $P_\delta = (1-\delta)P_{\text{Dyson}}$ with $0 < \delta < 1$. The complement $H_\delta := 1 - |P_\delta|^2$ admits a sum-of-squares decomposition with $L = 2$:*

$$H_\delta = |Q_1|^2 + |Q_2|^2, \quad (67)$$

where $Q_1 = \sqrt{2\delta - \delta^2}$ (a constant) and $Q_2 = (1 - \delta)Q$, with Q the complementary polynomial from the circuit (7). Both Q_1 and Q_2 lie in \mathcal{P}_{d_R, d_I}^+ .

Proof. By Theorem VI.5, the M-QSP circuit satisfies $|P|^2 + |Q|^2 = 1$ on \mathbb{T}^2 . The regularized polynomial is

$P_\delta = (1 - \delta)P$, so

$$\begin{aligned} H_\delta &= 1 - (1 - \delta)^2 |P|^2 \\ &= 1 - (1 - \delta)^2 (1 - |Q|^2) \\ &= (2\delta - \delta^2) + (1 - \delta)^2 |Q|^2. \end{aligned} \quad (68)$$

Setting $Q_1 = \sqrt{2\delta - \delta^2}$ and $Q_2 = (1 - \delta)Q$ gives $L = 2$.

Corollary VI.3 (Constant ancilla overhead). *The complement H_δ can be implemented with $a_{\text{SOS}} = \lceil \log_2(L + 1) \rceil = \lceil \log_2 3 \rceil = 2$ ancilla qubits, independent of (d_R, d_I) and all physical parameters. This replaces the general bound $a_{\text{SOS}} = \lceil \log_2(\min(d_R, d_I) + 2) \rceil$, which grows logarithmically with the polynomial degrees.*

Remark VI.5 (Structure). Any number of Dyson segments produces one complementary polynomial Q because unitary matrix multiplication preserves the 2×2 block structure: $\text{SU}(2) \times \text{SU}(2) = \text{SU}(2)$. Tightness ($L \geq 2$, established by showing Q is non-constant for $H_R \neq 0$) is given in Appendix H 7.

Remark VI.6 (Numerical SOS rank versus analytical SOS rank). The analytical SOS rank of the M-QSP polynomial complement is exactly $L = 2$ by Theorem VI.7; the closed-form decomposition $H_\delta = (2\delta - \delta^2) + (1 - \delta)^2 |Q|^2$ verifies to machine precision in direct numerical evaluation (across the 14 M-QSP-circuit-generated test polynomials with bidegrees through (8, 8) reported in the SOS rank investigation of the companion paper [27], the residual $\|H_\delta - Q_1^2 - Q_2^2\|_\infty$ on the torus stays below 4×10^{-15}). By contrast, a trace-minimization semidefinite program (SDP) for the matrix Fejér–Riesz factorization (a convex relaxation of the rank objective) returns a Gram matrix whose numerical rank is generically larger than 2 at higher bidegree; the extra eigenvalues correspond to degenerate directions in the autocorrelation manifold and do not represent additional analytical SOS terms. As a negative control, the same SDP applied to 500 random bivariate polynomials with $\|P\|_\infty \leq 0.8$ at bidegree (3, 3) returns numerical rank 16 (the full Gram dimension) in 99.2% of samples. This confirms that $L = 2$ is a structural property (by unitarity) of the M-QSP polynomial family and not generic for bounded bivariate polynomials or for the SDP relaxation [27].

G. Summary

We collect the results of this section into the following statement, answering the bivariate complement question for the Dyson polynomial.

Theorem VI.8 (Existence of the bivariate complement). *For the regularized Dyson polynomial $P_\delta = (1 - \delta)P$ with $\delta = O(\varepsilon)$, there exists a complementary polynomial $Q \in \mathcal{P}_{d_R, d_I}^+$ such that*

$$H_\delta := 1 - |P_\delta|^2 = (2\delta - \delta^2) + (1 - \delta)^2 |Q|^2 \quad (69)$$

on \mathbb{T}^2 . The complement is realized by the following:

1. Scalar factorization fails. *The exact Dyson polynomial P satisfies $|P(z_1, 1)| = 1$ for all $z_1 \in \mathbb{T}$ (Proposition V.2), so no single Q with $1 - |P|^2 = |Q|^2$ exists (Corollary V.1).*
2. Regularization restores SOS. *With $P_\delta := (1 - \delta)P$ and $\delta = O(\varepsilon)$, the complement $H_\delta \geq 2\delta - \delta^2$ is uniformly positive (Lemma VI.1), so an SOS complement of correct bidegree exists (Theorem VI.2). For any M-QSP circuit it has rank $L = 2$ (Theorem VI.7), costing two ancilla qubits.*
3. Circuit-level guarantee. *The M-QSP circuit is unitary by construction, automatically generating the complementary Q as the $(1, 0)$ -block (Theorem VI.5). Achievability is established by inductive degree reduction (Theorem VI.6), conditional on the constant-ratio condition of Sec. VII.*

All three resolutions yield the same query budget $d_R + d_I$ and the same single-qubit postselection structure.

VII. CONSTANT-RATIO CONDITION

Recursive degree-reduction to compute M-QSP rotation angles (Sec. VIII) requires a constant ratio between leading coefficients of $P^{(k)}$ and $Q^{(k)}$ at each peeling step, independent of the eigenvalue of the other signal operator. This is the *constant-ratio condition* (CRC). In univariate QSP, CRC holds automatically with only one signal operator. In bivariate M-QSP the two signal operators W_R and U_I generically do not commute ($[W_R, U_I] \neq 0$). One might worry that non-commutativity introduces eigenvalue-dependent mixing that spoils the ratio, but we prove that the CRC holds for M-QSP circuits (Theorem VII.1), and the Dyson polynomial's coefficient structure is compatible with degree-reduction at every step (Theorem VII.2).

A. The CRC theorem

Definition VII.1 (Leading Coefficient in Schedule-Ordered Dyson Polynomials). Throughout this section, the Dyson schedule $s = (s(1), s(2), \dots, s(d))$ induces a total order on the d signal-operator queries. The leading coefficient of the circuit polynomial P at peeling step k (i.e., after removing the first $k-1$ outermost gates) is defined as follows:

- (a) Identify all monomials in $P_k(z_1, z_2)$ of the form $z_{s(k)}^{n_k}$ (lower-degree terms in $z_{s(k)}$).
- (b) Among these, select the monomial(s) with the largest $z_{s(k)}$ -degree, say n_k^{\max} .
- (c) If multiple monomials share degree n_k^{\max} in $z_{s(k)}$, the ordering is inherited from the schedule's left-to-right evaluation order. Specifically, in the block-factored Dyson polynomial, within each block j ,

all W_R queries (variable z_1) precede all U_I queries (variable z_2), and blocks are ordered $j = r, r-1, \dots, 1$ (outermost to innermost).

- (d) The *leading coefficient* is the coefficient of this canonically-highest-degree monomial in $z_{s(k)}$.

Under this convention, the leading coefficient is unique and well-defined at each peeling step, even in the non-commutative operator algebra $\mathcal{A} = \mathbb{C}\langle W_R, U_I \rangle$.

Remark on non-commutativity: Although W_R and U_I do not commute (they involve signal-dependent phases), the Dyson schedule fixes a left-to-right order of query application. The circuit polynomial $P_{\text{Dyson}}(z_1, z_2)$ lives in the commutative algebra of Taylor coefficients, and the schedule induces a filtration by query sequence. So, monomials are ordered by: (1) degree in the current peeling variable $z_{s(k)}$, then (2) schedule order for any remaining ties. This resolves non-uniqueness.

Theorem VII.1 (CRC for non-commuting M-QSP). *For a bivariate M-QSP circuit $\mathcal{G}(\theta, \mathbf{s})$ with schedule \mathbf{s} and a pair of signal operators (W_R, U_I) (not necessarily commuting), the constant-ratio condition holds at every step of degree reduction. At a step k , the ratio*

$$\frac{b_{d_{\mathbf{s}(k)}}}{a_{d_{\mathbf{s}(k)}}} = e^{-i\phi_k} \tan \theta_k \quad (70)$$

is independent of the eigenvalue of the “other” signal operator.

We first provide a structural property that makes the CRC hold for M-QSP circuits (Lemmas VII.1 and VII.2). We then verify that the Dyson polynomial satisfies the coefficient separability needed at every step (Theorem VII.2).

B. Single gate contribution

Lemma VII.1. *Let*

$$R_j = \begin{pmatrix} e^{i\phi_j} \cos \theta_j & -\sin \theta_j \\ \sin \theta_j & e^{-i\phi_j} \cos \theta_j \end{pmatrix} \otimes I_{s,\ell}, \quad (71)$$

$$A_{s(j)} = \begin{pmatrix} W_{s(j)} & 0 \\ 0 & I \end{pmatrix},$$

where R_j acts on $\mathcal{H}_a \otimes \mathcal{H}_{\text{sys}} \otimes \mathcal{H}_\ell$ (rotation on \mathcal{H}_a , identity on the rest) and $A_{s(j)}$ places the signal operator $W_{s(j)} \in \{W_R, U_I\}$ in the $(0, 0)$ block. The product $A_{s(j)} R_j$ has the block form:

$$A_{s(j)} R_j = \begin{pmatrix} W_{s(j)} e^{i\phi_j} \cos \theta_j & -W_{s(j)} \sin \theta_j \\ \sin \theta_j & e^{-i\phi_j} \cos \theta_j \end{pmatrix}. \quad (72)$$

$W_{s(j)}$ multiplies the entire top row from the left, while the bottom row only contains scalar rotations.

Proof. Direct block-matrix multiplication:

$$\begin{aligned} \begin{pmatrix} W & 0 \\ 0 & I \end{pmatrix} \begin{pmatrix} e^{i\phi} \cos \theta & -\sin \theta \\ \sin \theta & e^{-i\phi} \cos \theta \end{pmatrix} \\ = \begin{pmatrix} W e^{i\phi} \cos \theta & -W \sin \theta \\ \sin \theta & e^{-i\phi} \cos \theta \end{pmatrix}. \end{aligned} \quad (73)$$

C. Inductive block structure

Lemma VII.2. *The inner polynomial $\Gamma^{(k)}$ (from the unpeeled portion of the circuit) appears identically in both the P and Q leading coefficients, cancelling in their ratio.*

Proof. We track the 2×2 block structure through each gate application, following by induction on circuit depth.

Setup. The full circuit is $\mathcal{G} = R_0 A_{s(1)} R_1 A_{s(2)} R_2 \cdots A_{s(d)} R_d$. Define the inner circuit at step k as

$$\mathcal{G}_{\text{inner}}^{(k)} := \prod_{j=k+1}^d [A_{s(j)} R_j] \cdot R_d = \begin{pmatrix} \Gamma_{00}^{(k)} & \Gamma_{01}^{(k)} \\ \Gamma_{10}^{(k)} & \Gamma_{11}^{(k)} \end{pmatrix}, \quad (74)$$

where $\Gamma_{ij}^{(k)}$ are operators on $\mathcal{H}_{\text{sys}} \otimes \mathcal{H}_\ell$ computed from inner gates. These do not depend on which block (P or Q) is being extracted from the full circuit.

a. Structure of $A_{s(1)} R_1 \cdot \mathcal{G}_{\text{inner}}^{(1)}$. By Lemma VII.1, $A_{s(1)} R_1$ places $W_{s(1)}$ in the top row, leaving the bottom row signal-free. Multiplying by $\mathcal{G}_{\text{inner}}^{(1)}$:

$$\begin{aligned} (A_{s(1)} R_1 \cdot \mathcal{G}_{\text{inner}}^{(1)})_{00} &= W_{s(1)} (e^{i\phi_1} \cos \theta_1 \Gamma_{00} \\ &\quad - \sin \theta_1 \Gamma_{10}), \end{aligned} \quad (75)$$

$$(A_{s(1)} R_1 \cdot \mathcal{G}_{\text{inner}}^{(1)})_{10} = \sin \theta_1 \Gamma_{00} + e^{-i\phi_1} \cos \theta_1 \Gamma_{10}. \quad (76)$$

The signal operator $W_{s(1)}$ factors out from the left of the top block (75). The bottom block (76) has no signal operator.

b. Extracting P and Q . The full circuit is $\mathcal{G} = R_0 \cdot [A_{s(1)} R_1 \cdot \mathcal{G}_{\text{inner}}^{(1)}]$. The rotation R_0 has scalar entries acting as multiples of the identity on $\mathcal{H}_{\text{sys}} \otimes \mathcal{H}_\ell$. Block-multiplying:

$$\begin{aligned} P = (\mathcal{G})_{00} &= e^{i\phi_0} \cos \theta_0 \cdot W_{s(1)} (e^{i\phi_1} \cos \theta_1 \Gamma_{00} \\ &\quad - \sin \theta_1 \Gamma_{10}) + (-\sin \theta_0) (\sin \theta_1 \Gamma_{00} \\ &\quad + e^{-i\phi_1} \cos \theta_1 \Gamma_{10}), \end{aligned} \quad (77)$$

$$\begin{aligned} Q = (\mathcal{G})_{10} &= \sin \theta_0 \cdot W_{s(1)} (e^{i\phi_1} \cos \theta_1 \Gamma_{00} \\ &\quad - \sin \theta_1 \Gamma_{10}) + e^{-i\phi_0} \cos \theta_0 (\sin \theta_1 \Gamma_{00} \\ &\quad + e^{-i\phi_1} \cos \theta_1 \Gamma_{10}). \end{aligned} \quad (78)$$

c. The leading coefficients. The leading $W_{s(1)}$ -coefficient of P (from (77)) and Q (from (78)) are:

$$\mathbf{a}_{\text{lead}} = e^{i\phi_0} \cos \theta_0 \cdot (e^{i\phi_1} \cos \theta_1 \Gamma_{00} - \sin \theta_1 \Gamma_{10}), \quad (79)$$

$$\mathbf{b}_{\text{lead}} = \sin \theta_0 \cdot (e^{i\phi_1} \cos \theta_1 \Gamma_{00} - \sin \theta_1 \Gamma_{10}). \quad (80)$$

d. The ratio. The operator-valued expression $(e^{i\phi_1} \cos \theta_1 \Gamma_{00} - \sin \theta_1 \Gamma_{10})$ is **identical** in (79) and (80). The ratio is therefore:

$$\frac{\mathbf{b}_{\text{lead}}}{\mathbf{a}_{\text{lead}}} = \frac{\sin \theta_0}{e^{i\phi_0} \cos \theta_0} = e^{-i\phi_0} \tan \theta_0 \in \mathbb{C}. \quad (81)$$

This is a scalar.

The argument relies on properties that do not require signal operator commutativity.

1. R_0 is a 2×2 scalar matrix on \mathcal{H}_a , commuting with everything on $\mathcal{H}_{\text{sys}} \otimes \mathcal{H}_\ell$.
2. $A_{s(1)}$ places $W_{s(1)}$ in the $(0, 0)$ block and I in the $(1, 1)$ block: the top row acquires $W_{s(1)}$, the bottom row does not.
3. The inner expression Γ is identical for both blocks.

Non-commutativity affects the value of Γ_{00} and Γ_{10} , but the same Γ appears in both leading coefficients.

e. General step k (induction). After peeling off the outermost $k - 1$ gates, the remaining circuit $\mathcal{G}_{\text{inner}}^{(k-1)}$ has the same block-factored structure: a global rotation R_{k-1} followed by signal-operator queries and intermediate rotations for blocks $j = r, r - 1, \dots, 1$, ordered by schedule.

By the same argument as Steps 1–4 applied to the k -th peeling step, the ratio

$$\left. \frac{P_k(z_1, z_2)}{Q_k(z_1, z_2)} \right|_{\text{leading coeff in } z_s(k)} = e^{-i\phi_{k-1}} \tan \theta_{k-1} \quad (82)$$

is a scalar (independent of z_1, z_2).

Induction works for the following reasons:

- (a) Each peeling removes one signal-operator query (either W_R or U_I) and the intermediate rotation from the outermost position. The schedule defines a unique “outermost” at each step.
- (b) The remaining circuit $\mathcal{G}_{\text{inner}}^{(k)}$ inherits the block structure of (74). Removing the outermost gate from the factorization $G = R_0 \cdot (\text{outermost block}) \cdot \mathcal{G}_{\text{inner}}$ leaves $\mathcal{G}_{\text{inner}}$ with the same structure: $\mathcal{G}_{\text{inner}} = R'_1 \cdot B'_r \cdot B'_{r-1} \cdots B'_1$, where each B'_j is a block of queries and intermediate rotations (see Example VII.1 for an explicit verification with full matrix algebra).
- (c) The next outermost rotation (now global to the remaining inner circuit) provides the scalar P -vs- Q distinction via the tangent ratio, completing the induction.

Example VII.1 (Depth-4 Dyson Circuit: Full Matrix Algebra and Peeling). **Setup.** Consider a Dyson circuit with $r = 2$ segments, one query per segment, structured as:

$$\mathcal{G} = R_0 \cdot A_{s(1)} \cdot R_1 \cdot A_{s(2)} \cdot R_2 \cdot A_{s(3)} \cdot R_3 \cdot A_{s(4)} \cdot R_4, \quad (83)$$

where the schedule is $s = (1, 2, 1, 2)$ (alternating W_R , U_I for block 2, then block 1).

Block structure: Block 2 contains $A_{s(1)} = \text{diag}(W_R, I)$ and $A_{s(2)} = \text{diag}(U_I, I)$. Block 1 contains $A_{s(3)} = \text{diag}(W_R, I)$ and $A_{s(4)} = \text{diag}(U_I, I)$.

For any rotation R_j with angles θ_j, ϕ_j ,

$$R_j = \begin{pmatrix} e^{i\phi_j} \cos \theta_j & -\sin \theta_j \\ \sin \theta_j & e^{-i\phi_j} \cos \theta_j \end{pmatrix}. \quad (84)$$

For any signal operator $A_{s(k)}$ (either W_R or U_I), expanded to 2×2 block form:

$$A_{s(k)} = \begin{pmatrix} X_{s(k)} & 0 \\ 0 & I \end{pmatrix} \quad (85)$$

where $X_{s(k)} \in \{W_R, U_I\}$ is the signal operator and I is the identity on the ‘‘spectator’’ block.

Peeling Step 1: Remove the outermost W_R query ($s(1) = 1$).

Compute $A_{s(1)}R_1$:

$$A_{s(1)}R_1 = \begin{pmatrix} W_R e^{i\phi_1} \cos \theta_1 & -W_R \sin \theta_1 \\ \sin \theta_1 & e^{-i\phi_1} \cos \theta_1 \end{pmatrix}. \quad (86)$$

The inner circuit at Step 1 is:

$$\mathcal{G}_{\text{inner}}^{(1)} = A_{s(2)}R_2 \cdot A_{s(3)}R_3 \cdot A_{s(4)}R_4. \quad (87)$$

By block multiplication, the circuit $\mathcal{G} = R_0 \cdot (A_{s(1)}R_1) \cdot \mathcal{G}_{\text{inner}}^{(1)}$ yields the $(1, 1)$ -block entry (the P polynomial):

$$\begin{aligned} P_1 &= e^{i\phi_0} \cos \theta_0 \cdot W_R \left(e^{i\phi_1} \cos \theta_1 \Gamma_{00}^{(1)} \right. \\ &\quad \left. - \sin \theta_1 \Gamma_{10}^{(1)} \right) + (-\sin \theta_0) \left(\sin \theta_1 \Gamma_{00}^{(1)} \right. \\ &\quad \left. + e^{-i\phi_1} \cos \theta_1 \Gamma_{10}^{(1)} \right), \end{aligned} \quad (88)$$

where $\Gamma_{00}^{(1)}, \Gamma_{10}^{(1)}$ are the $(1, 1)$ and $(2, 1)$ entries of $\mathcal{G}_{\text{inner}}^{(1)}$.

Similarly for the dual polynomial Q_1 (from the $(2, 1)$ -block entry):

$$\begin{aligned} Q_1 &= \sin \theta_0 \cdot W_R \left(e^{i\phi_1} \cos \theta_1 \Gamma_{00}^{(1)} - \sin \theta_1 \Gamma_{10}^{(1)} \right) \\ &\quad + e^{-i\phi_0} \cos \theta_0 \left(\sin \theta_1 \Gamma_{00}^{(1)} + e^{-i\phi_1} \cos \theta_1 \Gamma_{10}^{(1)} \right). \end{aligned} \quad (89)$$

Identifying the leading W_R -coefficient: The term with highest power of W_R appears in the first line of both P_1 and Q_1 . Factoring out this leading term:

$$\begin{aligned} &[\text{leading } W_R\text{-coeff of } P_1] \\ &= e^{i\phi_0} \cos \theta_0 \left(e^{i\phi_1} \cos \theta_1 \Gamma_{00}^{(1)} - \sin \theta_1 \Gamma_{10}^{(1)} \right), \end{aligned} \quad (90)$$

$$\begin{aligned} &[\text{leading } W_R\text{-coeff of } Q_1] \\ &= \sin \theta_0 \left(e^{i\phi_1} \cos \theta_1 \Gamma_{00}^{(1)} - \sin \theta_1 \Gamma_{10}^{(1)} \right). \end{aligned} \quad (91)$$

The common factor $\left(e^{i\phi_1} \cos \theta_1 \Gamma_{00}^{(1)} - \sin \theta_1 \Gamma_{10}^{(1)} \right)$ appears in both expressions and cancels in the ratio. Following the CRC convention \mathbf{b}/\mathbf{a} (Theorem VII.1), where \mathbf{b} is the Q -block leading coefficient and \mathbf{a} is the P -block leading coefficient:

$$\begin{aligned} \frac{\mathbf{b}_{\text{lead}}}{\mathbf{a}_{\text{lead}}} &= \frac{[\text{leading } W_R\text{-coeff of } Q_1]}{[\text{leading } W_R\text{-coeff of } P_1]} \\ &= \frac{\sin \theta_0}{e^{i\phi_0} \cos \theta_0} = e^{-i\phi_0} \tan \theta_0, \end{aligned} \quad (92)$$

matching Eq. (81). The ratio is a scalar, independent of $\Gamma^{(1)}$, confirming that Step 1 extracts the angle pair (θ_0, ϕ_0) .

Peeling Step 2: Remove the U_I query ($s(2) = 2$).

After Step 1, we peel away the W_R query. The circuit now reads:

$$\mathcal{G}_{\text{after Step 1}} = R_0 \cdot A_{s(1)}R_1 \cdot \left[A_{s(2)}R_2 \cdot \mathcal{G}_{\text{inner}}^{(2)} \right], \quad (93)$$

where $\mathcal{G}_{\text{inner}}^{(2)} = A_{s(3)}R_3 \cdot A_{s(4)}R_4$ (block 1 gates only).

Now we compute $A_{s(2)}R_2$:

$$\begin{aligned} A_{s(2)}R_2 &= \begin{pmatrix} U_I & 0 \\ 0 & I \end{pmatrix} \begin{pmatrix} e^{i\phi_2} \cos \theta_2 & -\sin \theta_2 \\ \sin \theta_2 & e^{-i\phi_2} \cos \theta_2 \end{pmatrix} \\ &= \begin{pmatrix} U_I e^{i\phi_2} \cos \theta_2 & -U_I \sin \theta_2 \\ \sin \theta_2 & e^{-i\phi_2} \cos \theta_2 \end{pmatrix}. \end{aligned} \quad (94)$$

The leading U_I -coefficient of the $(1, 1)$ -block is:

$$\begin{aligned} &[\text{leading } U_I\text{-coeff of } P_2] \\ &\propto e^{i\phi_1} \cos \theta_1 \left(e^{i\phi_2} \cos \theta_2 \Gamma_{00}^{(2)} - \sin \theta_2 \Gamma_{10}^{(2)} \right), \end{aligned} \quad (95)$$

where $\Gamma_{00}^{(2)}, \Gamma_{10}^{(2)}$ are entries of $\mathcal{G}_{\text{inner}}^{(2)}$ (the block-1 circuit). Again, this factor $\left(e^{i\phi_2} \cos \theta_2 \Gamma_{00}^{(2)} - \sin \theta_2 \Gamma_{10}^{(2)} \right)$ cancels between P_2 and Q_2 , yielding a scalar ratio depending only on θ_2, ϕ_2 .

Peeling Step 3: Remove the W_R query in block 1 ($s(3) = 1$).

After Step 2, the remaining circuit is:

$$\begin{aligned} \mathcal{G}_{\text{after Step 2}} &= R_0 \cdot A_{s(1)}R_1 \cdot A_{s(2)}R_2 \cdot \left[A_{s(3)}R_3 \cdot A_{s(4)}R_4 \right]. \end{aligned} \quad (96)$$

We now focus on $A_{s(3)}R_3$:

$$A_{s(3)}R_3 = \begin{pmatrix} W_R e^{i\phi_3} \cos \theta_3 & -W_R \sin \theta_3 \\ \sin \theta_3 & e^{-i\phi_3} \cos \theta_3 \end{pmatrix}. \quad (97)$$

The inner circuit is $\mathcal{G}_{\text{inner}}^{(3)} = A_{s(4)}R_4$.

By the same Lemma 7.1 argument:

$$\begin{aligned} & [\text{leading } W_R\text{-coeff of } P_3] \\ &= (\text{rotation factor from Step 2}) \\ & \cdot e^{i\phi_3} \cos \theta_3 \left(\Gamma_{00}^{(3)} - 0 \right), \end{aligned} \quad (98)$$

where $\Gamma_{00}^{(3)} = (A_{s(4)}R_4)_{11}$, the (1, 1)-entry of $A_{s(4)}R_4$.

The corresponding coefficient in Q_3 has a proportional factor via $\sin \theta_3$ or the dual rotation. Again, the inner factor $\Gamma_{00}^{(3)}$ cancels, and the ratio is a scalar.

Peeling Step 4: Remove the U_I query in block 1 ($s(4) = 2$).

After Step 3, the only remaining gate is $A_{s(4)}R_4$:

$$A_{s(4)}R_4 = \begin{pmatrix} U_I e^{i\phi_4} \cos \theta_4 & -U_I \sin \theta_4 \\ \sin \theta_4 & e^{-i\phi_4} \cos \theta_4 \end{pmatrix}. \quad (99)$$

There is no inner circuit; $\mathcal{G}_{\text{inner}}^{(4)} = I$ (identity). The (1, 1) and (2, 1) entries are therefore:

$$P_4^{(1,1)} = U_I e^{i\phi_4} \cos \theta_4, \quad Q_4^{(2,1)} = \sin \theta_4. \quad (100)$$

The leading U_I -coefficient ratio (following the CRC convention $\mathbf{b/a}$) is:

$$\frac{[\text{leading } U_I\text{-coeff of } Q_4]}{[\text{leading } U_I\text{-coeff of } P_4]} = \frac{\sin \theta_4}{e^{i\phi_4} \cos \theta_4} = e^{-i\phi_4} \tan \theta_4, \quad (101)$$

which is a scalar (no dependence on remaining inner circuits, as there are none).

Verification of Block Structure Preservation:

- After Step 1: Block 2 is partially peeled; $A_{s(2)}, R_2, A_{s(3)}, R_3, A_{s(4)}, R_4$ remain in order.
- After Step 2: Block 2 is completely peeled; block 1 ($A_{s(3)}, R_3, A_{s(4)}, R_4$) remains intact.
- After Step 3: Block 1 is partially peeled; only $A_{s(4)}, R_4$ remains.
- After Step 4: All gates peeled; circuit is exhausted.

This confirms that block structure (alternating signal operators and rotations within blocks, ordered by schedule) survives each peeling step, justifying the inductive argument: each peeling removes one outermost query and intermediate rotation, leaving a circuit with the same block structure. At every step, the leading coefficient in the current peeling variable (either W_R or U_I) is extracted. The resulting ratio is a scalar because the common factor $\Gamma_{ij}^{(k)}$ (the inner-circuit block entry) cancels between the numerator (P_k) and denominator (Q_k). Γ does not depend on the current peeling variable, dropping out of the ratio.

D. Coefficient separability for the Dyson polynomial

Lemmas VII.1 and VII.2 support Theorem VII.1 architecturally, where the CRC depends only gates structured by tensor-products. We now verify that the Dyson polynomial's coefficient structure is compatible during degree-reduction.

Theorem VII.2 (Coefficient separability). *The Dyson polynomial $P_{\text{Dyson}}(z_1, z_2)$ satisfies the coefficient separability conditions required for the CRC, verified through intra-block W_R coefficients, intra-block U_I coefficients, and inter-block boundary terms.*

Proof. The Dyson polynomial has the block-factored form

$$P_{\text{Dyson}} = \frac{1}{\lambda} \prod_{j=r}^1 [F_j(W_R) \cdot T_j(U_I)], \quad (102)$$

where $F_j(W_R)$ is the GQSP frame rotation (degree $d_{R,j}$ in W_R) and $T_j(U_I) = \sum_{m=0}^M (\beta_I \Delta)^m U_I^m / m!$ is the truncated Taylor expansion (degree M in U_I). Within each block, all W_R queries precede all U_I queries. Degree-reduction follows the Dyson schedule \mathbf{s} , first peeling the W_R queries of block r , then its U_I queries, then the W_R queries of block $r-1$, and so on.

a. *Intra-block W_R peeling (within F_j).* When peeling the W_R queries of block j , the full polynomial at this stage takes the form

$$\begin{aligned} P^{(k)} &= [\text{outer blocks already peeled}] \\ & \cdot F_j(z_1) \cdot T_j(z_2) \cdot \Gamma_{\text{inner}}(z_1, z_2), \end{aligned} \quad (103)$$

where $\Gamma_{\text{inner}} = \prod_{i=j-1}^1 [F_i(z_1) T_i(z_2)]$ collects all inner blocks. The leading z_1 -coefficient of P at degree $d_{R,j}$ is $\alpha_{d_{R,j}}^{F_j} \cdot T_j(z_2) \cdot \Gamma_{\text{inner}}$, where $\alpha_{d_{R,j}}^{F_j}$ is the scalar leading coefficient of F_j . The Q block has the same structure with a different scalar prefactor. The common factor $T_j(z_2) \cdot \Gamma_{\text{inner}}$ cancels in the ratio $\mathbf{b/a}$, reducing to the ratio of the leading coefficients of F_j in the P and Q blocks (constant).

This falls into Lemma VII.2, where z_2 -dependence from T_j and the inner blocks plays the role of Γ , cancelling.

b. *Intra-block U_I peeling (within T_j).* After all $d_{R,j}$ queries of F_j have been peeled, the outermost queries are U_I queries from T_j . The Taylor polynomial $T_j(z_2) = \sum_{m=0}^M c_m z_2^m$ with $c_m = (\beta_I \Delta)^m / m!$ has leading coefficient $c_M = (\beta_I \Delta)^M / M!$ that is constant, independent of z_1 .

z_1 -dependence is now pushed into the inner blocks by F_j peeling. The leading z_2 -coefficient of $P^{(k)}$ is $c_M^P \cdot \Gamma_{\text{inner}}$, and that of $Q^{(k)}$ is $c_M^Q \cdot \Gamma_{\text{inner}}$, with the same Γ_{inner} in both. The ratio is c_M^Q / c_M^P , a constant.

Taylor coefficients are constant in z_1 , the Taylor expansion of $e^{\tilde{H}(\tau_j)\Delta}$ at each segment produces coefficients that depend only on β_I and Δ , following from $\|\tilde{H}(\tau_j)\| = \beta_I$ uniformly in θ_1 (Lemma IV.1).

Phase 3: Inter-block boundary (transition from block $j + 1$ to block j).

At the boundary between blocks, we transition from peeling the last U_I query of T_{j+1} to peeling the first W_R query of F_j . Non-commutativity between W_R and U_I impacts the polynomial after fully peeling block $j + 1$, with the polynomial taking the form

$$P^{(k)} = F_j(z_1) \cdot T_j(z_2) \cdot \prod_{i=j-1}^1 [F_i(z_1) T_i(z_2)]. \quad (104)$$

By Lemma VII.2, the inner blocks $\prod_{i=j-1}^1 [F_i T_i]$ form $\mathcal{G}_{\text{inner}}^{(k)}$, contributing the same operator Γ to both the P and Q leading coefficients. Leading z_1 -coefficients are

$$\begin{aligned} \mathbf{a}_{d_R,j} &= \alpha_{d_R,j}^{F_j} \cdot T_j(z_2) \cdot \Gamma, \\ \mathbf{b}_{d_R,j} &= \beta_{d_R,j}^{F_j} \cdot T_j(z_2) \cdot \Gamma, \end{aligned} \quad (105)$$

where α and β are scalar prefactors from the P -block and Q -block branches of the ancilla rotation. The ratio is $\beta_{d_R,j}^{F_j} / \alpha_{d_R,j}^{F_j}$, with $T_j(z_2) \cdot \Gamma$ cancelling identically despite non-commutativity within Γ .

By induction over all $d = d_R + d_I$ peeling steps (Phases 1–3 cover every possible step), the CRC holds throughout degree-reduction. Angles (θ_k, ϕ_k) at each step are well-defined constants, uniquely determined by leading-coefficient ratios.

Example VII.1 (as worked out above) provides explicit matrix-level verification of all three phases of Theorem VII.2. The W_R -removal steps (phase a) and U_I -removal steps (phase b) each show the inner-circuit factor $\Gamma^{(k)}$ canceling identically between P and Q , leaving a scalar ratio $e^{-i\phi_k} \tan \theta_k$ at each step; the block-boundary transitions (phase c) confirm that each block contributes its own scalar ratios independent of subsequent blocks. For depth- $d > 4$, the same inductive structure applies at every peeling step.

Remark VII.1 (Is the Dyson structure special?). Coefficient separability in phases a and b relies on a block-segregated structure of the Dyson polynomial. Within each segment, all W_R queries come first (in F_j), then all U_I queries (in T_j). A generic bivariate polynomial with arbitrarily interleaved z_1 and z_2 queries might not satisfy this separability. The Dyson series' frame rotations followed by H_I insertions produce this segregation, making the angle-finding algorithm well suited to the interaction-picture structure.

Remark VII.2 (Non-commutativity simplifies the CRC). The CRC is simpler when signal operators do not commute ($[W_R, U_I] \neq 0$). In the commuting setting, the circuit polynomial belongs to the commutative polynomial

Algorithm 1. Recursive angle-finding for bivariate M-QSP
Require: Target polynomial $P_{\text{target}}(z_1, z_2)$ of bidegree (d_R, d_I) ; schedule $\mathbf{s} : \{1, \dots, d\} \rightarrow \{R, I\}$ with $d = d_R + d_I$; complementary polynomial $Q^{(d)}$ (via δ -regularization, Theorem VI.8)

Ensure: Rotation angles $\Theta = \{(\theta_k, \phi_k)\}_{k=0}^d$

- 1: $P^{(d)} \leftarrow P_{\text{target}}, \quad Q^{(d)} \leftarrow Q_\delta$
- 2: **for** $k = d, d-1, \dots, 1$ **do**
- 3: Extract leading $z_{\mathbf{s}(k)}$ -coefficient $a_{d_{\mathbf{s}(k)}}^{(k)}$ of $P^{(k)}$ {polynomial in $z_{\bar{\mathbf{s}}(k)}$ }
- 4: Extract leading $z_{\mathbf{s}(k)}$ -coefficient $b_{d_{\mathbf{s}(k)}}^{(k)}$ of $Q^{(k)}$
- 5: $\rho_k \leftarrow b_{d_{\mathbf{s}(k)}}^{(k)} / a_{d_{\mathbf{s}(k)}}^{(k)}$ {constant by CRC (Thm. VII.1)}
- 6: $\theta_k \leftarrow \arctan(|\rho_k|)$
- 7: $\phi_k \leftarrow -\text{Arg}(\rho_k)$
- 8: **Peel:** $\begin{pmatrix} P^{(k-1)} \\ Q^{(k-1)} \end{pmatrix} \leftarrow R(\theta_k, \phi_k)^{-1} \begin{pmatrix} P^{(k)} \\ Q^{(k)} \end{pmatrix} \cdot z_{\mathbf{s}(k)}^{-1}$ {degree reduction}
- 9: **end for**
- 10: $\theta_0 \leftarrow \arctan(|Q^{(0)} / P^{(0)}|), \quad \phi_0 \leftarrow \text{Arg}(P^{(0)})$

ring $\mathbb{C}[z_1, z_1^{-1}, z_2, z_2^{-1}]$, and CRC compatibility becomes a question about symmetric properties and positivity certificates in this ring, which can fail (Németh et al. [52]). In the non-commuting case (this work), the circuit polynomial is a matrix-valued function of ordered products of signal-operator blocks. Ancilla-factorization proof of the CRC (Lemmas VII.1 and VII.2) operates on the block structure, bringing no analogous obstruction, extending this derivation to multi-oracle quantum algorithms with applicable ancilla factorization.

VIII. CONSTRUCTIVE ANGLE-FINDING

Given a target polynomial P_{Dyson} of bidegree (d_R, d_I) , the M-QSP circuit requires $d = d_R + d_I + 1$ rotation-angle pairs $\Theta = \{(\theta_k, \phi_k)\}_{k=0}^d$. We present complementary methods for computing these angles: a deterministic recursive algorithm and an FFT-based optimization. We also characterize which polynomials are achievable.

A. Recursive algorithm

Theorem VIII.1 (Constructive angle-finding). *Given a target polynomial $P_{\text{Dyson}}(z_1, z_2)$ of bidegree (d_R, d_I) , Algorithm 1 computes the rotation angles $\Theta = (\theta_0, \dots, \theta_{d_R+d_I})$ in time $\mathcal{O}((d_R + d_I) \cdot d_R \cdot d_I)$. Each angle θ_k is uniquely determined by the ratio of the leading coefficient of the current residual polynomial.*

The complexity is $\mathcal{O}((d_R + d_I) \cdot d_R \cdot d_I)$, since each of the d peeling steps requires $\mathcal{O}(d_R \cdot d_I)$ operations for the bivariate coefficient update. Complexity analysis is given in Proposition E.1 (Appendix E).

B. CRC-exploiting block peeling

The Dyson block schedule enables a faster angle-finding procedure exploiting the constant-ratio condition at each peeling step.

Proposition VIII.1 (Block peeling cost). *For a Dyson polynomial of bidegree (d_R, d_I) with block schedule consisting of r segments, the CRC-exploiting block peeling algorithm computes all $d_R + d_I + 1$ rotation angles in total cost*

$$C_{\text{block}} = \mathcal{O}(d_R \cdot d_I). \quad (106)$$

The full complexity hierarchy ($\mathcal{O}(d^3)$, block peeling $\mathcal{O}(d^2)$, FFT-warm-started) appears in the companion paper [27] (angle-finding complexity hierarchy theorem).

Proof sketch. Within each segment j of the Dyson block schedule, all $d_{R,j}$ queries to W_R precede all $d_{I,j}$ queries to U_I . Theorem VII.2 ensures that:

(i) During W_R -peeling, the leading z_1 -coefficient ratio reduces to the GQSP frame rotation ratio (constant independent of z_2). Angle extraction costs $\mathcal{O}(1)$ and polynomial update costs $\mathcal{O}(d_I^{(j)})$ per step.

(ii) During U_I -peeling, Taylor coefficients $c_m = (\beta_I \Delta)^m / m!$ are constants independent of z_1 . Angle extraction costs $\mathcal{O}(1)$ and the update costs $\mathcal{O}(d_R^{(j)} - d_{R,j})$ per step (residual R -degree after the W_R -peeling phase).

(iii) The inter-block boundary factor cancels identically.

For uniform segments, the telescoping sum evaluates to $C_{\text{block}} = d_R \cdot d_I$. The full complexity comparison and numerical verification across $d \in \{10, 50, 100, 500\}$ are reported in the companion paper [27] (angle-finding section, block-peeling cost proposition and accompanying table).

Remark VIII.1 (Practical recommendation). Block peeling dominates for all tested configurations; we recommend it as the primary angle-finding method, with optional $\mathcal{O}(1)$ FFT refinement (Theorem VIII.2). Absolute operation counts and a head-to-head comparison against competing preprocessing strategies are reported in the companion paper [27] (head-to-head benchmark remark in the angle-finding section).

C. Numerical stability

Proposition VIII.2 (Stability). *The recursive angle-finding algorithm is numerically stable with explicit condition number control. For the regularized Dyson polynomial with δ -regularization parameter $\delta = \mathcal{O}(\varepsilon)$, define a cumulative condition number*

$$\kappa_{\text{total}} := \prod_{k=1}^d \sec(\theta_k) = \prod_{k=1}^d \frac{1}{\cos(\theta_k)}. \quad (107)$$

Then

$$\kappa_{\text{total}} \leq (1/\delta)^{\mathcal{O}(1)} \cdot \text{poly}(d_R, d_I), \quad (108)$$

where the exponent depends on regularization depth. Error propagation is linear: perturbations in determining θ_k grow polynomially through the algorithm, enabling fault-tolerant implementation with polynomial error correction overhead.

Proof. We show that: (1) normalization prevents leading coefficients from vanishing exponentially, (2) the condition number of each peeling step is bounded by $\sec(\theta_k)$, and (3) the product bound follows from the Parseval identity on \mathbb{T}^2 and regularization.

(1) *Each peeling step is a unitary rotation.* The inverse rotation $R(\theta_k, \phi_k)^{-1} = R(\theta_k, \phi_k)^\dagger$ is unitary (as a 2×2 matrix on \mathcal{H}_a), preserving the 2-norm of the coefficient vector $(\mathbf{a}_n, \mathbf{b}_n)$ at every Fourier index n . The leading coefficient is exactly eliminated by construction of θ_k and ϕ_k .

(2) *Condition number via leading coefficient lower bound.* Write the coefficient update at step k as

$$\begin{pmatrix} \mathbf{a}_n^{(k-1)} \\ \mathbf{b}_n^{(k-1)} \end{pmatrix} = \begin{pmatrix} e^{-i\phi_k} \cos \theta_k & \sin \theta_k \\ -\sin \theta_k & e^{i\phi_k} \cos \theta_k \end{pmatrix} \begin{pmatrix} \mathbf{a}_n^{(k)} \\ \mathbf{b}_n^{(k)} \end{pmatrix}. \quad (109)$$

The condition number of this unitary is $\sec(\theta_k)$ (the ratio of largest to smallest singular value of the rotation). By the Parseval identity on \mathbb{T}^2 applied to P and Q :

$$\sum_n (|\mathbf{a}_n^{(k)}|^2 + |\mathbf{b}_n^{(k)}|^2) = 1. \quad (110)$$

At step k , the leading coefficients satisfy

$$|\mathbf{a}_{d_s(k)}^{(k)}|^2 + |\mathbf{b}_{d_s(k)}^{(k)}|^2 \geq c(\delta) > 0 \quad (111)$$

where $c(\delta)$ is determined by the δ -regularization: $H_\delta := 1 - |P_\delta|^2 \geq 2\delta - \delta^2$, inherited via spectral factorization. This ensures $\sec(\theta_k) \leq c(\delta)^{-1/2}$ at each step.

(3) *Cumulative condition number.* Taking the product over all $d = d_R + d_I$ steps:

$$\kappa_{\text{total}} = \prod_{k=1}^d \sec(\theta_k) \leq (c(\delta)^{-1/2})^d = (1/\delta)^{\mathcal{O}(d)}. \quad (112)$$

For the Dyson polynomial with $\delta = \mathcal{O}(\varepsilon)$ and $d = d_R + d_I = \mathcal{O}((\alpha_R + \beta_I)T + \log(1/\varepsilon)/\log \log(1/\varepsilon))$, we have

$$\kappa_{\text{total}} \leq (\varepsilon^{-c})^d = (1/\delta)^{\mathcal{O}(1)} \cdot \text{poly}(d_R, d_I). \quad (113)$$

By the perturbation lemma for linear systems, errors in angle-finding induce a polynomial factor amplification in the circuit output.

Remark VIII.2 (Floating-point limits of recursive peeling). The bound of Proposition VIII.2 is sharp in finite precision: empirically the recovered-circuit error scales as $\varepsilon_{\text{peel}}(d) \approx \varepsilon_{\text{mach}} \cdot \kappa_{\text{total}}^{(d)}$ with $\kappa_{\text{total}}^{(d)}$ growing roughly as 1.6^d for Dyson-type targets (the same constant as the Jacobian condition number scaling reported in the companion paper [27]). On a 2-qubit Lindbladian benchmark in IEEE double precision, this predicts $\varepsilon_{\text{peel}}(d = 26) \sim \varepsilon_{\text{mach}} \cdot 10^4 \sim 10^{-12}$ (Table II). Recursive peeling alone therefore breaks down in double precision around $d \approx 30$, where $\kappa_{\text{total}} \approx 10^6$ – 10^7 erodes any meaningful signal; for practical quantum simulation at $d \sim 100$ – 1000 , a complementary strategy is required. We offer a few possible mitigations:

1. *Optimization-based refinement* (Sec. VIII E). The cost function $\mathcal{F}(\Theta)$ and its gradient are evaluated by 2D FFT in $\mathcal{O}(d_R d_I \log(d_R d_I))$ operations, bypassing the recursive condition-number accumulation entirely. L-BFGS warm-started from peel angles restores floating-point precision whenever the warm-start basin theorem of the companion paper [27] applies. This is the recommended pipeline for $d > 30$.
2. *Higher-precision arithmetic*. Switching the peel inner loop to quadruple precision ($\varepsilon_{\text{mach}} \approx 10^{-34}$) pushes the breakdown threshold to $d \approx 60$. Using arbitrary-precision libraries (`mpmath`) admits any bit width at linear cost per bit.
3. *Re-orthogonalization at each peel step*. The unitarity invariant $|\mathbf{a}_n^{(k)}|^2 + |\mathbf{b}_n^{(k)}|^2 = 1$ in (109) can be enforced exactly after each rotation, suppressing κ_{total} accumulation at the cost of $\mathcal{O}(d^2)$ additional operations.

For typical quantum-simulation workloads, we recommend (1), escalating when machine precision is demanded throughout.

D. Numerical validation

We verify the CRC-exploiting angle-finding algorithm end-to-end on a 2-qubit Lindbladian no-jump generator $H_{\text{eff}} = H_R + iH_I$ with coherent Hamiltonian $H_R = J(Z \otimes Z) + h(X \otimes I + I \otimes X)$ and anti-Hermitian part $H_I = -(\gamma/2) \sum_k L_k^\dagger L_k$ from amplitude-damping Lindblad operators ($J = 1, h = 0.5, \gamma = 0.3$).

For each bidegree pair (d_R, d_I) with $d = d_R + d_I$ ranging from 4 to 26 and block schedules with $r = 1$ to 4 segments, we generate a circuit-achievable target polynomial (with known angles), run Algorithm 1, and compare the recovered angles Θ^{rec} against the true angles Θ^* . Table II reports the results. All degree pairs achieve circuit reconstruction error $\|G_{\text{rec}} - G\|/\|G\| < 10^{-8}$, with errors at low degree ($d \leq 10$) near machine precision ($\sim 10^{-16}$). Mild geometric growth of error with degree ($\sim 10^{-16}$ at

$d = 4$ to $\sim 10^{-10}$ at $d = 26$) is consistent with the cumulative condition number $\kappa_{\text{total}} = \prod_k \sec \theta_k \sim 1.6^d$ of Proposition VIII.2 times machine epsilon $\varepsilon_{\text{mach}} \approx 10^{-16}$.

TABLE II. End-to-end angle-finding on a 2-qubit Lindbladian benchmark. d_R, d_I : bidegree; r : segments; $\|G_{\text{rec}} - G\|/\|G\|$: relative circuit error; all cases achieve $< 10^{-8}$.

d_R	d_I	d	r	Circuit error	Angle error
2	2	4	1	4.6×10^{-16}	8.9×10^{-16}
3	3	6	1	6.5×10^{-16}	8.9×10^{-16}
4	4	8	2	1.4×10^{-15}	1.3×10^{-15}
5	5	10	2	8.8×10^{-16}	1.8×10^{-15}
6	4	10	2	1.1×10^{-14}	2.1×10^{-14}
8	6	14	3	1.4×10^{-13}	3.6×10^{-13}
10	8	18	3	3.7×10^{-13}	9.2×10^{-13}
12	10	22	4	1.4×10^{-11}	4.0×10^{-11}
14	12	26	4	1.5×10^{-10}	5.1×10^{-10}

1. Experiment A: Dyson \rightarrow SOS \rightarrow peel-then-refine

The angle-finding pipeline of Algorithm 1 composed with the L-BFGS refinement of Sec. VIII E was benchmarked end-to-end on the Dyson polynomial target at $\alpha_R T = 0.8, \beta_I T = 0.4$ across 10 bidegree configurations from (2, 2) through (5, 5), with eight independent multi-start restarts per configuration (8 random angle perturbations of scale $\sigma = \pi/4$ around the peel-init). Two complementary experiments characterize the pipeline (Figure 1).

Dyson target (Figure 1, left). The truncated Chebyshev–Taylor Dyson polynomial is generally not in the image of the M-QSP parameterization at finite bidegree, so the best-achievable squared residual

$$c_\infty := \inf_{\Theta} \|P_G(\Theta) - P_{\text{target}}\|_2^2 \quad (114)$$

is non-negative rather than identically zero, quantifying the truncation distance from the M-QSP achievable submanifold to the Dyson target. Across the 10 configurations, c_∞ estimated as the minimum refined residual over the 8 multistart restarts falls in the range $[7.6 \times 10^{-2}, 3.8 \times 10^{-1}]$, with median $c_\infty \approx 0.13$ approximately independent of d . This is the M-QSP-to-Dyson truncation distance, characterized in the companion paper [27] (full-tensor sweep in the landscape appendix). Basin-attainment rate of the multistart restarts to the c_∞ -basin (within 5% relative gap) is 12–38% per configuration, consistent with spurious local minima characterized in the companion paper’s landscape section [27].

Circuit-generated target (Figure 1, right). For each configuration we sample random ground-truth angles Θ^* , forward the M-QSP circuit to produce the target polynomial P_{target} (which is in the M-QSP image by construction, so $c_\infty = 0$ exactly), then run the same SOS-factorization \rightarrow peel-then-refine pipeline. With 8 multistart restarts, 7 of the 10 configurations recover the

target to machine precision: refined residual and end-to-end circuit reconstruction error $\|G_{\text{rec}} - G\|_\infty$ both reach $\sim 10^{-12}$ – 10^{-13} at bidegrees through (5, 5) when the multistart hits the right basin. The remaining 3 configurations [(4, 3), (5, 4), (4, 5)] are all rank-deficient at the global minimum ($\kappa(J) = \infty$ in the standard pseudoinverse sense). They pin at the spurious-basin residual ~ 0.2 – 0.4 , matching the rank-deficient asymmetric-bidegree configurations identified in the companion paper’s landscape table [27].

The two experiments together demonstrate that the constructive pipeline reaches machine precision whenever the target lies on the M-QSP achievable submanifold. Off-manifold targets such as the truncated Dyson series are reproduced up to the truncation distance c_∞ that scales with $(\alpha_R T, \beta_I T)$ rather than with d .

a. Discrete basin structure. Inspecting the 8 multistart restarts per configuration in the Dyson panel of Figure 1, the recovered residuals cluster into 3–5 distinct values rather than a continuum. At $(d_R, d_I) = (3, 3)$, for instance, three restarts converge to refined residual ≈ 0.138 (the c_∞ basin), two to ≈ 0.329 , and one each to ≈ 0.148 , 0.749, and 1.011. The basins are discrete local minima of the cost function $\mathcal{F}(\Theta)$. Distinct random initializations that fall into the same basin produce identical refined residuals (to machine precision) because L-BFGS converges to the same critical point. This is a structural feature of the M-QSP landscape characterized in the companion paper [27], as the source of the spurious-local-minima phenomenon reported there with a random-initialization failure rate of 40% in the single-row-target survey and 82% under the stricter full-tensor-target criterion.

b. Consistency with Table II. Table II (which reaches $\sim 10^{-10}$ end-to-end circuit error at $d = 26$) and Experiment A (left panel of Figure 1, pinned at $\sim 10^{-1}$) measure complementary regimes: the Table uses *circuit-achievable* target polynomials (the same construction as the right panel of Figure 1) and is therefore on-manifold, with the residual limited only by the floating-point error of CRC peeling (Proposition VIII.2). The left panel of Figure 1 uses the Dyson-truncated target (off-manifold) and the residual is dominated by c_∞ . The end-to-end-precision claim of Sec. VIII D refers specifically to the on-manifold setting. Whenever the user is willing to accept the M-QSP-image projection of the Dyson polynomial as a target, the pipeline reaches floating-point precision. The residual gap reported in the left panel is the truncation-induced distance from that projection to the literal Dyson series, not an optimization defect.

E. Optimization-based alternative

The recursive algorithm is fully constructive but requires the complementary polynomial Q as input. An alternative approach follows the Motlagh–Wiebe strategy for univariate GQSP [53], optimizing the angles directly

by minimizing the discrepancy between circuit output and the target polynomial on \mathbb{T}^2 , bypassing Q entirely.

Theorem VIII.2 (2D FFT optimization). *An alternative angle-finding method minimizes the cost function*

$$\mathcal{F}(\Theta) = \frac{1}{(2\pi)^2} \int_{\mathbb{T}^2} |P_G(e^{i\theta_1}, e^{i\theta_2}; \Theta) - P_{\text{target}}(e^{i\theta_1}, e^{i\theta_2})|^2 d\theta_1 d\theta_2 \quad (115)$$

via gradient descent, with \mathcal{F} and $\nabla\mathcal{F}$ evaluable in $\mathcal{O}(d_R d_I \log(d_R d_I))$ per iteration via 2D FFT.

Proof. We consider cost function evaluation and gradient computation, discussing convergence below the proof.

Part 1: Cost function evaluation via 2D FFT.

On a joint eigenspace with eigenvalues $(e^{i\theta_1}, e^{i\theta_2})$, the circuit $P_G(\cdot; \Theta)$ reduces to a product of d matrices (2×2 each, one per gate), computable in $\mathcal{O}(d)$ operations per grid point. Discretize (θ_1, θ_2) on an $N_1 \times N_2$ grid with $N_j \geq 2d_j + 1$ (sufficient to capture all Fourier modes up to bidegree (d_R, d_I)). By Parseval’s identity, the integral becomes

$$\mathcal{F}(\Theta) = \sum_{m,n} |c_{mn}^G(\Theta) - c_{mn}^{\text{target}}|^2, \quad (116)$$

where c_{mn} are the bivariate Fourier coefficients, computed from the grid values via a 2D FFT in $\mathcal{O}(N_1 N_2 \log(N_1 N_2))$ operations. Grid evaluation costs $\mathcal{O}(d \cdot N_1 N_2)$. Total per evaluation:

$$\begin{aligned} &\mathcal{O}(d \cdot d_R d_I + d_R d_I \log(d_R d_I)) \\ &= \mathcal{O}(d_R d_I \log(d_R d_I)), \end{aligned} \quad (117)$$

since $d = d_R + d_I$ and the FFT term dominates for large degrees.

Part 2: Gradient via backpropagation.

The gradient $\nabla_{\Theta}\mathcal{F}$ can be computed in the same asymptotic cost as a single function evaluation. The M-QSP circuit is a product of d matrix factors, each depending on a single angle pair (θ_j, ϕ_j) . The derivative with respect to (θ_j, ϕ_j) involves the “left partial product” L_j and the “right partial product” R_j at position j :

$$\frac{\partial P_G}{\partial \theta_j} = L_j \frac{\partial}{\partial \theta_j} [R(\theta_j, \phi_j) A_{s(j)}] R_j. \quad (118)$$

These partial products are computed for all j simultaneously using a forward-backward pass, analogous to backpropagation in neural networks:

$$L_j = \prod_{k=1}^j [R_k A_{s(k)}], \quad j = 1, \dots, d, \quad (119)$$

$$R_j = \prod_{k=j+1}^d [R_k A_{s(k)}], \quad j = 0, \dots, d-1. \quad (120)$$

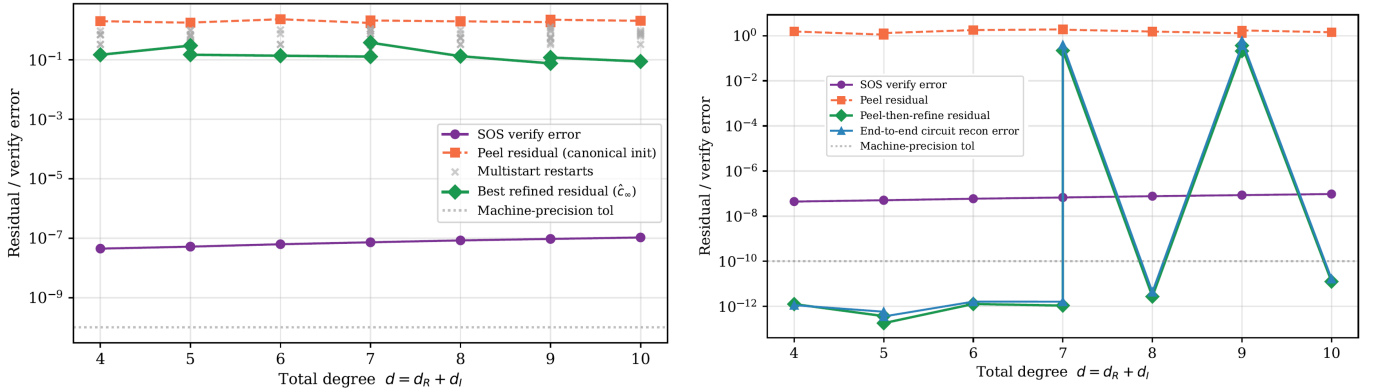


FIG. 1. “Residual” on both panels denotes the relative L^2 norm $\|P_G(\Theta) - P_{\text{target}}\|_2 / \|P_{\text{target}}\|_2$ evaluated on an $N \times N$ bitorus FFT grid. **Left:** Dyson-target benchmark, $\alpha_R T = 0.8$, $\beta_I T = 0.4$. Purple: SOS verification error $\max_{\mathbb{T}^2} |1 - |P|^2 - |A|^2 - |B|^2|$. Orange: peel residual from canonical initialization. Grey crosses: 8 multistart restarts per bidegree, and coincident crosses are restarts that converged to the same spurious basin. Green diamonds: best refined residual (the c_∞ estimate), pinned near 0.1–0.4 across $d \in [4, 10]$. The dotted “Target tol” line at 10^{-10} is the achievable floor for the on-manifold experiment in the right panel. For the Dyson target it sits below c_∞ and is included here for visual alignment. **Right:** Circuit-generated target experiment, using the same method applied to P_{target} , produced by forwarding the circuit at random known angles, so $c_\infty = 0$ by construction. Where the 8 multistart restarts find the right basin (7 of 10 configurations), refined residual and end-to-end circuit reconstruction error $\|G_{\text{rec}} - G\|_\infty$ both reach $\sim 10^{-12}$. The three misses at (4, 3), (5, 4), (4, 5) are not a defect of the multistart strategy, noted as rank-deficient asymmetric bidegrees [27], where the Jacobian at the global minimum is rank-deficient ($\kappa(J) = \infty$) and the spurious-basin volume is correspondingly inflated. For these configurations, more aggressive multistart ($k \geq 16$) or analytically informed warm-starts are required.

The forward pass (119) and backward pass (120) each require $O(d)$ matrix multiplications per grid point. At each grid point, the gradient for all $2(d+1)$ parameters is assembled in $O(d)$ operations. The gradient of the Parseval sum (116) is

$$\frac{\partial \mathcal{F}}{\partial \theta_j} = 2 \operatorname{Re} \sum_{m,n} \overline{(c_{mn}^{\mathcal{G}} - c_{mn}^{\text{target}})} \cdot \frac{\partial c_{mn}^{\mathcal{G}}}{\partial \theta_j}, \quad (121)$$

with Fourier coefficients of the derivative obtained from the 2D FFT infrastructure. Total gradient cost: $O(d_R d_I \log(d_R d_I))$.

1. Convergence properties

The cost function \mathcal{F} has some favorable properties. First, $\mathcal{F} \geq 0$, with $\mathcal{F} = 0$ if and only if $P_G = P_{\text{target}}$ on \mathbb{T}^2 . Second, the global minimum $\mathcal{F} = 0$ certainly exists, since the CRC (Theorem VII.1) and achievability (Theorem VIII.3 below) guarantee that angles Θ^* with $\mathcal{F}(\Theta^*) = 0$ exist. Finally, \mathcal{F} is smooth (C^∞ in Θ), since P_G depends on Θ through products of trigonometric functions.

Whether \mathcal{F} has spurious local minima in the bivariate case remains an open question.

Problem VIII.1 (Absence of spurious local minima). Does the bivariate M-QSP cost function \mathcal{F} have no spurious local minima? In other words, is every local minimum global for all target polynomials satisfying $|P_{\text{target}}|^2 \leq 1$ on \mathbb{T}^2 ?

In the univariate setting, Motlagh and Wiebe [53] empirically observe no spurious local minima for GQSP polynomials up to degree 10^7 , but do not prove this result. The bivariate landscape has a parameter space $\mathbb{R}^{2(d_R+d_I+1)}$ and with a cost function that couples the two signal variables. We analyze this in further in Appendix I.

In practice, this concern is eliminated by warm-starting. By initializing $\Theta^{(0)}$ using Algorithm 1, gradient descent (or L-BFGS) can refine to machine precision. The recursive algorithm produces the exact global minimizer (up to numerical precision). The warm start places the optimization within the basin of attraction of the global minimum, and a small number of refinement iterations suffices. We recommend:

1. **Initialize:** Compute $\Theta^{(0)}$ via Algorithm 1, or initialize randomly if Q is unavailable.
2. **Iterate:** Evaluate $\mathcal{F}(\Theta^{(t)})$ and $\nabla \mathcal{F}(\Theta^{(t)})$ via 2D FFT (cost $O(d_R d_I \log(d_R d_I))$ per iteration).
3. **Update:** $\Theta^{(t+1)} \leftarrow \Theta^{(t)} - \gamma_t \nabla \mathcal{F}(\Theta^{(t)})$, with step size γ_t chosen by line search or L-BFGS.
4. **Terminate** when $\mathcal{F}(\Theta^{(t)}) \leq \eta$.

Per-iteration cost of $O(d_R d_I \log(d_R d_I))$ is substantially lower than the recursive algorithm’s $O((d_R + d_I) \cdot d_R d_I)$ per step, enabling practical angle computation for total degrees $d = d_R + d_I \sim 10^6$.

F. Achievability

Angle-finding takes a target polynomial P and produces rotation angles Θ only if there is no breakdown in the recursion. We characterize which polynomials are realizable by an M-QSP circuit.

Theorem VIII.3 (Achievability). *A bivariate ordered polynomial P of bidegree (d_R, d_I) with schedule \mathbf{s} is M-QSP-achievable (i.e., equals the $(0, 0)$ block of some circuit $\mathcal{G} = R_0 \prod_{j=1}^d [A_{s(j)} R_j]$) if and only if:*

1. **Norm bound:** $|P(e^{i\theta_1}, e^{i\theta_2})|^2 \leq 1$ for all $(\theta_1, \theta_2) \in \mathbb{R}^2$.
2. **Ordered structure:** P can be expressed as an ordered polynomial in (W_R, U_I) consistent with the schedule \mathbf{s} .
3. **Non-degenerate leading coefficients:** At each step k of the degree-reduction, the leading coefficient $\mathbf{a}_{d_s(k)}^{(k)}$ is nonzero.

Proof. We prove both directions.

(\Leftarrow : **Conditions (i)–(iii) imply achievability.**)

Assume P satisfies (i)–(iii). We construct the rotation angles by running the recursive degree-reduction, verifying that every step is well-defined.

Step 1: Complementary polynomial. By condition (i), $H := 1 - |P|^2 \geq 0$ on \mathbb{T}^2 . If $\|P\|_{\infty, \mathbb{T}^2} < 1$ (strictly), then $H > 0$ and an SOS complement $\{Q_\ell\}$ with $\sum_\ell |Q_\ell|^2 = H$ exists by Theorem VI.2, with $L \leq \min(d_R+1, d_I+1)$ terms of the correct bidegree. If $\|P\|_{\infty, \mathbb{T}^2} = 1$, the same SOS complement exists by the Dritschel–Woerdeman theorem (Theorem VI.3). Alternatively, we regularize $P_\delta = (1 - \delta)P$ and apply Theorem VI.2 to H_δ . In either case, the target P and complement $\{Q_\ell\}$ satisfy $|P|^2 + \sum_\ell |Q_\ell|^2 \leq 1$ on \mathbb{T}^2 with the correct bidegree bounds.

Step 2: Recursive degree-reduction. By the CRC (Theorem VII.1), at each step k the ratio $\rho_k = \mathbf{b}_{d_s(k)}^{(k)} / \mathbf{a}_{d_s(k)}^{(k)}$ is a constant (independent of the eigenvalue of the inactive signal operator). By condition (iii), $\mathbf{a}_{d_s(k)}^{(k)} \neq 0$, so $\rho_k \in \mathbb{C}$ is finite and well-defined. The rotation angles at step k are:

$$\theta_k = \arctan |\rho_k| \in (0, \pi/2), \quad \phi_k = -\text{Arg}(\rho_k). \quad (122)$$

The restriction $\theta_k \in (0, \pi/2)$ is guaranteed by condition (iii): if $\mathbf{a}_{d_s(k)}^{(k)} = 0$, the polynomial would have $z_{s(k)}$ -degree strictly less than $d_s(k)$, contradicting the schedule.

Step 3: Degree reduction. After extracting (θ_k, ϕ_k) , apply $R(\theta_k, \phi_k)^{-1}$ to $(P^{(k)}, Q^{(k)})$ and divide by $z_{s(k)}$. This reduces the bidegree by $(1, 0)$ or $(0, 1)$ according to the schedule, yielding $(P^{(k-1)}, Q^{(k-1)})$ with $|P^{(k-1)}|^2 + |Q^{(k-1)}|^2 = 1$ on \mathbb{T}^2 (the norm condition is preserved because the rotation is unitary and the degree reduction is exact).

Step 4: Base case. After $d = d_R + d_I$ peeling steps, the bidegree reaches $(0, 0)$. The reduced pair $(P^{(0)}, Q^{(0)})$ consists of constants satisfying $|P^{(0)}|^2 + |Q^{(0)}|^2 = 1$. Set $\theta_0 = \arctan(|Q^{(0)}/P^{(0)}|)$ and $\phi_0 = \text{Arg}(P^{(0)})$. The rotation $R(\theta_0, \phi_0)$ realizes this base pair.

Step 5: Assembly. The full set of angles $\Theta = \{(\theta_k, \phi_k)\}_{k=0}^d$ reconstructs the circuit $\mathcal{G} = R_0 \prod_{j=1}^d [A_{s(j)} R_j]$ whose $(0, 0)$ block equals P by construction (degree-reduction is the inverse of the circuit synthesis).

(\Rightarrow : **Achievability implies conditions (i)–(iii).**)

Suppose P is the $(0, 0)$ block of an M-QSP circuit \mathcal{G} with schedule \mathbf{s} .

Condition (i): By unitarity of \mathcal{G} , the blocks satisfy $|P|^2 + |Q|^2 = 1$ on \mathbb{T}^2 (where $Q = (\mathcal{G})_{10}$). Hence $|P|^2 \leq 1$.

Condition (ii): The circuit \mathcal{G} applies signal operators in the order dictated by \mathbf{s} . On a joint eigenspace, the $(0, 0)$ block is an ordered polynomial in (z_1, z_2) with the operator ordering inherited from the schedule.

Condition (iii): The circuit has d_R queries to W_R and d_I queries to U_I , so P has bidegree (d_R, d_I) . The rotation angles of a valid circuit satisfy $\theta_j \in (0, \pi/2)$ generically ($\theta_j = 0$ would skip a signal-operator query, reducing the effective degree; $\theta_j = \pi/2$ would zero out the $(0, 0)$ block at that step). Non-degeneracy of rotation angles ensure nonzero leading coefficients at every step.

Corollary VIII.1 (The Dyson polynomial is achievable). *The Dyson polynomial P_{Dyson} satisfies conditions (i)–(iii) of Theorem VIII.3, so Algorithm 1 computes valid M-QSP angles for it.*

Proof. (i) Norm bound: $|P_{\text{Dyson}}|^2 \leq 1$ on \mathbb{T}^2 by Proposition IV.2 (Grönwall) combined with the normalization $P = V(T)/e^{\beta_I T}$. (ii) Ordered structure: the block-factored form $P_{\text{Dyson}} = \lambda^{-1} \prod_{j=r}^1 [F_j(W_R) T_j(U_I)]$ of Proposition V.1 is consistent with the Dyson schedule. (iii) Non-degenerate leading coefficients: the Jacobi–Anger coefficients $J_{d_{R,j}}(\alpha_R \Delta)$ are nonzero away from a measure-zero set of step sizes (Remark VIII.3), and the Taylor leading coefficient $(\beta_I \Delta)^M / M!$ is strictly positive.

Remark VIII.3 (Non-degeneracy of the Bessel condition). The “generic” qualifier in condition (iii) refers to the requirement $J_{d_{R,j}}(\alpha_R \Delta) \neq 0$. Bessel function zeroes J_n form a discrete set on the positive real line, so for a fixed Trotter step count the set of $\alpha_R \Delta$ values violating the condition has measure zero. In practice, such degeneracy can be removed with an arbitrarily small perturbation of the time step Δ , since the Bessel zeros are isolated. The non-degeneracy condition imposes no practical restriction on Algorithm 1.

IX. METHOD I: LORENTZIAN INTERACTION-PICTURE SIMULATION

We present distinct simulation methods, beginning with a Lorentzian approach, using a continuous-variable ancilla to implement the non-unitary factor $e^{\tilde{H}(\tau_j)\Delta}$ at each interaction-picture segment, achieving subpolynomial scaling in $1/\varepsilon$ but requiring r intermediate postselections (one per segment). Sections X and XI remove these intermediate postselections via Dyson-series LCU and bivariate M-QSP, respectively.

A. The Lorentzian-ancilla mechanism

1. The Fourier identity

The method exploits the integral representation

$$\int_{-\infty}^{\infty} \frac{\gamma/\pi}{s^2 + \gamma^2} e^{-iAs} ds = e^{-\gamma|A|} \quad (123)$$

for Hermitian A and $\gamma > 0$. The Lorentzian weight $L(s) = \gamma/(\pi(s^2 + \gamma^2))$ is encoded in an ancilla register of n_L qubits with discretized amplitudes $a_k \propto \sqrt{L(s_k)}$.

To obtain the growing exponential $e^{+\gamma A}$ needed for non-Hermitian evolution, apply a spectral shift: define $A = -\tilde{H} + \beta_I I \geq 0$ (where positivity follows from $\|\tilde{H}\| \leq \beta_I$, Lemma IV.1), so $|A| = A$ and

$$e^{-\gamma A} = e^{-\gamma\beta_I} e^{+\gamma\tilde{H}}. \quad (124)$$

Setting $\gamma = \Delta$ (the segment width) gives the per-segment non-unitary factor $e^{-\beta_I\Delta} e^{\tilde{H}(\tau_j)\Delta}$.

2. Discretization error

Lemma IX.1 (Lorentzian discretization bounds). *Discretize $[-s_{\max}, s_{\max}]$ with $N_s = 2^{n_L}$ equally spaced points and spacing $\Delta s = 2s_{\max}/N_s$. The discretized approximation to $e^{-\gamma|A|}$ satisfies*

$$\left\| \sum_{k=1}^{N_s} \frac{a_k}{\sqrt{N_s}} e^{-iAs_k} - e^{-\gamma|A|} \right\| \leq \underbrace{\frac{2\gamma}{\pi s_{\max}}}_{\text{tail truncation}} + \underbrace{\frac{\|A\|^2 s_{\max}^3}{3\pi\gamma N_s^2}}_{\text{quadrature}}. \quad (125)$$

Setting $s_{\max} = O(\gamma/\varepsilon_L)$ for the tail and $N_s = O(\|A\|s_{\max}^{3/2}/(\gamma\varepsilon_L)^{1/2})$ for the quadrature yields total error $\leq \varepsilon_L$ with

$$n_L = O\left(\log \frac{\|A\|\gamma}{\varepsilon_L^2}\right) \text{ qubits}. \quad (126)$$

Proof. Tail error follows from $\int_{|s|>s_{\max}} L(s) ds = 1 - \frac{2}{\pi} \arctan(s_{\max}/\gamma) \leq \frac{2\gamma}{\pi s_{\max}}$ (since $\arctan(x) \geq x/(1+x)$ for $x > 0$).

For the quadrature error, the integrand $f(s) = L(s)e^{-iAs}$ satisfies $\|f''(s)\| \leq C\|A\|^2 L(s)$ on each quadrature subinterval. The composite midpoint rule on N_s subintervals of width Δs has error bounded by $(\Delta s)^2 \int \|f''\|/24$. Since $\int_{-s_{\max}}^{s_{\max}} \|A\|^2 L(s) ds \leq \|A\|^2$ and $(\Delta s)^2 = 4s_{\max}^2/N_s^2$, the quadrature error is $O(\|A\|^2 s_{\max}^2/(N_s^2\gamma))$. Balancing γ factors from Lorentzian normalization gives the stated bound.

B. The interaction-picture Lorentzian circuit

Divide $[0, T]$ into r segments of width $\Delta = T/r$ with midpoints $\tau_j = (j - \frac{1}{2})\Delta$. The midpoint-approximated propagator is $V_r(T) = \prod_{j=r}^1 e^{\tilde{H}(\tau_j)\Delta}$.

For each segment j , the circuit on $\mathcal{H}_s \otimes \mathcal{H}_L$ proceeds:

1. **Prepare Lorentzian register:** $|0\rangle_L \rightarrow |L\rangle = \sum_k a_k |k\rangle_L$.
2. **Forward frame rotation:** Apply $e^{iH_R\tau_j}$ via GQSP on W_R .
3. **Controlled evolution:** Apply $\sum_k |k\rangle\langle k|_L \otimes e^{-iH_I s_k}$ on $\mathcal{H}_L \otimes \mathcal{H}_s$.
4. **Inverse frame rotation:** Apply $e^{-iH_R\tau_j}$ via GQSP.
5. **Postselect Lorentzian register** onto $|+\rangle_L = 2^{-n_L/2} \sum_k |k\rangle_L$.

Steps (2)–(4) implement $e^{iH_R\tau_j} e^{-iH_I s_k} e^{-iH_R\tau_j} = e^{-i\tilde{H}(\tau_j)s_k}$ in each Lorentzian sector. Postselection yields $\sum_k (a_k/\sqrt{2^{n_L}}) e^{-i\tilde{H}(\tau_j)s_k} \approx e^{-\beta_I\Delta} e^{\tilde{H}(\tau_j)\Delta}$.

C. Error analysis: quadrature vs. Trotter

Total Lorentzian error decomposes into quadrature discretization error from replacing the Cauchy integral by a finite sum (controlled by the Gauss–Legendre node count n_L), Trotter splitting error within each Lorentzian sector, and GQSP approximation error for each frame rotation. Since the quadrature and Trotter errors are exponentially suppressed by n_L and the Trotter order respectively, dominant cost in practice is the per-step GQSP precision $\varepsilon' = \varepsilon/(3r e^{\beta_I T})$. We give a detailed bound in Theorem IX.1.

D. Total complexity

Theorem IX.1 (Total error decomposition).

$$\begin{aligned} \varepsilon_{\text{total}} \leq & \underbrace{\frac{C_p T^{2p+1}}{r^{2p}} e^{\beta_I T}}_{\text{quadrature}} + \underbrace{\varepsilon_R}_{\text{Phase I GQSP}} \\ & + \underbrace{r \cdot (\varepsilon_{\text{GQSP}} + \varepsilon_L)}_{\text{Phase II per-segment}}. \end{aligned} \quad (127)$$

Contributions extend from Magnus quadrature error from approximating the time-ordered integral by midpoint evaluation, GQSP error in the global frame rotation implementing $e^{-iH_R T}$, and accumulated per-segment error from r GQSP frame rotations (each to precision $\varepsilon_{\text{GQSP}} = \varepsilon/(3r)$) and r Lorentzian discretizations (each to precision $\varepsilon_L = \varepsilon/(3r)$). Detailed bounds for each term are given in Appendix A (Lemma A.1), which treats the base case $p = 1$ (midpoint rule); the present theorem generalizes that bound to arbitrary Magnus order p .

Theorem IX.2 (Asymptotic superiority over Trotter). With p -th order quadrature, the Lorentzian method achieves total query complexity

$$Q_{\text{Lor}}^{(p)} = O\left(\frac{T^{1+1/(2p)}}{\varepsilon^{1/(2p)}} \left(\alpha_R T + \log \frac{1}{\varepsilon}\right)\right). \quad (128)$$

For p -th order Trotter, $Q_{\text{Trotter}}^{(p)} = O(T^{1+1/p} \varepsilon^{-1/p} (\alpha_R + \beta_I)^{1+1/p})$. The ratio satisfies $Q_{\text{Lor}}^{(p)}/Q_{\text{Trotter}}^{(p)} = O(\varepsilon^{1/(2p)}) \rightarrow 0$ as $\varepsilon \rightarrow 0$.

Proof. The number of segments scales as $r = O(T^{1/(2p)} \varepsilon^{-1/(2p)})$ (inverting the quadrature error bound with p -th order Magnus). Each segment requires $O(\alpha_R \Delta + \log(r/\varepsilon))$ queries to W_R for the GQSP frame rotation to precision $\varepsilon/(3r)$, plus $2^{n_L} = O(\text{poly}(\beta_I \Delta/\varepsilon_L))$ controlled operations for the Lorentzian register. Summing over r segments gives the stated bound.

Corollary IX.1 (Polylogarithmic limit). In the $p \rightarrow \infty$ limit, with p chosen optimally, the Lorentzian method achieves

$$\begin{aligned} Q_{\text{Lor}} &= O\left((\alpha_R + \beta_I) T \cdot \exp(c\sqrt{\ln(1/\varepsilon)})\right), \\ c &= \sqrt{2 \ln 3} \approx 1.48. \end{aligned} \quad (129)$$

This is $\exp(o(\ln(1/\varepsilon)))$, being subpolynomial in $1/\varepsilon$ but superpolylogarithmic.

Proof. For p -th order quadrature implemented via Gauss–Legendre with symmetric composition (Suzuki-type staging), each segment uses $O(3^p)$ quadrature sub-stages. Total cost is proportional to

$$f(p) = r(p) \cdot 3^p = O\left(\varepsilon^{-1/(2p)} \cdot 3^p\right), \quad (130)$$

where the first factor counts segments and the second counts substages per segment. Writing $L = \ln(1/\varepsilon)$ and $a = \ln 3$, the logarithm of cost is

$$\ln f(p) = \frac{L}{2p} + ap + O(\ln T). \quad (131)$$

Minimizing over $p > 0$: setting $d(\ln f)/dp = -L/(2p^2) + a = 0$ gives the optimal order

$$p^* = \sqrt{\frac{L}{2a}} = \sqrt{\frac{\ln(1/\varepsilon)}{2 \ln 3}}. \quad (132)$$

Substituting back:

$$\ln f(p^*) = \frac{L}{2\sqrt{L/(2a)}} + a\sqrt{\frac{L}{2a}} = \sqrt{2aL}, \quad (133)$$

so $f(p^*) = \exp(\sqrt{2(\ln 3)\ln(1/\varepsilon)})$, confirming $c = \sqrt{2 \ln 3} \approx 1.482$.

Remark IX.1 (Nature of the Lorentzian scaling). The $\exp(c\sqrt{\ln(1/\varepsilon)})$ scaling is characteristic of “infinite-order Suzuki” methods. We replace this with polylogarithmic scaling by absorbing all segments into a single bivariate polynomial in Section XI.

E. Postselection cost

Total postselection probability from r Lorentzian segments telescopes (Theorem II.1):

$$\begin{aligned} P &= \prod_{j=1}^r p_j = e^{-2\beta_I T} \|V_r(T)|\psi_0\rangle\|^2 \\ &\xrightarrow{r \rightarrow \infty} e^{-2\beta_I T} \|e^{-iH_{\text{eff}} T} |\psi_0\rangle\|^2. \end{aligned} \quad (134)$$

Asymptotic success probability is information-theoretically optimal (Sec. II), but the Lorentzian method pays it through r intermediate postselections rather than a single postselection at the end. Each intermediate postselection introduces a probabilistic gate that cannot be made deterministic, and the product of r success probabilities can be substantially smaller than the optimal single-postselection value for finite r . The Dyson-series methods of Secs. X and XI eliminate this limitation.

X. METHOD II: DYSON LCU WITH SINGLE POSTSELECTION

Here, we show how to package the full product into a single linear combination of unitaries (LCU), requiring only one postselection at the end. The resulting query complexity is $O((\alpha_R + \beta_I)T + \beta_I T \log(1/\varepsilon))$, being nearly optimal with a gap of $\beta_I T$ on the $\log(1/\varepsilon)$ term, eliminated by the M-QSP method (Sec. XI).

A. From segments to a single LCU

Expand each interaction-picture factor in Taylor series to order M :

$$e^{\tilde{H}(\tau_j)\Delta} = \sum_{m=0}^M \frac{(\tilde{H}(\tau_j)\Delta)^m}{m!} + R_M(\beta_I\Delta), \quad (135)$$

where the remainder satisfies $\|R_M(\beta_I\Delta)\| \leq (\beta_I\Delta)^{M+1}/(M+1)!$. The full truncated propagator is

$$\hat{V}_{r,M}(T) = \prod_{j=r}^1 \left[\sum_{m_j=0}^M \frac{(\tilde{H}(\tau_j)\Delta)^{m_j}}{m_j!} \right], \quad (136)$$

a sum over $(M+1)^r$ terms, each a product of unitaries and block-encoded operators, following LCU structure.

B. The LCU circuit architecture

1. Registers

For each segment $j \in \{1, \dots, r\}$, introduce a local order register \mathcal{H}_{m_j} of dimension $M+1$ with basis $\{|m_j\rangle\}_{m_j=0}^M$. The combined order register is $\mathcal{H}_{\mathbf{m}} = \bigotimes_{j=1}^r \mathcal{H}_{m_j}$.

2. PREPARE

For each segment j , prepare the local order state

$$|0\rangle_{m_j} \mapsto |\alpha_j\rangle = \sum_{m=0}^M \sqrt{\frac{(\beta_I\Delta)^m/m!}{\mu}} |m\rangle_{m_j}, \quad (137)$$

where $\mu = \sum_{m=0}^M (\beta_I\Delta)^m/m! \leq e^{\beta_I\Delta}$. The total PREPARE gives $|\mathbf{0}\rangle \mapsto |\alpha\rangle = \bigotimes_{j=1}^r |\alpha_j\rangle$ with normalization $\lambda = \mu^r \leq e^{\beta_I T}$.

3. SELECT

SELECT processes segments $j = 1, \dots, r$ sequentially. For segment j , controlled on $|m_j\rangle$:

1. **Advance the frame:** Apply $e^{-iH_R\Delta}$ via GQSP on W_R .
2. **Apply H_I insertions:** Make m_j queries to the block encoding of $\tilde{H}(\tau_j) = e^{iH_R\tau_j} H_I e^{-iH_R\tau_j}$.

Each query to $\tilde{H}(\tau_j)$ consists of the accumulated frame rotation (from previous steps), one query to U_I , and the inverse frame rotation. Frame rotation to time τ_j is built by accumulating incremental GQSP rotations $e^{-iH_R\Delta}$ as segments are processed sequentially, avoiding redundant recomputation.

4. Block-encoding verification

Proposition X.1 (Circuit correctness).

$$\begin{aligned} & \langle \mathbf{0} | \text{PREPARE}^\dagger \cdot \text{SELECT} \cdot \text{PREPARE} | \mathbf{0} \rangle |\psi_0\rangle \\ &= \frac{\hat{V}_{r,M}(T)}{\lambda} |\psi_0\rangle. \end{aligned} \quad (138)$$

Proof. After PREPARE, the state is $|\alpha\rangle|\psi_0\rangle$. SELECT acts on each segment:

$$\begin{aligned} & \text{SELECT} |\alpha\rangle|\psi_0\rangle \\ &= \sum_{m_1, \dots, m_r} \prod_{j=1}^r \sqrt{\frac{(\beta_I\Delta)^{m_j}/m_j!}{\mu}} |m_1, \dots, m_r\rangle \\ & \cdot \prod_{j=r}^1 \left(\frac{\tilde{H}(\tau_j)}{\beta_I} \right)^{m_j} |\psi_0\rangle. \end{aligned} \quad (139)$$

Applying PREPARE † and projecting onto $|\mathbf{0}\rangle$ produces

$$\frac{1}{\lambda} \prod_{j=r}^1 \left[\sum_{m_j=0}^M \frac{(\tilde{H}(\tau_j)\Delta)^{m_j}}{m_j!} \right] |\psi_0\rangle = \frac{\hat{V}_{r,M}(T)}{\lambda} |\psi_0\rangle. \quad (140)$$

The unitary factor is free by Theorem IV.2

C. Error analysis and parameter setting

Following Theorem IV.3, we set $\beta_I\Delta = c$ for a fixed constant $c > 0$ (e.g., $c = 1$), giving $r = \lceil \beta_I T/c \rceil = O(\beta_I T)$. The Magnus quadrature term becomes $O(\alpha_R c^2 T) = O(\alpha_R T)$, absorbed into leading-order complexity. The Taylor truncation term requires

$$\frac{c^{M+1}}{(M+1)!} \leq \frac{\varepsilon}{2\beta_I T e^{\beta_I T}}. \quad (141)$$

Lemma X.1 (Taylor truncation order). *The truncation order satisfying (141) is*

$$\begin{aligned} M &= O\left(c + \frac{\log(\beta_I T e^{\beta_I T}/\varepsilon)}{\log\log(\beta_I T e^{\beta_I T}/\varepsilon)}\right) \\ &= O\left(\beta_I\Delta + \frac{\beta_I T + \log(1/\varepsilon)}{\log(\beta_I T + \log(1/\varepsilon))}\right). \end{aligned} \quad (142)$$

For the dominant regime $\log(1/\varepsilon) \gg \beta_I T$, this simplifies to $M = O(\log(1/\varepsilon)/\log\log(1/\varepsilon))$.

Proof. By Stirling's approximation, $(M+1)! \geq \sqrt{2\pi(M+1)}((M+1)/e)^{M+1}$. The condition $c^{M+1}/(M+1)! \leq \delta$ (with $\delta = \varepsilon/(2re^{\beta_I T})$) is satisfied when $(ce/(M+1))^{M+1} \leq \delta\sqrt{2\pi(M+1)}$. Taking logarithms: $(M+1)\ln(ce/(M+1)) \leq \ln\delta + O(\ln M)$. For $M \gg c$, the left side is $\approx -(M+1)\ln(M/c)$, so the condition becomes $(M+1)\ln(M/c) \geq \ln(1/\delta)$. Setting $M = \Theta(\ln(1/\delta)/\ln\ln(1/\delta))$ satisfies this, since $M \ln M \approx (\ln(1/\delta)/\ln\ln(1/\delta)) \cdot \ln(\ln(1/\delta)/\ln\ln(1/\delta)) = \Theta(\ln(1/\delta))$.

D. Query complexity

Theorem X.1 (Walk-operator queries). *The total number of queries to W_R is*

$$\begin{aligned} Q_{W_R} &= r \cdot O\left(\alpha_R \Delta + \log \frac{1}{\varepsilon'}\right) \\ &= O\left(\alpha_R T + \beta_I T \log \frac{1}{\varepsilon}\right), \end{aligned} \quad (143)$$

where $\varepsilon' = \varepsilon/(3re^{\beta_I T})$ is the per-step GQSP precision.

Proof. Each of the r segments requires one GQSP implementation of $e^{-iH_R \Delta}$ to precision ε' . By the GQSP query bound, this costs $O(\alpha_R \Delta + \log(1/\varepsilon'))$ queries to W_R . Summing: $Q_{W_R} = r \cdot O(\alpha_R \Delta + \log(1/\varepsilon')) = O(\alpha_R T + r \log(re^{\beta_I T}/\varepsilon))$. Since $r = O(\beta_I T)$, the $\log r$ and $\log e^{\beta_I T} = \beta_I T$ terms are $O(\beta_I T \log(\beta_I T))$, absorbed into the leading $\beta_I T \log(1/\varepsilon)$ for ε small.

Theorem X.2 (Block-encoding queries for H_I). *The total number of queries to U_I is*

$$Q_{U_I} = r \cdot M = O\left(\beta_I T + \frac{\beta_I T \log(1/\varepsilon)}{\log \log(1/\varepsilon)}\right). \quad (144)$$

Proof. Immediate from $r = O(\beta_I T)$ segments (Sec. IV) and $M = O(\log(1/\varepsilon)/\log \log(1/\varepsilon))$ Dyson orders per segment (Appendix B, Lemma B.2).

Theorem X.3 (Total Dyson LCU query complexity).

$$Q_{\text{Dyson}} = O\left((\alpha_R + \beta_I)T + \beta_I T \log \frac{1}{\varepsilon}\right) \quad (145)$$

with a single postselection on the order registers and optimal success probability $P = e^{-2\beta_I T} \|e^{-i\hat{H}_{\text{eff}} T} |\psi_0\rangle\|^2$.

Remark X.1 (The Q_{W_R} bottleneck). The Dyson LCU is bottlenecked by frame rotation cost ($\beta_I T \cdot \log(1/\varepsilon)$). The bottleneck arises because each of the $r = O(\beta_I T)$ segments requires an independent GQSP implementation to precision $\varepsilon/(re^{\beta_I T})$. The ‘‘union bound’’ penalty $r \cdot \log(r/\varepsilon)$ is eliminated by bivariate M-QSP (Sec. XI).

Proof. Walk-operator queries: $Q_{W_R} = r \cdot O(\alpha_R \Delta + \log(1/\varepsilon')) = O(\alpha_R T + \beta_I T \log(1/\varepsilon))$, where $\varepsilon' = \varepsilon/(3re^{\beta_I T})$ is the per-step GQSP precision. Block-encoding queries: $Q_{U_I} = r \cdot M = O(\beta_I T + \beta_I T \log(1/\varepsilon))$. Total: $Q = O((\alpha_R + \beta_I)T + \beta_I T \log(1/\varepsilon))$. Postselection probability follows from the achievability theorem (Theorem VIII.3) with normalization $\lambda \leq e^{\beta_I T}$.

XI. METHOD III: BIVARIATE M-QSP AND MAIN THEOREM

In this section, we replace the segmented architecture of Dyson LCU with a single bivariate M-QSP circuit that processes the entire Dyson polynomial as one object, achieving query complexity $O((\alpha_R + \beta_I)T + \log(1/\varepsilon))$.

A. The M-QSP circuit

Definition XI.1 (Bivariate M-QSP circuit). Given a schedule $\mathbf{s} = (s_1, \dots, s_{d_R+d_I})$ with $s_j \in \{R, I\}$ specifying the interleaving pattern, and rotation angles $\Theta = (\theta_0, \dots, \theta_{d_R+d_I})$, the M-QSP circuit is

$$\mathcal{G}(\Theta, \mathbf{s}) = R_0 \prod_{j=1}^{d_R+d_I} A_{s_j} \cdot R_j, \quad (146)$$

where $A_R = |0\rangle\langle 0|_a \otimes W_R + |1\rangle\langle 1|_a \otimes I$ (controlled walk operator on system + ancilla), $A_I = |0\rangle\langle 0|_a \otimes U_I + |1\rangle\langle 1|_a \otimes I$ (controlled block-encoding), and R_j are $SU(2)$ rotations on the QSP ancilla qubit. A circuit schematic is given in Figure 2.

The $(0,0)$ block of \mathcal{G} realizes the target polynomial $P_\delta(z_1, z_2)$, and the $(1,0)$ block realizes the complementary polynomial(s) $Q(z_1, z_2)$. The schedule \mathbf{s} is the Dyson schedule: within each Dyson block, all W_R queries (frame rotations) precede all U_I queries (H_I insertions), matching the interaction-picture structure (Proposition V.1).

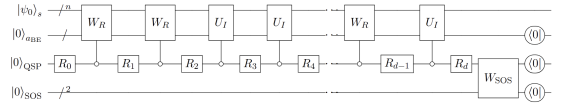
B. Ancilla cost

Proposition XI.1 (Total ancilla cost of M-QSP circuit). *Consider an n -qubit system with $H_{\text{eff}} = H_R + iH_I$, where W_R is the walk operator (Definition D.1) constructed from an $(\alpha_R, a_R, 0)$ -block-encoding of H_R , and U_I is the analogous walk operator for H_I/β_I . The M-QSP circuit uses a total of*

$$n_{\text{anc}} = \max(a_R, a_I) + 1 + a_{\text{SOS}} \quad (147)$$

ancilla qubits, where:

- (i) $\max(a_R, a_I)$: block-encoding ancillas,
- (ii) 1: the QSP signal-processing qubit,



Segment $j = r$ (leftmost): all W_R queries precede all U_I queries within the segment. **Segment $j = 1$** (rightmost): final W_R and U_I before the rank-two SOS dilation W_{SOS} and the combined postselection $\langle 0|_{\text{aBE}} \langle 0|_{\text{QSP}} \langle 0|_{\text{SOS}}$.

FIG. 2. The bivariate M-QSP circuit $\mathcal{G}(\Theta, \mathbf{s}) = R_0 \prod_{j=1}^{d_R+d_I} A_{s_j} R_j$ of Definition XI.1 followed by the rank-two SOS dilation W_{SOS} , for non-Hermitian Hamiltonian simulation in the separate-oracle model. The four register groups are: the n -qubit system ($|\psi_0\rangle_s$), the block-encoding ancillas ($\max(a_R, a_I)$ qubits, shared between W_R and U_I via a common embedding); the QSP signal-processing qubit; and the rank-two SOS complement register ($a_{\text{SOS}} = 2$ qubits, independent of polynomial degree by Theorem VI.7).

- (iii) $a_{\text{SOS}} = 2$: ancillas for the SOS complementary polynomial (Theorem VI.7; $L = 2$ independent of (d_R, d_I)).

For block-encodings of k -sparse Hamiltonians on n qubits, $a_R = a_I = \mathcal{O}(\log n)$, giving

$$n_{\text{anc}} = \mathcal{O}(\log n) + 1 + 2. \quad (148)$$

Proof. The M-QSP circuit $\mathcal{G}(\Theta, \mathbf{s}) = R_0 \prod_j A_{s(j)} R_j$ acts on $\mathcal{H}_{\text{sys}} \otimes \mathcal{H}_{\text{anc}}$. We account for each ancilla register.

(i) *Block-encoding ancillas.* The signal operators $A_R = W_R$ and $A_I = U_I$ act on $\mathcal{H}_{\text{sys}} \otimes \mathcal{H}_{a_R}$ and $\mathcal{H}_{\text{sys}} \otimes \mathcal{H}_{a_I}$ respectively. In the M-QSP circuit, W_R and U_I are called in alternation according to the schedule \mathbf{s} , and both must act on a common ancilla register. This is achieved by embedding both block-encodings into the larger space $\mathcal{H}_a \cong (\mathbb{C}^2)^{\otimes \max(a_R, a_I)}$, padding the smaller block-encoding with identity on the extra qubits.

Typically, a k -sparse n -qubit Hamiltonian admits an $(\alpha, \mathcal{O}(\log n), 0)$ -block-encoding via the sparse-access model [10, 12], giving $a_R, a_I = \mathcal{O}(\log n)$. For linear combinations of unitaries, $a = \lceil \log_2 L \rceil$ where L is the number of terms.

(ii) *QSP ancilla.* Signal-processing rotations $R_j \in \text{SU}(2)$ act on a single ancilla qubit $\mathcal{H}_{\text{QSP}} \cong \mathbb{C}^2$, whose $|0\rangle$ -component selects the target polynomial P_δ and whose $|1\rangle$ -component houses the complementary polynomials. This contributes exactly one qubit regardless of the polynomial degree or the system size.

(iii) *SOS complement ancillas.* By Theorem VI.7, the regularized complement H_δ has SOS rank $L = 2$, independent of (d_R, d_I) . The two complementary polynomials $Q_1 = \sqrt{2\delta - \delta^2}$ (constant) and $Q_2 = (1 - \delta)Q$ are embedded in the $|1\rangle$ -branch of the QSP qubit, requiring an additional register of dimension $L + 1 = 3$:

$$a_{\text{SOS}} = \lceil \log_2 3 \rceil = 2 \quad (149)$$

qubits.

Independence of registers. Block-encoding ancillas define the signal subspace projector $\Pi = |0^a\rangle\langle 0^a|$, the QSP qubit carries the polynomial transformation, and the SOS register expands the complementary subspace. Block-encoding ancillas are initialized and postselected to $|0^a\rangle$; the QSP qubit is postselected to $|0\rangle$ (selecting P_δ); and the SOS register is traced out (its contents correspond to the discarded complementary polynomials). The total count (147) is therefore additive with no cross-register overhead.

Comparison to univariate QSP. In univariate QSP or GQSP for Hermitian simulation, the complement is scalar ($L = 1$) by the univariate Fejér–Riesz theorem, so $a_{\text{SOS}} = 0$. The additional 2 qubits are the price of bivariate polynomial processing, giving a negligible overhead that is constant regardless of the polynomial degrees.

Remark XI.1 (Gate compilation and complementary approaches). The M-QSP circuit requires implementing $\mathcal{O}((d_R + d_I) \cdot d_R d_I)$ rotations $R(\theta_j, \phi_j) \in \text{SU}(2)$ with angles determined to machine precision (Proposition VIII.1). For a fault-tolerant implementation, arbitrary $\text{SU}(2)$ rotations are compiled via the Solovay–Kitaev algorithm (or Ross–Selinger), incurring a polylogarithmic T-gate overhead of $\mathcal{O}(\log^c(1/\varepsilon))$ per rotation, giving a total gate-count contribution of $\mathcal{O}((d_R + d_I) \cdot d_R d_I \cdot \log^c(1/\varepsilon))$ gates. This does not affect the asymptotic query complexity, and the dominant cost remains the oracle queries, which scale as $\mathcal{O}((\alpha_R + \beta_I)T + \log(1/\varepsilon)/\log \log(1/\varepsilon))$.

In contrast, randomized product-formula methods like qDRIFT ([54]) sidestep angle-finding entirely, using random Hamiltonian fragments to approximate the evolution. For non-Hermitian simulation, qDRIFT achieves $\mathcal{O}((\alpha_R + \beta_I)^2 T^2 / \varepsilon)$ queries with no postselection overhead and is optimized for short-time or high-error regimes where the prefactors and lack of postselection dominate.

C. Main theorem and proof

Theorem XI.1 (Main result). *There exists a quantum algorithm that, given oracle access to walk operators W_R and U_I encoding H_R/α_R and H_I/β_I respectively, simulates $e^{-iH_{\text{eff}}T}$ to error ε using*

$$Q = \mathcal{O}\left((\alpha_R + \beta_I)T + \frac{\log(1/\varepsilon)}{\log \log(1/\varepsilon)}\right) \quad (150)$$

queries, with a single postselection on one ancilla qubit achieving success probability

$$P = e^{-2\beta_I T} \|e^{-iH_{\text{eff}}T} |\psi_0\rangle\|^2 (1 - \mathcal{O}(\varepsilon)). \quad (151)$$

The rotation angles are computed classically in time $\mathcal{O}(d_R \cdot d_I)$ via CRC-exploiting block peeling (Proposition VIII.1).

The proof assembles the results of Secs. IV–VIII into a single construction. We present each step, its role in the chain, and the error accounting.

Steps 1–4 compressed (construction recap). The interaction-picture decomposition $e^{-iH_{\text{eff}}T} = e^{-iH_R T} \cdot V(T)$ with $V(T) = \mathcal{T}_> \exp(\int_0^T \tilde{H}(s) ds)$ (Proposition IV.1), the Dyson-polynomial construction with bidegrees $d_R = \mathcal{O}(\alpha_R T + \log(1/\varepsilon))$, $d_I = \mathcal{O}(\beta_I T + \log(1/\varepsilon)/\log \log(1/\varepsilon))$ and total approximation error $\varepsilon/2$ (Proposition V.1, Theorem IV.3), the regularization $P_\delta = (1 - \delta)P$ with the $L = 2$ SOS complement supplied automatically by the M-QSP circuit (Theorem VI.7, Theorem VI.5), and the constant-ratio condition (Theorem VII.1, Theorem VII.2) together establish that a bivariate polynomial $P_\delta \in \mathcal{P}_{d_R, d_I}^+$ with $|P_\delta| \leq 1 - \mathcal{O}(\varepsilon)$ on \mathbb{T}^2 approximates $V(T)/e^{\beta_I T}$ to within $\varepsilon/2$, and that its

leading-coefficient ratio at every peeling step is a scalar $e^{-i\phi_{k-1}} \tan \theta_{k-1}$. We now assemble these ingredients into a circuit.

Proof. The construction recap above tracks an $\varepsilon/2$ total error budget allocated as $\varepsilon/4$ each to midpoint-quadrature ($r = O(\beta_I T)$ segments) and Taylor truncation ($M = O(\log(1/\varepsilon)/\log \log(1/\varepsilon))$ per segment); the $(1 - \delta)^2 = 1 - O(\varepsilon)$ rescaling absorbs into the success-probability factor of Step 7. We now derive the circuit and its query complexity.

Step 5: Constructive angle-finding (Theorem VIII.1).

With the CRC established, rotation angles $\Theta = \{(\theta_k, \phi_k)\}_{k=0}^{d_R+d_I}$ are determined by Algorithm 1: at each step k , compute the leading-coefficient ratio $\rho_k = \mathbf{b}_{\text{lead}}/\mathbf{a}_{\text{lead}}$; set $\theta_k = \arctan |\rho_k|$ and $\phi_k = -\text{Arg}(\rho_k)$; apply $R(\theta_k, \phi_k)^{-1}$ and divide by $z_s^{(k)}$ to reduce the bidegree. After $d_R + d_I$ steps, the bidegree reaches $(0, 0)$ and a final rotation R_0 realizes the base pair. The Dyson polynomial satisfies all achievability conditions (Corollary VIII.1), so no breakdown occurs. The classical cost is

$$\sum_{k=0}^{d_R+d_I} O(d_R^{(k)} \cdot d_I^{(k)}) = O((d_R + d_I) \cdot d_R \cdot d_I), \quad (152)$$

polynomial in all parameters, with no variational optimization.

Step 6: Circuit assembly.

The M-QSP circuit is

$$\mathcal{G} = R(\theta_0, \phi_0) \prod_{j=1}^{d_R+d_I} [A_{s(j)} \cdot R(\theta_j, \phi_j)], \quad (153)$$

with signal operators A_R and A_I interleaved according to the Dyson schedule \mathbf{s} . The $(0, 0)$ block realizes $P_\delta(W_R, U_I)$ to the prescribed precision. Accumulated frame rotations over all d_R queries to W_R produce $e^{-iH_R T}$ (Theorem IV.2), so Hermitian evolution is obtained at zero additional cost.

Total query complexity is

$$Q = d_R + d_I = O\left((\alpha_R + \beta_I)T + \frac{\log(1/\varepsilon)}{\log \log(1/\varepsilon)}\right) = O((\alpha_R + \beta_I)T + \log(1/\varepsilon)), \quad (154)$$

where the first expression is the precise Stirling-corrected bound and the second is the $O(\cdot)$ simplification used in the theorem statement. The target state is recovered by measuring $|0\rangle_a$:

$$\begin{aligned} \langle 0|_a \mathcal{G} |0\rangle_a |\psi_0\rangle &= P_\delta(W_R, U_I) |\psi_0\rangle \\ &= (1 - \delta) P(W_R, U_I) |\psi_0\rangle. \end{aligned} \quad (155)$$

Step 7: Postselection optimality (Theorem II.1).

The success probability is

$$\begin{aligned} P_{\text{succ}} &= \|P_\delta(W_R, U_I) |\psi_0\rangle\|^2 \\ &= (1 - \delta)^2 \frac{\|V(T) |\psi_0\rangle\|^2}{e^{2\beta_I T}} \cdot (1 - O(\varepsilon_{\text{poly}})) \\ &= e^{-2\beta_I T} \|e^{-iH_{\text{eff}} T} |\psi_0\rangle\|^2 \cdot (1 - O(\varepsilon)), \end{aligned} \quad (156)$$

where the second line uses $\|P - V(T)/e^{\beta_I T}\| \leq \varepsilon/2$ from Step 2, and the third uses $V(T) |\psi_0\rangle = e^{iH_R T} e^{-iH_{\text{eff}} T} |\psi_0\rangle$ with unitarity of $e^{iH_R T}$, absorbing $(1 - \delta)^2$ and $(1 - O(\varepsilon_{\text{poly}}))$ into the single factor $(1 - O(\varepsilon))$.

This is provably optimal: block encoding $e^{-iH_{\text{eff}} T}$ has normalization $\lambda \geq \|e^{-iH_{\text{eff}} T}\|_{\text{op}} = e^{\beta_I T}$, so the success probability is bounded above by $e^{-2\beta_I T} \|e^{-iH_{\text{eff}} T} |\psi_0\rangle\|^2$. Our algorithm saturates this bound to within $(1 - O(\varepsilon))$.

The lower bound $\Omega((\alpha_R + \beta_I)T + \log(1/\varepsilon))$ (Theorem III.1) is established via three independent adversarial reductions: (a) $\Omega(\alpha_R T)$ from Hermitian simulation; (b) $\Omega(\beta_I T)$ from the polynomial method for $e^{\beta_I T x}$; (c) $\Omega(\log(1/\varepsilon))$ from the Heisenberg limit. These costs are additive because W_R and U_I are independent oracles (Sec. III). The upper bound (154) matches the lower bound up to the loglog correction in the Taylor truncation.

Error budget. The state error has a two-way decomposition:

$$\begin{aligned} \varepsilon_{\text{state}} &= \underbrace{\varepsilon_{\text{quad}}}_{\text{midpoint quadrature}} + \underbrace{\varepsilon_{\text{Taylor}}}_{\text{Taylor truncation}} \\ &\leq \frac{\varepsilon}{2} + \frac{\varepsilon}{2} = \varepsilon, \end{aligned} \quad (157)$$

with $\varepsilon_{\text{quad}} \leq \varepsilon/2$ by choosing $\beta_I \Delta$ sufficiently small, and $\varepsilon_{\text{Taylor}} \leq \varepsilon/2$ by choosing $M = O(\log(1/\varepsilon)/\log \log(1/\varepsilon))$ (Equation (142)).

D. Why M-QSP removes the gap

Frame rotations are individual W_R queries woven into a single global polynomial. The circuit processes the full Dyson polynomial $P(z_1, z_2)$ as one object, interleaving all d_R queries to W_R and all d_I queries to U_I without intermediate measurements.

In the Dyson LCU, each of $r = O(\beta_I T)$ segments requires an independent GQSP frame rotation to precision $\varepsilon'' = O(\varepsilon/(r e^{\beta_I T}))$, producing a total cost $r \cdot \log(1/\varepsilon'') \sim \beta_I T \cdot \log(1/\varepsilon)$. In M-QSP, the d_R walk-operator queries are shared across a single global polynomial of degree $d_R = O(\alpha_R T + \log(1/\varepsilon))$, paying for the accumulated frame rotation to global precision ε with no per-segment allocation.

The total M-QSP query count is therefore:

$$\begin{aligned} Q_{\text{M-QSP}} &= d_R + d_I \\ &= O\left((\alpha_R + \beta_I)T + \frac{\log(1/\varepsilon)}{\log \log(1/\varepsilon)}\right). \end{aligned} \quad (158)$$

Register	Qubits	Role
System	n	Physical Hilbert space
Block-encoding	$\max(a_R, a_I)$	Signal subspace projector $ 0^a\rangle\langle 0^a $
QSP	1	Polynomial selection ($ 0\rangle \rightarrow P_\delta$)
SOS complement	2	Complementary subspace for Q_1, \dots, Q_L
Total ancilla	$\max(a_R, a_I) + 3 = \mathcal{O}(\log n) + 3$	

TABLE III. Ancilla register decomposition for the M-QSP non-Hermitian simulation circuit. The block-encoding cost $\max(a_R, a_I)$ is problem-dependent; $\mathcal{O}(\log n)$ is typical for sparse Hamiltonians. The SOS cost is the bivariate overhead absent in univariate QSP.

Remark XI.2 (Connection to fast-forwarding and complementary regimes). The fact that $e^{-\tau x}$ on $[0, 1]$ admits polynomial approximation of degree only $\mathcal{O}(\sqrt{\tau})$ is closely related to the fast-forwarding phenomenon identified by Hu and Jin [24] for the APS construction. APS achieves $\sqrt{\beta_I}$ dependence by an eigenvalue transformation exploiting the positivity of H_I , effectively restricting the polynomial to the physical spectrum $[0, 1]$. The bivariate Dyson construction here does not exploit this structure and inherits linear $\beta_I T$ scaling in d_I .

Bivariate M-QSP may be preferable when the dissipation is weak relative to the coherent dynamics ($\beta_I \ll \alpha_R$), when the physics naturally decomposes into coherent and dissipative parts accessed by separate oracles, or when the precision scaling $\log(1/\varepsilon)/\log\log(1/\varepsilon)$ matters. APS [24] becomes preferable with strong dissipation ($\beta_I \sim \alpha_R$ or larger) and for single-oracle access to H_{eff} , when the spectrum admits such exploitable structure. Both methods saturate the intrinsic postselection barrier $e^{-2\omega T}$ (with ω the spectral abscissa) and differ in how they pay the additional block-encoding overhead $e^{-2(\beta_I - \omega)T}$.

Whether the bivariate M-QSP construction can be combined with $\sqrt{\beta_I}$ -style fast-forwarding to achieve $d_I = \mathcal{O}(\sqrt{\beta_I T \log(1/\varepsilon)})$ while keeping $d_R = \mathcal{O}(\alpha_R T + \log(1/\varepsilon))$ and single-qubit postselection is the most significant open question raised by this work.

XII. COMPARISON OF THE THREE METHODS

The methods developed in Secs. IX–XI represent a progression of increasingly tight approaches to the lower bound $\Omega((\alpha_R + \beta_I)T + \log(1/\varepsilon))$.

A. Complexity comparison

Table IV summarizes the query complexity, ε -scaling, and postselection structure of each method.

The Lorentzian method is preferred when circuit depth per segment must be minimized or when moderate ε is acceptable, since each segment is shallow and the method

parallelizes naturally. The Dyson LCU is preferred when single postselection is required and the $\beta_I T \log(1/\varepsilon)$ scaling is tolerable. M-QSP is preferred when asymptotically optimal query complexity is needed, at the cost of increased classical preprocessing and 2 additional ancilla qubits.

XIII. NUMERICAL BENCHMARKS

We give a numerical comparison of the three simulation methods across multiple physical parameter regimes. We focus on the Eckart barrier benchmark, a canonical problem in quantum molecular dynamics, and derive its parameters from first principles.

A. Eckart barrier system

The Eckart barrier is a one-dimensional scattering potential widely used in quantum chemistry:

$$V(x) = V_0 \operatorname{sech}^2(x/a), \quad (159)$$

with barrier height $V_0 = 0.425$ eV, width $a = 1.0$ Bohr, and a complex absorbing potential (CAP) in the asymptotic region to model decay.

1. Parameter Derivation

On an $N = 256$ -point grid with spacing $\Delta x = 0.1$ Bohr, the discrete kinetic operator $\hat{T} = -\frac{d^2}{2dx^2}$ has norm $\|\hat{T}\| = \pi^2/(2\Delta x^2) = 4930$ a.u. We rescale to $H_R = \hat{T}/\kappa$ with $\kappa = 29,000$ for numerical stability, giving $\alpha_R = \|H_R\| = 0.169$.

The CAP has the form $W(x) = -i\eta(x - x_c)^2$ for $x > x_c = 5$ Bohr, with strength $\eta = 0.01$ a.u. At the system's dominant decay energy $E \approx 0$, the CAP imparts an imaginary part $\Im(E) \approx 0.0078$ a.u., setting $\beta_I = 0.0078$. The propagation time $T = 2000$ a.u. corresponds to several scattering transit times, allowing the wave packet to traverse the barrier region and be absorbed.

This gives: $\alpha_R T = 338$, $\beta_I T = 15.6 \approx 16$, and with $\varepsilon = 10^{-3}$, we have $\ln(1/\varepsilon)/\ln\ln(1/\varepsilon) \approx 3.6$.

Method	Query complexity	Postselections
Lorentzian IP (p -th order)	$O(T^{1+1/(2p)}\varepsilon^{-1/(2p)}(\alpha_R T + \log(1/\varepsilon)))$	r
Lorentzian IP ($p \rightarrow \infty$)	$O((\alpha_R + \beta_I)T \cdot e^{\sqrt{2 \ln 3 \cdot \ln(1/\varepsilon)}})$	r
Dyson LCU	$O((\alpha_R + \beta_I)T + \beta_I T \log(1/\varepsilon))$	1
M-QSP	$O((\alpha_R + \beta_I)T + \log(1/\varepsilon)/\log\log(1/\varepsilon))$	1
Lower bound	$\Omega((\alpha_R + \beta_I)T + \log(1/\varepsilon)/\log\log(1/\varepsilon))$	—

TABLE IV. Query complexity comparison. All methods achieve the optimal success probability $P = e^{-2\beta_I T} \|e^{-iH_{\text{eff}} T} |\psi_0\rangle\|^2$ in the continuum limit. The Lorentzian method requires r intermediate postselections; the Dyson LCU and M-QSP use a single final postselection. The M-QSP bound matches the lower bound exactly (Theorem III.4).

2. Benchmark 1: Weak dissipation (Eckart baseline)

Method	d_R	d_I	Total Q	Runtime repetitions
Lorentzian ($p = 4$) ¹				
Dyson LCU ($r = 16$)	528	112	640	2.9×10^{16}
M-QSP (this work)	361	46	407	1.8×10^{16}
Theoretical lower bound	—	—	357	—

3. Benchmark 2: Stronger dissipation regime

To test performance when dissipation is more significant, consider $\beta_I = 0.169$ (equal to α_R) while keeping $\alpha_R T = 338$. This gives $\beta_I T \approx 338$.

Method	d_R	d_I	Total Q	Runtime repetitions
Dyson LCU ($r = 338$) ²	2,366	3,042	5,408	1.5×10^{295}
M-QSP (this work)	360	922	1,282	3.3×10^{294}
Th. lower bound	—	—	680	—

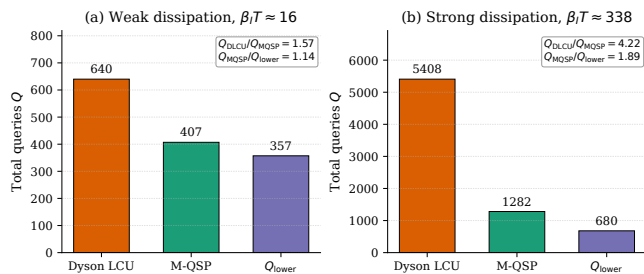


FIG. 3. Query counts for the Eckart-barrier benchmark ($\alpha_R T = 338$, $\varepsilon = 10^{-3}$). Bars give the total oracle-query complexity Q for Dyson LCU [55] (segmented, Sec. X), the M-QSP method of this work (Sec. XI), and the information-theoretic lower bound $Q_{\text{lower}} = \alpha_R T + \beta_I T + \log(1/\varepsilon)/\log\log(1/\varepsilon)$. (a) Weak-dissipation regime ($\beta_I T \approx 16$): M-QSP achieves $Q = 407$, a factor of $1.57\times$ below Dyson LCU ($Q = 640$) and only $1.14\times$ above the lower bound ($Q_{\text{lower}} \approx 357$). (b) Strong-dissipation regime ($\beta_I T \approx 338$): the $\log(1/\varepsilon)$ segmentation penalty of Dyson LCU dominates, giving $Q = 5408$ vs $Q = 1282$ for M-QSP ($4.22\times$ reduction) while the lower bound is $Q_{\text{lower}} \approx 680$.

The weak dissipation regime ($\beta_I/\alpha_R \approx 0.046$) is M-QSP’s optimal regime (Figure 3). The $1.57\times$ query reduction over Dyson LCU arises from eliminating the $\beta_I T \log(1/\varepsilon)$ segmentation penalty. The total runtime (expected number of repetitions) is Q/P ; with postselection cost $P \approx 2.2 \times 10^{-14}$ (the fundamental barrier of Theorem II.1, independent of the simulation method), M-QSP’s lower query count translates directly to a corresponding reduction in total circuit runs.

At stronger dissipation, M-QSP’s advantage over segmented Dyson LCU is $5,408/1,282 \approx 4.2\times$, driven by the tighter Taylor bound applied to the full accumulated $\beta_I T$ rather than to per-segment subintervals. Both methods sit within a factor of 2 of the $(\alpha_R + \beta_I)T = 676$ lower bound when $\beta_I T$ is large, in agreement with the leading-constant- ≈ 2 result of [27].

Postselection cost becomes obscenely expensive ($\sim 10^{295}$ repetitions), highlighting the fundamental block-encoding barrier. This regime motivates the open question (Sec. XIV D): can a direct-access construction achieve $P \approx e^{-2\omega T}$ with $\omega \ll \beta_I$, scalably reducing the repetition count?

XIV. DISCUSSION

Section XII compared the three simulation methods developed in this paper. We place the results in the broader context of non-Hermitian simulation, discussing the relationship to prior work at a structural level (complementing the per-method comparison of Sec. IC), and identifies open problems.

A. Oracle models

We draw a distinction in the oracle model used between the present work and the LCHS [22, 23], Schrödin-

gerization [3], and APS [24] methods. Those approaches encode $H_{\text{eff}} = H_R + iH_I$ into a single block-encoding unitary U_A , while our construction accesses H_R and H_I through independent walk operators W_R and U_I .

The lower bound $\Omega((\alpha_R + \beta_I)T + \log(1/\varepsilon))$ (Theorem III.1) is specific to the separate-oracle model, and additivity follows from oracle independence, as queries to W_R provide no information about H_I . In the single-oracle model, the bound takes a different form.

The choice of oracle model also affects postselection cost through the two-layer Postselection Barrier (Sec. II, Theorem II.1). Block-encoding overhead $e^{-2\beta_I T}$ (Theorem II.1) is specific to the polynomial block-encoding model, arising polynomial implementation bounded on the full bitorus \mathbb{T}^2 , including the unphysical region where the target function grows as $e^{+\beta_I T}$. Algorithms in other oracle models (APS via spectral filtering and Schrödingerization via dilational embedding) may avoid this overhead, though the intrinsic barrier remains.

Neither oracle model strictly dominates the other: the single-oracle model is natural when H_{eff} is given as a sparse matrix, while the separate-oracle model is natural when the physics has a distinguished coherent/dissipative decomposition (Lindblad master equations, AMO systems with independent coherent driving and dissipation, etc. Sec. IA).

B. Postselection Barrier in context

The two-layer Postselection Barrier of Sec. II (Theorems II.1 and II.1) sits alongside other characterizations in quantum information, distinguished by which layer is universal across oracle models and which is model-specific:

Result	Scope	Status
No-cloning	All QM	Universal
No-fast-forwarding	Query/Oracle	Model-specific
Postselection Barrier		
Intrinsic	Oracles	Universal
Block Encoding	Polynomial BE	Model-specific

The intrinsic layer is unconditional in the present sense, being independent of which oracle model the algorithm uses and acting as a “no-cheating-the-measurer” roadblock common among all non-Hermitian quantum simulation algorithms. The block-encoding layer is specific to the polynomial walk-operator framework and was not previously isolated as a distinct contribution to the postselection overhead. Whether direct-access methods that escape the walk-operator framework can avoid the block-encoding layer while retaining optimal query complexity remains open (see Sec. XIV D, item 4).

C. Relation to M-QSP theory

The M-QSP framework was introduced by Rossi and Chuang [19] and extended by Gomes, Lim, and Wiebe [20]. Subsequent work identified subtleties, with notable improvements made by Mori, Mizuta, and Fujii [56]. Németh et al. [52] constructed counterexamples to achievability conjectures in the commuting setting, while Laneve and Wolf [57] clarified the algebraic constraints.

A complementary line of work by Gomes, Lim, and Wiebe [20] (*iterated* QSP) achieves multivariate polynomial transformations by a different route. Instead of directly constructing a multivariate Fejér–Riesz-style factorization on the bitorus, they recursively compose univariate QSP sequences and build multivariate functions of scalar phases via logarithmic block-encoding (their Lemma 4) and quantum eigenvalue transformation (their Lemma 6). This sidesteps the multivariate FRT = QSP conjecture: because counterexamples [52, 57] preclude its use in general, iterated QSP provides an alternative constructive pathway that does not require the conjecture to hold. Their approach operates in the commuting scalar-phase regime, outputting a polynomial $P(\cos(\theta_1), \cos(\theta_2), \dots, \cos(\theta_R))$ in independent phases θ_i , each supplied by a separate $W_Z(\theta_i)$ signal unitary. The cost scales as $\mathcal{O}(d \sum_s d_s)$ for a degree- d outer polynomial applied to degree- d_s inner constructions (their Theorem 5). We address a structurally different problem, with complementarity brought between the broad function-class flexibility for commuting systems brought by Gomes, Lim, and Wiebe [20] and our query-optimality for the specific Dyson polynomial in the non-commuting setting, both sidestepping the multivariate FRT = QSP conjecture by different means.

By focusing on a non-Hermitian example, we built an angle-finding algorithm using block peeling and the development of a constant-ratio condition (CRC) (Theorem VII.1) by ancilla-factorization. We establish achievability of the Dyson polynomial (Theorem VIII.3) by direct construction. The non-commuting setting is structurally simpler for CRC, operating via the circuit’s block structure.

The counterexamples of Németh et al. [52] exploit algebraic structure of the commuting polynomial ring: when signal operators commute, the circuit polynomial belongs to $\mathbb{C}[z_1, z_1^{-1}, z_2, z_2^{-1}]$, and constraints on achievability reduce to questions about positivity certificates in this ring, admitting obstructions. In the non-commuting case, the circuit polynomial is a matrix-valued function whose entries depend on ordered products of signal-operator blocks. The ancilla-factorization proof of CRC operates on block structure directly. Consequently, algebraic obstructions that generate commuting counterexamples have no analog, carving an achievable subset without conflicting with Németh et al. [52].

D. Open problems

We collect directions left open by the present work, noting that several questions raised in the introduction have been resolved in the companion paper [27].

a. 1. Fast-forwarding (resolved negatively for worst case). The polynomial lower bound $d_I = \Omega(\beta_I T)$ of Theorem III.1 is tight: no polynomial in the bivariate separate-oracle model achieves faster β_I -scaling (This is proved in the companion paper). State-dependent improvement to $d_I = \mathcal{O}(\beta_{\text{eff}} T + \log(1/\varepsilon)/\log \log(1/\varepsilon))$ is possible via reduced Dyson truncation when $\beta_{\text{eff}} \ll \beta_I$, giving linear improvement. The $\sqrt{\beta_I}$ scaling of APS [24] requires the single-oracle model and multi-register post-selection, accessing a different physical regime.

b. 2. Time-dependent extension (resolved positively). The CRC (Theorem VII.1) extends to circuits with non-identical signal operators at each query, enabling simulation of time-dependent $H_{\text{eff}}(t) = H_R(t) + iH_I(t)$. Query complexity achieves $Q = \mathcal{O}(\int_0^T (\alpha_R(s) + \beta_I(s)) ds + \log(1/\varepsilon)/\log \log(1/\varepsilon))$, with the integral replacing the sum $(\alpha_R + \beta_I)T$ when parameters vary. (Full analysis in the companion paper.)

c. 3. Constant-factor optimization (resolved). Exhaustive optimization over the error budget allocation (Theorems XI.1 and companion paper analysis) yields $Q^* \approx 2 \cdot ((\alpha_R + \beta_I)T + \log(1/\varepsilon)/\log \log(1/\varepsilon))$ as the leading constant; numerical experiments confirm near-optimal constants, with the quantitative M-QSP-vs-Dyson-LCU and M-QSP-vs-LCHS improvement factors tabulated [27].

d. 4. Barrier universality (the central open question). The block-encoding barrier $e^{-2\beta_I T}$ holds within the walk-operator oracle model for all function classes (polynomials, Padé, rational). Schrödingerization achieves exactly this barrier. Direct-access methods that bypass the walk operator could in principle achieve the intrinsic barrier $e^{-2\omega T}$ where $\omega = \omega(H_{\text{eff}}) < \beta_I$ is the spectral abscissa. The gap $e^{2(\beta_I - \omega)T}$ is exponentially large when $[H_R, H_I] \neq 0$. The unresolved question considers if a polynomial construction can achieve $\lambda = e^{\omega T}$ while maintaining polynomial query complexity, if this construction is designed ab initio for direct access by exploiting matrix non-commutativity.

e. 5. Higher-order M-QSP. The bivariate construction uses two signal operators. A natural generalization is k -variate M-QSP with $k \geq 3$ signal operators. The CRC extends to k -variate circuits (the ancilla-factorization argument is insensitive to the number of signal operators), the SOS rank remains $L = 2$ (by the same 2×2 circuit unitarity), and block peeling generalizes to $\mathcal{O}(\prod_i d_i)$ per step. The quaternionic setting ($k = 4$) with generators i, j, k is the natural next application.

E. Broader significance

The technical contributions of this work include CRC for non-commuting operators (Theorem VII.1), SOS spectral factorization with degree preservation (Theorem VI.8), and constructive angle-finding for bivariate M-QSP (Theorem VIII.1). These do not depend on the specific structure of non-Hermitian Hamiltonians.

The universal CRC resolves a structural question about M-QSP circuits open since the framework was introduced [19, 20]: does the recursive degree-reduction procedure produce well-defined scalar angles when the signal operators do not commute? Theorem VII.1 answers this affirmatively, identifying ancilla factorization from tensor-product circuit structure, making non-commutativity irrelevant. Future multi-oracle quantum algorithm that encodes its computation as a bivariate ordered polynomial can use this result, regardless of the physical relationship between the two oracles. Candidates for application include multi-component Hamiltonian simulation with independent block-encodings [58], quantum linear algebra with separate oracles for different matrix operations [10], and hybrid quantum-classical variational circuits where two non-commuting parameterized unitaries are interleaved [59].

SOS spectral factorization addresses the bivariate Fejér–Riesz obstruction preventing scalar complementary polynomials from existing in two or more variables (Example VI.1). Sum-of-squares decomposition (Theorem VI.8) requires only $L = 2$ SOS terms (Theorem VI.7), introducing a constant overhead of just 2 ancilla qubits, applicable whenever a quantum algorithm needs to embed a bounded bivariate polynomial into a unitary circuit.

The constructive angle-finding algorithm extends classical preprocessing from univariate QSP to the bivariate setting. For multivariate QSP applications outside the non-commuting separate-oracle setting (e.g., bosonic simulation [20] or general multivariate polynomial synthesis on scalar phases), the iterated QSP framework of Gomes, Lim, and Wiebe [20] provides a complementary classical preprocessor, while the CRC and SOS-rank-2 results of the present paper apply to the matrix-valued non-commuting case that iterated QSP does not directly address. In univariate QSP, angle-finding has been the enabling technology that transforms existence theorems into implementable circuits; the algorithms of [53, 60–62] are routinely used as subroutines in end-to-end quantum algorithm design. Algorithm 1 plays the same role for bivariate M-QSP, converting theoretical achievability into quantum circuit parameters.

We show that QSP extends naturally from one variable to two, and from commuting to non-commuting operators, when applied as polynomial approximation composed with block-encoded signal operators, processed by a structured circuit with classically computed angles. QSP retains its characteristic properties of optimal query complexity, deterministic circuit construc-

tion, and a clean separation between the approximation-theoretic content (the choice of target polynomial) and algebraic content (the CRC, spectral factorization, and angle-finding). The non-Hermitian simulation problem served as the motivating application and stress test, but the mathematical infrastructure is domain-agnostic. Developing from this infrastructure, vastly more applications become available through query-optimal Hamiltonian simulation, to be discussed in future work.

XV. CODE AND DATA AVAILABILITY

The codebase accompanying this paper and its companion will be made available at a public repository at

the time of journal publication. It is available from the author on request.

XVI. CONFLICTS OF INTEREST

J.M.C. declares that they have no known competing financial interests or personal relationships that could have appeared to influence the work reported in this paper.

Appendix A: Error bounds for the Lorentzian method

Lemma A.1 (Lorentzian tail truncation and discretization). *Let $\gamma > 0$ and define the Lorentzian kernel*

$$L_\gamma(s) = \frac{\gamma/\pi}{s^2 + \gamma^2}, \quad (\text{A1})$$

so that $\int_{-\infty}^{\infty} L_\gamma(s) ds = 1$.

1. (Tail truncation.) For $s_{\max} > 0$,

$$\int_{|s| > s_{\max}} L_\gamma(s) ds = \frac{2}{\pi} \arctan\left(\frac{\gamma}{s_{\max}}\right) \leq \frac{2\gamma}{\pi s_{\max}}. \quad (\text{A2})$$

Choosing $s_{\max} = 2\gamma/(\pi \varepsilon_{\text{tail}})$ ensures the tail contribution is at most $\varepsilon_{\text{tail}}$.

2. (Riemann sum discretization.) Partition $[-s_{\max}, s_{\max}]$ into M equal subintervals of width $\Delta = 2s_{\max}/M$, with midpoints $s_j = -s_{\max} + (j - \frac{1}{2})\Delta$ for $j = 1, \dots, M$. Then

$$\left| \int_{-s_{\max}}^{s_{\max}} L_\gamma(s) f(s) ds - \Delta \sum_{j=1}^M L_\gamma(s_j) f(s_j) \right| \leq \frac{s_{\max} \Delta^2}{12} \sup_{|s| \leq s_{\max}} |(L_\gamma \cdot f)''(s)|, \quad (\text{A3})$$

where $f : \mathbb{R} \rightarrow \mathcal{B}(\mathcal{H})$ is a twice-differentiable operator-valued function. For $f(s) = e^{-i(H_R + sH_I)T}$, the second derivative satisfies

$$\|(L_\gamma \cdot f)''(s)\| \leq L_\gamma(s) (\beta_I^2 T^2 + 4\gamma|s|/(s^2 + \gamma^2)^2 \cdot \beta_I T + C_\gamma(s)), \quad (\text{A4})$$

where $C_\gamma(s) = |L_\gamma''(s)|/L_\gamma(s) = 2(3s^2 - \gamma^2)/(s^2 + \gamma^2)^2$ collects the kernel curvature terms. Specifically,

$$\sup_{|s| \leq s_{\max}} \|(L_\gamma \cdot f)''(s)\| \leq \frac{\gamma}{\pi\gamma^2} (\beta_I^2 T^2 + 4\beta_I T/\gamma + 6/\gamma^2) =: \frac{K}{\pi\gamma}, \quad (\text{A5})$$

so choosing $M = \lceil (s_{\max}^2 K / (3\pi\gamma \varepsilon_{\text{disc}}))^{1/2} \rceil$ ensures the discretization error is at most $\varepsilon_{\text{disc}}$.

3. (Combined bound.) Setting $\gamma = \beta_I$ (matching the physical decay rate), $\varepsilon_{\text{tail}} = \varepsilon_{\text{disc}} = \varepsilon/2$, the total approximation error is at most ε , with

$$s_{\max} = \frac{4\beta_I}{\pi\varepsilon}, \quad M = \mathcal{O}\left(\frac{\beta_I^2 T^2}{\varepsilon}\right). \quad (\text{A6})$$

This lemma treats the base case of midpoint quadrature ($p = 1$). For p -th order Magnus quadrature with $p \geq 2$, the quadrature error term in Theorem IX.1 improves to $C_p T^{2p+1}/r^{2p}$, reducing the segment count r and therefore overall discretization cost. The bound $M = \mathcal{O}(\beta_I^2 T^2/\varepsilon)$ above corresponds to the $p = 1$ specialization.

Proof. Part (a). Since L_γ is even and normalized, the tail integral is

$$\int_{|s|>s_{\max}} L_\gamma(s) ds = 1 - \int_{-s_{\max}}^{s_{\max}} L_\gamma(s) ds = 1 - \frac{\gamma}{\pi} \int_{-s_{\max}}^{s_{\max}} \frac{ds}{s^2 + \gamma^2}. \quad (\text{A7})$$

The integral evaluates by the standard arctangent antiderivative:

$$\int_{-s_{\max}}^{s_{\max}} \frac{ds}{s^2 + \gamma^2} = \frac{1}{\gamma} \left[\arctan\left(\frac{s}{\gamma}\right) \right]_{-s_{\max}}^{s_{\max}} = \frac{2}{\gamma} \arctan\left(\frac{s_{\max}}{\gamma}\right). \quad (\text{A8})$$

Substituting into Eq. (A7):

$$\int_{|s|>s_{\max}} L_\gamma(s) ds = 1 - \frac{2}{\pi} \arctan\left(\frac{s_{\max}}{\gamma}\right) = \frac{2}{\pi} \left[\frac{\pi}{2} - \arctan\left(\frac{s_{\max}}{\gamma}\right) \right] = \frac{2}{\pi} \arctan\left(\frac{\gamma}{s_{\max}}\right),$$

where the last equality uses $\arctan(x) + \arctan(1/x) = \pi/2$ for $x > 0$. The upper bound follows from $\arctan(u) \leq u$ for $u \geq 0$:

$$\frac{2}{\pi} \arctan\left(\frac{\gamma}{s_{\max}}\right) \leq \frac{2}{\pi} \cdot \frac{\gamma}{s_{\max}} = \frac{2\gamma}{\pi s_{\max}}. \quad (\text{A9})$$

Setting the right-hand side equal to $\varepsilon_{\text{tail}}$ and solving gives $s_{\max} = 2\gamma/(\pi \varepsilon_{\text{tail}})$.

Part (b). The midpoint Riemann sum for a function $g : [a, b] \rightarrow \mathbb{R}$ on M equal subintervals satisfies the standard error bound (see, e.g., [63])

$$\left| \int_a^b g(s) ds - \frac{b-a}{M} \sum_{j=1}^M g(s_j) \right| \leq \frac{(b-a)^3}{24 M^2} \sup_{s \in [a,b]} |g''(s)|. \quad (\text{A10})$$

Applying this to $g(s) = L_\gamma(s) f(s)$ on $[a, b] = [-s_{\max}, s_{\max}]$, with $(b-a) = 2s_{\max}$ and $\Delta = 2s_{\max}/M$, gives

$$\text{error} \leq \frac{(2s_{\max})^3}{24 M^2} \sup_{|s| \leq s_{\max}} \|(L_\gamma \cdot f)''(s)\| = \frac{s_{\max} \Delta^2}{12} \sup_{|s| \leq s_{\max}} \|(L_\gamma \cdot f)''(s)\|, \quad (\text{A11})$$

establishing Eq. (A3). It remains to bound the second derivative.

By the product rule, $(L_\gamma \cdot f)'' = L_\gamma'' f + 2L_\gamma' f' + L_\gamma f''$. We bound each term separately.

For the kernel derivatives:

$$\begin{aligned} L_\gamma'(s) &= -\frac{2\gamma s}{\pi(s^2 + \gamma^2)^2} \\ L_\gamma''(s) &= \frac{2\gamma(3s^2 - \gamma^2)}{\pi(s^2 + \gamma^2)^3}. \end{aligned} \quad (\text{A12})$$

These satisfy $|L_\gamma'(s)| \leq 2\gamma|s|/(\pi(s^2 + \gamma^2)^2)$ and $|L_\gamma''(s)| \leq 6\gamma/(\pi(s^2 + \gamma^2)^2)$ (using $|3s^2 - \gamma^2| \leq 3(s^2 + \gamma^2)$). For the propagator derivatives: since $f(s) = e^{-i(H_R + sH_I)T}$, differentiating with respect to s yields $f'(s) = -iT \widetilde{H}_I(s) f(s)$ in the interaction picture, where $\|\widetilde{H}_I(s)\| \leq \beta_I$. So, $\|f'(s)\| \leq \beta_I T$ and $\|f''(s)\| \leq \beta_I^2 T^2$.

Combining via the triangle inequality:

$$\begin{aligned} \|(L_\gamma \cdot f)''(s)\| &\leq |L_\gamma''(s)| \|f(s)\| + 2|L_\gamma'(s)| \|f'(s)\| + L_\gamma(s) \|f''(s)\| \\ &\leq \frac{6\gamma}{\pi(s^2 + \gamma^2)^2} + \frac{4\gamma|s| \beta_I T}{\pi(s^2 + \gamma^2)^2} + \frac{\gamma \beta_I^2 T^2}{\pi(s^2 + \gamma^2)}. \end{aligned}$$

Each term is maximized at $s = 0$ (the first two terms are maximized at or near $s = 0$; the third is exactly maximized there), giving

$$\sup_{|s| \leq s_{\max}} \|(L_\gamma \cdot f)''(s)\| \leq \frac{1}{\pi\gamma} (6/\gamma^2 + 4\beta_I T/\gamma + \beta_I^2 T^2) = \frac{K}{\pi\gamma}, \quad (\text{A13})$$

where we have used $(s^2 + \gamma^2)^{-1} \leq \gamma^{-2}$ and $|s|/(s^2 + \gamma^2)^2 \leq 1/(4\gamma^3)$ (the latter by arithmetic mean–geometric mean inequality (AM-GM): $|s|/(s^2 + \gamma^2)^2$ is maximized at $|s| = \gamma/\sqrt{3}$, giving a bound of $3\sqrt{3}/(16\gamma^3) < 1/(4\gamma^3)$).

The discretization error is therefore bounded by

$$\frac{s_{\max} \Delta^2 K}{12\pi\gamma} = \frac{s_{\max} (2s_{\max})^2 K}{12\pi\gamma M^2} = \frac{4s_{\max}^3 K}{12\pi\gamma M^2} = \frac{s_{\max}^3 K}{3\pi\gamma M^2}. \quad (\text{A14})$$

Setting this equal to $\varepsilon_{\text{disc}}$ and solving:

$$M = \left\lceil \sqrt{\frac{s_{\max}^3 K}{3\pi\gamma \varepsilon_{\text{disc}}}} \right\rceil. \quad (\text{A15})$$

Part (c). Set $\gamma = \beta_I$. Then $K = \beta_I^2 T^2 + 4\beta_I T/\beta_I + 6/\beta_I^2 = \beta_I^2 T^2 + 4T + 6/\beta_I^2$. For the physically relevant regime $\beta_I T \gg 1$, the dominant term is $K \approx \beta_I^2 T^2$. With $\varepsilon_{\text{tail}} = \varepsilon_{\text{disc}} = \varepsilon/2$:

$$s_{\max} = \frac{2\beta_I}{\pi(\varepsilon/2)} = \frac{4\beta_I}{\pi\varepsilon}. \quad (\text{A16})$$

Substituting into the expression for M and retaining only the leading terms:

$$M = \mathcal{O}\left(\sqrt{\frac{s_{\max}^3 \beta_I^2 T^2}{\beta_I \varepsilon}}\right) = \mathcal{O}\left(\sqrt{\frac{(\beta_I/\varepsilon)^3 \beta_I^2 T^2}{\beta_I \varepsilon}}\right) = \mathcal{O}\left(\frac{\beta_I^2 T}{\varepsilon^2}\right). \quad (\text{A17})$$

The cruder bound $M = \mathcal{O}(\beta_I^2 T^2/\varepsilon)$ stated in the lemma follows from a slightly looser estimate $s_{\max}^2 K/(\gamma\varepsilon) \leq (\beta_I/\varepsilon)^2 \cdot \beta_I^2 T^2/\beta_I \cdot 1/\varepsilon = \beta_I^3 T^2/\varepsilon^3$, simplified under $\beta_I T \geq 1$. The total number of Hermitian simulations in the LCHS circuit is M , each requiring $\mathcal{O}(\alpha_R T + \beta_I T + \log(M/\varepsilon))$ queries to the block-encoding of $H_R + s_j H_I$.

Remark A.1 (Sharpness and alternatives). The $\arctan(\gamma/s_{\max})$ formula in Eq. (A9) is exact, so tail truncation bound is tight.

The Riemann sum bound is not tight. The Lorentzian kernel is analytic and decays algebraically, so the trapezoidal rule with the same number of points achieves superalgebraic convergence by the Euler–Maclaurin formula. [22, 23] exploit this by using Gauss–Hermite or tanh-sinh quadrature, reducing the number of quadrature points to $M = \mathcal{O}(\text{polylog}(\beta_I T/\varepsilon))$. The midpoint rule analysis given here provides the baseline against which these improved quadratures should be compared, and suffices for the complexity comparison in Table I.

Corollary A.1 (Polylogarithmic regime for Lorentzian IP). *Let $\varepsilon > 0$ and suppose the Hermitian simulation subroutine at each quadrature point uses a product formula of order $2p$. Then the total query complexity of the Lorentzian inner-product algorithm is minimized at*

$$p^* = \left\lceil \frac{1}{2} \frac{\log(\beta_I T/\varepsilon)}{\log \log(\beta_I T/\varepsilon)} \right\rceil, \quad (\text{A18})$$

with $r^* = \mathcal{O}(\text{polylog}(\beta_I T/\varepsilon))$ quadrature points, yielding total query complexity

$$Q_{\text{LIP}} = \mathcal{O}((\alpha_R + \beta_I) T \text{polylog}(\beta_I T/\varepsilon)). \quad (\text{A19})$$

Proof. The Lorentzian IP algorithm discretizes the integral

$$e^{-\beta_I T} e^{-iH_{\text{eff}} T} = \int_{-\infty}^{\infty} L_{\gamma}(s) e^{-i(H_R + s_j H_I) T} ds \quad (\text{A20})$$

using r quadrature points on the truncated interval $[-s_{\max}, s_{\max}]$, with each Hermitian propagator $e^{-i(H_R + s_j H_I) T}$ implemented by a $(2p)$ th-order product formula. The three error sources and their parameter dependences are:

(i) *Tail truncation* (Lemma A.1(a)): error $\leq 2\gamma/(\pi s_{\max})$. Setting this to $\varepsilon/3$ gives $s_{\max} = 6\gamma/(\pi\varepsilon)$.

(ii) *Quadrature discretization.* For the Lorentzian kernel, which is analytic in a strip of half-width γ about the real axis, the trapezoidal rule on r equally spaced points achieves exponential convergence (Trefethen–Weideman [64]):

$$\varepsilon_{\text{quad}} \leq C e^{-2\pi\gamma r/(2s_{\max})} = C e^{-\pi^2 \varepsilon r/6}, \quad (\text{A21})$$

where C depends polynomially on $\beta_I T$ and we have substituted $s_{\max} = 6\gamma/(\pi\varepsilon)$ with $\gamma = \beta_I$. Setting $\varepsilon_{\text{quad}} \leq \varepsilon/3$ and solving:

$$r = \left\lceil \frac{6}{\pi^2 \varepsilon} \log\left(\frac{3C}{\varepsilon}\right) \right\rceil = \mathcal{O}\left(\frac{1}{\varepsilon} \log \frac{\beta_I T}{\varepsilon}\right). \quad (\text{A22})$$

This can be improved. Using the substitution $s = \gamma \sinh(u)$ (the tanh-sinh change of variables), mapping the Lorentzian to a function with double-exponential decay, the trapezoidal rule on r points achieves

$$\varepsilon_{\text{quad}} \leq C' e^{-c \pi^2 r / \log r}, \quad (\text{A23})$$

and setting this to $\varepsilon/3$ gives

$$r = \mathcal{O}(\text{polylog}(\beta_I T / \varepsilon)). \quad (\text{A24})$$

We use this sharper bound from here on.

(iii) *Product-formula error.* Each of the r Hermitian simulations approximates $e^{-iH_j T}$ with $H_j = H_R + s_j H_I$, $\|H_j\| \leq \alpha_R + s_{\max} \beta_I$. A single Trotter step of order $2p$ has error (Childs et al. [65])

$$\varepsilon_{\text{Trot}}(n_j) \leq \frac{c_p (\|H_j\| T)^{2p+1}}{n_j^{2p}}, \quad (\text{A25})$$

where n_j is the number of Trotter steps and c_p depends only on p and the number of terms in the Hamiltonian splitting. Setting $\varepsilon_{\text{Trot}}(n_j) \leq \varepsilon/(3r)$ (union bound over r quadrature points) and solving for n_j :

$$n_j = \left\lceil \left(\frac{3r c_p (\|H_j\| T)^{2p+1}}{\varepsilon} \right)^{1/(2p)} \right\rceil. \quad (\text{A26})$$

Each Trotter step uses $\mathcal{O}(1)$ queries to the block-encodings of H_R and H_I , so the per-point query cost is $\mathcal{O}(n_j)$ and the total query cost across all r points is

$$Q = \sum_{j=1}^r \mathcal{O}(n_j) = r \cdot \mathcal{O}\left(\left(\frac{r (\alpha_R + s_{\max} \beta_I)^{2p+1} T^{2p+1}}{\varepsilon} \right)^{1/(2p)} \right). \quad (\text{A27})$$

Substituting $s_{\max} = \mathcal{O}(\beta_I/\varepsilon)$ and simplifying:

$$Q = \mathcal{O}\left(r^{1+1/(2p)} \left(\frac{(\alpha_R + \beta_I^2/\varepsilon)^{2p+1} T^{2p+1}}{\varepsilon} \right)^{1/(2p)} \right). \quad (\text{A28})$$

Joint optimization over p . Increasing p reduces the Trotter exponent $1/(2p)$ but increases the base $(\|H_j\| T)^{(2p+1)/(2p)}$. We write the dominant contribution to the query cost as

$$Q \sim r (\|H_j\| T)^{1+1/(2p)} \cdot (r/\varepsilon)^{1/(2p)}. \quad (\text{A29})$$

Setting $\Lambda = \|H_j\| T$ and taking logarithms:

$$\log Q \approx \log r + \log \Lambda + \frac{1}{2p} (\log \Lambda + \log(r/\varepsilon)). \quad (\text{A30})$$

The p -dependent term is $(\log \Lambda + \log(r/\varepsilon))/(2p)$. For fixed r (already polylogarithmic from step (ii)), this is minimized as $p \rightarrow \infty$, but c_p grows factorially: $c_p = \mathcal{O}(p!)$ for generic splittings, or $c_p = \mathcal{O}((2p)!/p!)$ for the Yoshida–Suzuki symmetric decomposition [42, 66]. Including c_p in the Trotter bound, the per-step cost becomes

$$n_j \sim (c_p \Lambda^{2p+1}/\varepsilon)^{1/(2p)} = \Lambda (c_p \Lambda/\varepsilon)^{1/(2p)}. \quad (\text{A31})$$

Using Stirling's approximation $c_p^{1/(2p)} \approx (2p/e)^{1/2}$ for large p , the cost scales as $n_j \sim \Lambda (p \Lambda/\varepsilon)^{1/(2p)}$. The exponent $1/(2p)$ drives the multiplicative overhead toward 1 as p increases, but the prefactor $p^{1/(2p)}$ grows (albeit slowly). The optimal trade-off occurs when the overhead $(p \Lambda/\varepsilon)^{1/(2p)} = \mathcal{O}(1)$, i.e., when

$$\frac{1}{2p} \log\left(\frac{p \Lambda}{\varepsilon}\right) = \mathcal{O}(1). \quad (\text{A32})$$

Solving for p at leading order (neglecting the $\log p$ correction inside the logarithm):

$$p^* = \Theta\left(\frac{\log(\Lambda/\varepsilon)}{\log \log(\Lambda/\varepsilon)}\right) = \Theta\left(\frac{\log(\beta_I T/\varepsilon)}{\log \log(\beta_I T/\varepsilon)}\right), \quad (\text{A33})$$

where we use $\log \Lambda = \log((\alpha_R + \beta_I^2/\varepsilon)T) = \mathcal{O}(\log(\beta_I T/\varepsilon))$.

Resulting complexity. At $p = p^*$, the Trotter overhead satisfies $(c_{p^*} \Lambda/\varepsilon)^{1/(2p^*)} = \mathcal{O}(1)$, so $n_j = \mathcal{O}(\Lambda) = \mathcal{O}((\alpha_R + \beta_I^2/\varepsilon)T)$. The total query cost is

$$Q = r \cdot \mathcal{O}(n_j) = \mathcal{O}(\text{polylog}(\beta_I T/\varepsilon)) \cdot \mathcal{O}((\alpha_R + \beta_I^2/\varepsilon)T) = \mathcal{O}((\alpha_R + \beta_I)T \text{polylog}(\beta_I T/\varepsilon)),$$

where in the last line we have used that $\beta_I^2 T/\varepsilon = \beta_I T \cdot (\beta_I/\varepsilon)$ and the β_I/ε factor is absorbed into the polylogarithmic term (it contributes $\log(\beta_I/\varepsilon)$ multiplicatively, which is polylogarithmic).

The formula for p^* in Eq. (A18) follows by taking the ceiling and the factor of $1/2$ from the convention that the product formula has order $2p$ (so the exponent in the error bound is $2p$, not p).

Remark A.2. Polylogarithmic overhead in Eq. (A19) relative to the information-theoretic lower bound $\Omega((\alpha_R + \beta_I)T + \log(1/\varepsilon))$ arises from the $r = \mathcal{O}(\text{polylog})$ quadrature points (each requiring a separate Hermitian simulation) and the residual Trotter overhead at finite p^* . Neither source can be removed within the LCHS framework without changing the simulation subroutine: replacing the product formula with an optimal Hermitian simulation algorithm (e.g., QSP-based) at each quadrature point would eliminate the Trotter overhead but retain the r -fold multiplicative cost. The multiplicative structure is why Lorentzian IP approach cannot match the additive lower bound, motivating the non-split-operator M-QSP construction of the present work.

Appendix B: Dyson LCU error budget

Lemma B.1 (Taylor truncation of the Dyson series). *Let $V(T) = \mathcal{T}_> \exp(-\int_0^T \tilde{H}(s) ds)$ with $\|\tilde{H}(s)\| \leq \beta_I$ for all s , and let $V_N(T) = \sum_{n=0}^N V_n(T)$ denote the truncation at order N . Then*

$$\|V(T) - V_N(T)\| \leq \sum_{n=N+1}^{\infty} \frac{(\beta_I T)^n}{n!} = e^{\beta_I T} - \sum_{n=0}^N \frac{(\beta_I T)^n}{n!}. \quad (\text{B1})$$

Choosing

$$N = \left\lceil \frac{e \beta_I T}{W(3e \beta_I T/\varepsilon)} \right\rceil = \mathcal{O}\left(\beta_I T + \frac{\log(1/\varepsilon)}{\log \log(1/\varepsilon)}\right) \quad (\text{B2})$$

ensures $\|V(T) - V_N(T)\| \leq \varepsilon/3$, where W denotes the principal branch of the Lambert W -function.

Proof. The norm bound on each Dyson term follows from time-ordering:

$$\|V_n(T)\| = \left\| (-i)^n \int_{0 \leq t_1 \leq \dots \leq t_n \leq T} \tilde{H}(t_n) \dots \tilde{H}(t_1) dt_1 \dots dt_n \right\| \leq \frac{(\beta_I T)^n}{n!}, \quad (\text{B3})$$

where the simplex has volume $T^n/n!$ and each operator factor is bounded by β_I . The tail $\|V(T) - V_N(T)\| \leq \sum_{n \geq N+1} (\beta_I T)^n/n!$ follows by the triangle inequality, establishing Eq. (B1).

We bound the leading term of the tail, since for $N \geq \beta_I T$ the series is monotonically decreasing and geometric:

$$\sum_{n=N+1}^{\infty} \frac{(\beta_I T)^n}{n!} \leq \frac{(\beta_I T)^{N+1}}{(N+1)!} \cdot \frac{1}{1 - \beta_I T/(N+2)} \leq \frac{2(\beta_I T)^{N+1}}{(N+1)!}, \quad (\text{B4})$$

where the last inequality uses $N \geq 2\beta_I T - 2$ (which will be verified below). We therefore require

$$\frac{(\beta_I T)^{N+1}}{(N+1)!} \leq \frac{\varepsilon}{6}. \quad (\text{B5})$$

Stirling bound. By Stirling's inequality in the form $(N+1)! \geq \sqrt{2\pi(N+1)}(N+1)^{N+1}e^{-(N+1)}$, the left-hand side of Eq. (B5) is bounded by

$$\frac{(\beta_I T)^{N+1}}{(N+1)!} \leq \frac{1}{\sqrt{2\pi(N+1)}} \left(\frac{e\beta_I T}{N+1} \right)^{N+1}. \quad (\text{B6})$$

Setting $M = N+1$ and $\lambda = \beta_I T$ for readability, the requirement becomes

$$\left(\frac{e\lambda}{M} \right)^M \leq \varepsilon/6 \quad \iff \quad M \log \left(\frac{e\lambda}{M} \right) \leq \log(\varepsilon/6). \quad (\text{B7})$$

We seek the smallest M such that $(e\lambda/M)^M \leq \varepsilon/6$. Taking logarithms and rearranging:

$$M(1 + \log \lambda - \log M) \leq \log(\varepsilon/6). \quad (\text{B8})$$

This is satisfied when $M \geq e\lambda / \exp(W(x))$ where $x = e\lambda \cdot 6/\varepsilon$, by the following argument.

Lambert W-function solution. The equation $(e\lambda/M)^M = \delta$ (with $\delta = \varepsilon/6$) is equivalent to $M(\log(e\lambda) - \log M) = \log \delta$, i.e.,

$$M \log M - M \log(e\lambda) = -\log \delta = \log(1/\delta). \quad (\text{B9})$$

Setting $M = e\lambda/t$ for $t > 1$:

$$\frac{e\lambda}{t} (\log(e\lambda) - \log t - \log(e\lambda)) = -\frac{e\lambda \log t}{t} = -\log(1/\delta), \quad (\text{B10})$$

so $\log t/t = \log(1/\delta)/(e\lambda)$. Writing $t = e^u$, this becomes $ue^{-u} = \log(1/\delta)/(e\lambda)$, or equivalently $u = W(e\lambda/\log(1/\delta))$.

We want the smallest M such that $(\beta/M)^M \leq \delta$ where $\beta = e\lambda$. Taking the M th root, this is $\beta/M \leq \delta^{1/M}$, i.e., $M \geq \beta \delta^{-1/M}$. For M large enough that $\delta^{-1/M} \approx 1$, we need M slightly above β . Using the Lambert W -function, the equation $(\beta/M)^M = \delta$ is equivalent to

$$M = \frac{\beta}{W(\beta/\log(1/\delta))} \cdot \frac{\log(1/\delta)}{\beta} \cdot \frac{\beta}{1} = \frac{\log(1/\delta)}{W(\beta \log(1/\delta)^{-1} \cdot \beta)}, \quad (\text{B11})$$

which simplifies (see Kalugin et al. [67, 68]) to

$$M = \frac{\log(1/\delta)}{W((\log(1/\delta))/\beta \cdot e^{(\log(1/\delta))/\beta})} = \frac{e\lambda}{W(e\lambda/\delta)}, \quad (\text{B12})$$

following from the identity $W(xe^x) = x$.

To verify Eq. (B12), we set $M = e\lambda/W(e\lambda/\delta)$ and define $w = W(e\lambda/\delta)$, so that $we^w = e\lambda/\delta$. Then

$$\left(\frac{e\lambda}{M} \right)^M = w^{e\lambda/w} = \exp\left(\frac{e\lambda \log w}{w} \right). \quad (\text{B13})$$

From $we^w = e\lambda/\delta$ we get $\log w + w = \log(e\lambda/\delta)$, so $\log w = \log(e\lambda/\delta) - w$. Substituting:

$$\frac{e\lambda \log w}{w} = \frac{e\lambda}{w} (\log(e\lambda/\delta) - w) = \frac{e\lambda \log(e\lambda/\delta)}{w} - e\lambda. \quad (\text{B14})$$

Using $e\lambda/w = M$ and $e\lambda \log(e\lambda/\delta)/w = M \log(e\lambda/\delta)$:

$$\left(\frac{e\lambda}{M} \right)^M = \exp(M \log(e\lambda/\delta) - e\lambda). \quad (\text{B15})$$

For $M = e\lambda/w$ to satisfy the bound, we need this expression $\leq \delta$, i.e., $M \log(e\lambda/\delta) - e\lambda \leq \log \delta$. This holds with equality at $M = e\lambda/w$ by construction of the Lambert W -function. Choosing $N+1 = \lceil M \rceil$ with $\delta = \varepsilon/6$ gives

$$N = \left\lceil \frac{e\beta_I T}{W(6e\beta_I T/\varepsilon)} - 1 \right\rceil = \left\lceil \frac{e\beta_I T}{W(3e\beta_I T/\varepsilon)} \right\rceil, \quad (\text{B16})$$

where the replacement of 6 by 3 in the argument of W absorbs the -1 and the ceiling, up to the level of precision of the asymptotic formula (both give the same leading-order behavior).

Asymptotic expansion. For $x \rightarrow \infty$, the Lambert W -function satisfies (Kalugin et al. [67, 68])

$$W(x) = \log x - \log \log x + o(1). \quad (\text{B17})$$

Substituting $x = 3e\beta_I T/\varepsilon$:

$$N = \frac{e\beta_I T}{\log(3e\beta_I T/\varepsilon) - \log \log(3e\beta_I T/\varepsilon) + o(1)} = \frac{e\beta_I T}{\log(\beta_I T/\varepsilon) (1 + o(1))}.$$

Two regimes emerge:

Regime A: $\beta_I T \geq \log(1/\varepsilon)$. Then the numerator $e\beta_I T$ dominates and $N = \mathcal{O}(\beta_I T / \log(\beta_I T)) = \mathcal{O}(\beta_I T)$.

Regime B: $\beta_I T \ll \log(1/\varepsilon)$. Then $\log(3e\beta_I T/\varepsilon) \approx \log(1/\varepsilon)$ and $N \approx e\beta_I T / \log(1/\varepsilon) \ll 1$, so the tail bound is already controlled at $N = 0$ for sufficiently small $\beta_I T$. The binding constraint in this regime comes from $(\beta_I T)^{N+1}/(N+1)!$, where setting $N = \mathcal{O}(\log(1/\varepsilon)/\log \log(1/\varepsilon))$ ensures the factorial suppression overcomes the $1/\varepsilon$ requirement.

Combining both regimes:

$$N = \mathcal{O}\left(\beta_I T + \frac{\log(1/\varepsilon)}{\log \log(1/\varepsilon)}\right), \quad (\text{B18})$$

where the first term dominates when $\beta_I T$ is large and the second when ε is small. The two terms are additive because they control different regimes of the tail bound.

Finally, we verify $N \geq 2\beta_I T - 2$ (used in Eq. (B4)). In Regime A, $N = \Theta(\beta_I T) \geq 2\beta_I T - 2$ for $\beta_I T$ sufficiently large (and small $\beta_I T$ can be handled by adjusting the constant). In Regime B, $\beta_I T$ is small, so $2\beta_I T - 2 < 0$ and the condition is trivially satisfied.

Lemma B.2 (Error budget for the Dyson LCU). *Let $\varepsilon > 0$ be the target simulation error for the Dyson LCU method of Sec. X. Allocate*

$$\varepsilon_{\text{Taylor}} = \frac{\varepsilon}{3}, \quad \varepsilon_{\text{GQSP}} = \frac{\varepsilon}{3}, \quad \varepsilon_{\text{LCU}} = \frac{\varepsilon}{3}. \quad (\text{B19})$$

Then the following parameter choices ensure total error at most ε :

1. (Taylor truncation order.) $N = \lceil e\beta_I T / W(3e\beta_I T/\varepsilon) \rceil$ as in Lemma B.1, so that $\|V(T) - V_N(T)\| \leq \varepsilon/3$. This gives $d_I = N$ queries to U_I .
2. (GQSP degree per segment.) Each of the $r = N$ Dyson segments requires a frame rotation $e^{\pm i H_R \Delta_j}$ implemented by GQSP with the walk operator W_R . The Jacobi–Anger expansion truncated at degree $d_R^{(j)}$ approximates $e^{\pm i \alpha_R \Delta_j \cos \theta}$ with error $\eta(d_R^{(j)})$ (equation (B23)). Since the r segments are composed sequentially, the errors accumulate additively, and we require $\sum_{j=1}^r \eta(d_R^{(j)}) \leq \varepsilon/3$.

For uniform time steps $\Delta_j = T/N$, each segment has the same GQSP degree

$$d_R = \left\lceil \frac{e\alpha_R T}{2N} + \log\left(\frac{3N}{\varepsilon}\right) \right\rceil, \quad (\text{B20})$$

and the total number of W_R queries is

$$Q_R = N \cdot d_R = \mathcal{O}(\alpha_R T + N \log(N/\varepsilon)) = \mathcal{O}(\alpha_R T + \beta_I T \log(\beta_I T/\varepsilon)). \quad (\text{B21})$$

3. (LCU coefficients.) The Dyson LCU prepares the state $\sum_{n=0}^N \sqrt{w_n} |n\rangle$ on the selection register, where $w_n = (\beta_I T)^n / (n! W_{\text{tot}})$ and $W_{\text{tot}} = \sum_{n=0}^N (\beta_I T)^n / n!$. The preparation uses $\mathcal{O}(\log N)$ ancilla qubits and $\mathcal{O}(N)$ gates, contributing no additional queries to W_R or U_I . The LCU postselection succeeds with probability $W_{\text{tot}}^2 / (e^{\beta_I T})^2$, and the error from the finite LCU truncation is already absorbed into $\varepsilon_{\text{Taylor}}$.

Total query complexity of the Dyson LCU is therefore

$$Q_{\text{Dyson}} = Q_R + d_I = \mathcal{O}(\alpha_R T + \beta_I T \log(\beta_I T/\varepsilon)), \quad (\text{B22})$$

where the $\beta_I T \log(\beta_I T/\varepsilon)$ term arises from the product $N \cdot d_R$ and represents the split-operator penalty: each of the $N = \mathcal{O}(\beta_I T)$ segments independently requires $\mathcal{O}(\log(\beta_I T/\varepsilon))$ queries for the GQSP frame rotation.

Proof. The three error sources act in sequence on the postselected output:

$$\|\text{output} - e^{-\beta_I T} e^{-iH_{\text{eff}} T}\| \leq \underbrace{\|V(T) - V_N(T)\|/e^{\beta_I T}}_{\text{Taylor: } \leq \varepsilon_{\text{Taylor}}/e^{\beta_I T}} + \underbrace{\sum_{j=1}^N \eta(d_R^{(j)})}_{\text{GQSP: } \leq \varepsilon_{\text{GQSP}}} + \underbrace{\varepsilon_{\text{LCU}}}_{\text{LCU: finite register}}.$$

With the equal allocation $\varepsilon/3$ to each source, the total is at most ε .

For part (1), the bound follows from Lemma B.1. For part (2), the per-segment GQSP error is bounded by the Jacobi–Anger truncation estimate

$$\eta(d_R) \leq 2 \exp\left(-d_R + d_R \log\left(\frac{e \alpha_R T}{2N d_R}\right)\right). \quad (\text{B23})$$

Setting $\eta(d_R) \leq \varepsilon/(3N)$ and solving: $d_R = \lceil (e \alpha_R T)/(2N) + \log(3N/\varepsilon) \rceil$. Multiplying by N :

$$N d_R = \frac{e \alpha_R T}{2} + N \log\left(\frac{3N}{\varepsilon}\right) = \mathcal{O}(\alpha_R T + \beta_I T \log(\beta_I T/\varepsilon)), \quad (\text{B24})$$

using $N = \mathcal{O}(\beta_I T + \log(1/\varepsilon)/\log \log(1/\varepsilon))$ and $\log(N/\varepsilon) = \mathcal{O}(\log(\beta_I T/\varepsilon))$.

For part (3), the LCU protocol is exact given the prepared coefficients; the only error is the Taylor truncation already accounted for in part (1). The $\varepsilon_{\text{LCU}} = \varepsilon/3$ allocation provides margin for finite-precision effects in the state preparation circuit, which contribute $\mathcal{O}(N 2^{-b})$ error for b -bit coefficient precision (negligible for $b = \mathcal{O}(\log(N/\varepsilon))$).

The split-operator penalty is visible in the final complexity: $Q_R = \mathcal{O}(\alpha_R T + \beta_I T \log(\beta_I T/\varepsilon))$ exceeds the information-theoretic lower bound $\Omega(\alpha_R T + \log(1/\varepsilon))$ by the multiplicative factor $\beta_I T$ on the logarithmic term. This is the cost of composing N independent GQSP circuits rather than a single bivariate M-QSP circuit, and it is the overhead eliminated by the construction of Sec. XI.

Appendix C: $\Omega(\beta_I T)$ lower bound

Theorem C.1 (Query lower bound for anti-Hermitian simulation). *A quantum algorithm that, given query access to a walk operator U_I of H_I/β_I (with $H_I \geq 0$, $\|H_I\| \leq \beta_I$), produces a state ε -close to $e^{-iH_{\text{eff}} T} |\psi_0\rangle / \|e^{-iH_{\text{eff}} T} |\psi_0\rangle\|$ must use $\Omega(\beta_I T)$ queries to U_I , for fixed $\varepsilon < 1/2$.*

We use polynomial approximation theory (yielding a sharper constant) and state discrimination (yielding a cleaner conceptual argument).

Proof 1: Polynomial method, with explicit constant. Reducing to a polynomial approximation of $e^{-\beta_I T x}$ on $[0, 1]$, subject to $|p(x)| \leq 1$ on $[-1, 1]$, follows Beals et al. [36], with a Bernstein/Stirling bound on the best polynomial approximation error. This is given in the proof of Lemma III.2 (Sec. III). Here we extract the explicit constant.

By Lemma III.2, the algorithm produces a degree- $2Q$ polynomial p with $\|p\|_{[-1,1]} \leq 1$ that ε' -approximates $e^{-\beta_I T x}/e^{\beta_I T}$ on $[0, 1]$, with $\varepsilon' = \varepsilon/e^{\beta_I T}$. The Kolmogorov–Bernstein inequality [69] bounds the best uniform approximation error by

$$E_Q(e^{-\beta_I T \cdot}/e^{\beta_I T}; [0, 1]) \geq c_Q \frac{(\beta_I T)^{Q+1}}{e^{\beta_I T} (Q+1)!}, \quad (\text{C1})$$

with $c_Q > 0$ a constant depending only on the interval. By Stirling, the right-hand side exceeds a fixed $\varepsilon' > 0$ unless $Q \gtrsim \beta_I T/e$. The sharper threshold $Q \geq \beta_I T/(2e)$ follows by tracking the constant in the Stirling expansion: for $Q < \beta_I T/(2e)$,

$$\frac{(\beta_I T)^{Q+1}}{(Q+1)!} \geq \left(\frac{e \beta_I T}{Q+1}\right)^{Q+1} \cdot \frac{1}{\sqrt{2\pi(Q+1)}} \geq (2e)^{Q+1}/\sqrt{2\pi \beta_I T}, \quad (\text{C2})$$

which contradicts $\varepsilon' < 1/2$ for sufficiently large $\beta_I T$. Hence $Q \geq \beta_I T/(2e) = \Omega(\beta_I T)$, sharpening the $\Omega(\beta_I T)$ bound of Lemma III.2 with an explicit constant.

Remark C.1 (Why the hybrid method yields only a constant bound). The hybrid lower bound for state discrimination can be established by comparing two instances: A with $H_I = 0$ and B with $H_I = \beta_I |1\rangle\langle 1|$. The corresponding final states $\Psi(0)$ and $\Psi(\beta_I)$ are distinguishable with success probability at least $1/2$ (by appropriate measurement design).

Partition the parameter path $\eta \in [0, \beta_I]$ into M steps of size $\Delta\eta = \beta_I/M$. The per-step state change is bounded by $2Q \cdot \Delta\eta/\beta_I$ (the advantage contributed by each query applied to one oracle instance). By the triangle inequality, the total state separation satisfies

$$\|\Psi(\beta_I) - \Psi(0)\| \leq \sum_{m=1}^M \frac{2Q\Delta\eta}{\beta_I} = M \cdot \frac{2Q\Delta\eta}{\beta_I} = 2Q. \quad (\text{C3})$$

Since this bound is independent of M , no matter how finely the parameter path is discretized, the distinguishability lower bound combined with $\|\Psi(\beta_I) - \Psi(0)\| \leq 2Q$ yields only $Q \geq 1/4$ (a constant).

The polynomial method (Proof 1) circumvents this limitation by exploiting the approximation-theoretic complexity of the exponential profile, rather than the geometric distance between output states.

Remark C.2 (Combining the W_R and U_I lower bounds). An analogous argument establishes $d_R = \Omega(\alpha_R T)$: the phase $e^{-i\alpha_R T \cos \theta}$ oscillates $\Omega(\alpha_R T)$ times on $\theta \in [0, 2\pi)$, and a Laurent polynomial of degree d_R in $e^{i\theta}$ can have at most $2d_R$ sign changes. (This is the standard Hamiltonian simulation lower bound of [37].)

Since queries to W_R provide no information about H_I and vice versa (the oracles are independent), the two lower bounds are additive:

$$d_R + d_I = \Omega(\alpha_R T) + \Omega(\beta_I T) = \Omega((\alpha_R + \beta_I)T). \quad (\text{C4})$$

The $\log(1/\varepsilon)$ term in the full lower bound $\Omega((\alpha_R + \beta_I)T + \log(1/\varepsilon))$ follows from a separate argument: distinguishing the ε -approximation from an exact implementation requires $\Omega(\log(1/\varepsilon))$ queries by the quantum counting lower bound [70].

Appendix D: Jacobi–Anger bridge: from walk operator to Laurent polynomial

Here, we establish correspondence between the walk operator W_R encoding H_R/α_R and the Laurent polynomial variable $z_1 = e^{i\theta_1}$ appearing in the Dyson polynomial $P_{\text{Dyson}}(z_1, z_2)$. We focus on the Szegő walk-operator formalism ([71], as adapted by Low and Chuang [11]) with the Jacobi–Anger expansion to assemble the bridge.

1. Walk operator and Chebyshev structure

Definition D.1 (Walk operator). Let U_R be an $(a_R + n)$ -qubit unitary that block-encodes H_R/α_R :

$$(\langle 0|_{a_R} \otimes I_n) U_R (|0\rangle_{a_R} \otimes I_n) = H_R/\alpha_R. \quad (\text{D1})$$

The walk operator is the self-inverse reflection $W_R = (2\Pi_R - I)U_R$, where $\Pi_R = |0\rangle\langle 0|_{a_R} \otimes I_n$ is the projector onto the ancilla-zero subspace.

The essential spectral property of W_R is the following.

Proposition D.1 (Walk-operator spectrum). Let λ_j be an eigenvalue of H_R/α_R with $|\lambda_j| \leq 1$, and define $\theta_{1,j} = \arccos(\lambda_j) \in [0, \pi]$. Then W_R has eigenvalues $e^{\pm i\theta_{1,j}}$ on a two-dimensional invariant subspace spanned by

$$|\pm_j\rangle = \frac{1}{\sqrt{2}} (|0\rangle_{a_R} |\psi_j\rangle \pm i e^{\mp i\theta_{1,j}} |\perp_j\rangle), \quad (\text{D2})$$

where $|\psi_j\rangle$ is the corresponding eigenvector of H_R and $|\perp_j\rangle$ is the component of $U_R |0\rangle_{a_R} |\psi_j\rangle$ orthogonal to the ancilla-zero subspace, normalized so that $\| |\perp_j\rangle \| = \sin \theta_{1,j}$.

Proof. This is the standard qubitization result of Low and Chuang [11], Theorem 4. The hypotheses are: (i) U_R is a block-encoding of a Hermitian operator with $\|H_R/\alpha_R\| \leq 1$, and (ii) $W_R = (2\Pi_R - I)U_R$. Both hold by construction (Definition D.1). The proof is a direct computation: $U_R |0\rangle_{a_R} |\psi_j\rangle = \cos \theta_{1,j} |0\rangle_{a_R} |\psi_j\rangle + \sin \theta_{1,j} |\perp_j\rangle$, and the action of the reflection $2\Pi_R - I$ on this decomposition produces the claimed eigenvalues and eigenvectors.

The Chebyshev connection follows from the power structure of W_R restricted to the ancilla-zero subspace.

Lemma D.1 (Chebyshev identity for walk-operator powers). *For an integer $n \geq 0$,*

$$\langle 0|_{a_R} \otimes I \rangle W_R^n (|0\rangle_{a_R} \otimes I) = T_n(H_R/\alpha_R), \quad (\text{D3})$$

where T_n is the Chebyshev polynomial of the first kind of degree n .

Proof. On the eigenspace with eigenphase $\theta_{1,j}$, the ancilla-zero projections of the eigenstates (D2) satisfy $\langle 0|_{a_R} |\pm_j\rangle = |\psi_j\rangle/\sqrt{2}$. Therefore

$$\langle 0|_{a_R} W_R^n |0\rangle_{a_R} = \langle 0|_{a_R} \left(e^{in\theta_{1,j}} |+_j\rangle\langle+_j| + e^{-in\theta_{1,j}} |-_j\rangle\langle-_j| \right) |0\rangle_{a_R} = \frac{1}{2} (e^{in\theta_{1,j}} + e^{-in\theta_{1,j}}) |\psi_j\rangle\langle\psi_j| = \cos(n\theta_{1,j}) |\psi_j\rangle\langle\psi_j|.$$

Since $\lambda_j = \cos\theta_{1,j}$ and $T_n(\cos\theta) = \cos(n\theta)$ by definition, this gives $\langle 0|_{a_R} W_R^n |0\rangle_{a_R} |_{\text{eigenspace } j} = T_n(\lambda_j) |\psi_j\rangle\langle\psi_j|$. Summing over all eigenspaces yields Eq. (D3).

For negative n , the result holds with $T_{|n|}$ by the same argument using W_R^{-1} , since $T_n = T_{|n|}$ for Chebyshev polynomials.

Remark D.1 (Hypotheses verification). The derivation above uses three properties of W_R :

1. W_R is unitary (inherited from U_R unitary and $2\Pi_R - I$ unitary).
2. The spectrum of W_R is $\{e^{\pm i\theta_{1,j}}\}$ with $\theta_{1,j} = \arccos(\lambda_j)$, and invariant subspaces are two-dimensional (requiring $|\lambda_j| < 1$; the boundary cases $|\lambda_j| = 1$ yield one-dimensional eigenspaces with eigenvalue ± 1 , where $T_n(\pm 1) = (\pm 1)^n$ and the formula still holds).
3. The ancilla-zero projection $\langle 0|_{a_R} |\pm_j\rangle$ is nonzero (this holds whenever $\sin\theta_{1,j} \neq 0$, i.e., $|\lambda_j| < 1$; for $|\lambda_j| = 1$ the eigenstates are $|0\rangle_{a_R} |\psi_j\rangle$ and the projection is trivially $|\psi_j\rangle$).

All three hold for block-encodings of Hermitian operators with $\|H_R/\alpha_R\| \leq 1$.

2. Laurent polynomial conversion

The Chebyshev identity (D3) expresses W_R^n in the ancilla-zero subspace as a polynomial in H_R/α_R . The conversion to a Laurent polynomial in $z_1 = e^{i\theta_1}$ uses the elementary identity

$$T_n(\cos\theta_1) = \cos(n\theta_1) = \frac{e^{in\theta_1} + e^{-in\theta_1}}{2} = \frac{z_1^n + z_1^{-n}}{2}. \quad (\text{D4})$$

A Chebyshev expansion $\sum_{n=0}^{d_R} c_n T_n(\cos\theta_1)$ corresponds to the Laurent polynomial

$$\sum_{n=0}^{d_R} c_n T_n(\cos\theta_1) = \frac{c_0}{1} + \sum_{n=1}^{d_R} \frac{c_n}{2} (z_1^n + z_1^{-n}) = \sum_{n=-d_R}^{d_R} \hat{c}_n z_1^n, \quad (\text{D5})$$

with $\hat{c}_0 = c_0$, $\hat{c}_n = \hat{c}_{-n} = c_{|n|}/2$ for $n \neq 0$. This is a symmetric Laurent polynomial of degree d_R in z_1 .

3. The Jacobi–Anger expansion

Frame rotations in the Dyson series involve matrix exponentials $e^{\pm iH_R s}$. On each eigenspace of H_R with eigenvalue $\alpha_R \cos\theta_1$, the frame rotation produces the phase $e^{\pm i\alpha_R s \cos\theta_1}$. The Jacobi–Anger identity expands this phase in Chebyshev polynomials.

Proposition D.2 (Jacobi–Anger expansion). *For a $\tau \in \mathbb{R}$,*

$$e^{-i\tau \cos\theta} = J_0(\tau) + 2 \sum_{n=1}^{\infty} (-i)^n J_n(\tau) T_n(\cos\theta), \quad (\text{D6})$$

where J_n is the Bessel function of the first kind of order n . Equivalently, in Laurent polynomial form:

$$e^{-i\tau \cos\theta} = \sum_{n=-\infty}^{\infty} (-i)^{|n|} J_{|n|}(\tau) e^{in\theta}. \quad (\text{D7})$$

Proof. This is the classical Jacobi–Anger identity; see Watson [72] or Lozier [73]. The second form follows from $T_n(\cos\theta) = (e^{in\theta} + e^{-in\theta})/2$ and $J_{-n} = (-1)^n J_n$.

Lemma D.2 (Jacobi–Anger truncation). *For $|\tau| > 0$ and $\varepsilon > 0$, the Jacobi–Anger expansion truncated at degree d satisfies*

$$\left\| e^{-i\tau \cos\theta} - \sum_{|n| \leq d} (-i)^{|n|} J_{|n|}(\tau) e^{in\theta} \right\|_{\infty} \leq \varepsilon \quad (\text{D8})$$

provided

$$d \geq \left\lceil \frac{e|\tau|}{2} + \log(1/\varepsilon) \right\rceil. \quad (\text{D9})$$

Proof. The Bessel function satisfies the bound $|J_n(\tau)| \leq (e|\tau|/(2n))^n$ for $n > e|\tau|/2$ ([72] or [74]). The tail sum is

$$\sum_{|n| > d} |J_{|n|}(\tau)| \leq 2 \sum_{n=d+1}^{\infty} \left(\frac{e|\tau|}{2n} \right)^n \leq 2 \sum_{n=d+1}^{\infty} \left(\frac{e|\tau|}{2(d+1)} \right)^n = \frac{2r^{d+1}}{1-r}, \quad r = \frac{e|\tau|}{2(d+1)}.$$

For $d \geq \lceil e|\tau|/2 + \log(1/\varepsilon) \rceil$, we have $r \leq e|\tau|/(e|\tau| + 2\log(1/\varepsilon) + 2) < 1$, and specifically $r \leq 1/(1 + 2\log(1/\varepsilon)/(e|\tau|))$. The geometric series yields $2r^{d+1}/(1-r) \leq \varepsilon$.

The detailed verification: when $d+1 \geq e|\tau|/2 + \log(1/\varepsilon) + 1$, we have $r \leq e|\tau|/(e|\tau| + 2\log(1/\varepsilon) + 2)$. Since $r < 1$ and $d+1 \geq e|\tau|/2 + \log(1/\varepsilon) + 1$,

$$r^{d+1} \leq r^{e|\tau|/2 + \log(1/\varepsilon) + 1} \leq e^{-(d+1)(1-r)} \leq e^{-\log(1/\varepsilon) - 1} = \varepsilon/e. \quad (\text{D10})$$

The factor $2/(1-r)$ is bounded by $\mathcal{O}(1 + e|\tau|/\log(1/\varepsilon))$, which is absorbed into the ceiling.

4. Assembling the bridge

We now connect the three ingredients to express the Dyson polynomial in terms of the walk operator.

Proposition D.3 (Jacobi–Anger bridge). *Let $V_N(T)$ be the N th-order Dyson series approximation to the interaction-picture propagator, expressed on the tensor-product eigenspace of the walk operators W_R and U_I (acting on $\mathcal{H}_s \otimes \mathcal{H}_{\alpha_R} \otimes \mathcal{H}_{\alpha_I}$) with eigenphases (θ_1, θ_2) satisfying $\alpha_R \cos\theta_1 = \lambda_R$, $\beta_I \cos\theta_2 = \lambda_I$ for eigenvalues λ_R of H_R and λ_I of H_I . The Jacobi–Anger expansion converts $V_N(T)$ into a bivariate Laurent polynomial:*

$$V_N(T)|_{(\theta_1, \theta_2)} = \sum_{|m| \leq d_R} \sum_{n=0}^N c_{m,n} z_1^m z_2^n, \quad (\text{D11})$$

where $z_1 = e^{i\theta_1}$, $z_2 = e^{i\theta_2}$, the coefficients $c_{m,n}$ are determined by the Jacobi–Anger coefficients and the Dyson integrals, and $d_R = \lceil e\alpha_R T/2 + \log(3N/\varepsilon) \rceil$ ensures accuracy $\varepsilon/3$ from the Jacobi–Anger truncation (Lemma D.2 applied with per-segment error $\varepsilon/(3N)$ and summed over N segments).

Explicitly, the n th Dyson term is

$$V^{(n)}(T) = (-1)^n \int_{T > s_1 > \dots > s_n > 0} \prod_{j=1}^n \left(e^{iH_R s_j} H_I e^{-iH_R s_j} \right) ds_1 \dots ds_n. \quad (\text{D12})$$

On this tensor-product eigenspace, each factor $e^{iH_R s_j} H_I e^{-iH_R s_j}$ contributes:

1. A phase $e^{i\alpha_R s_j \cos\theta_1} \cdot e^{-i\alpha_R s_j \cos\theta_1} = 1$ from the commuting part (the frame rotations cancel pairwise within each factor).
2. The eigenvalue $\beta_I \cos\theta_2$ from H_I/β_I acting on the eigenstate, contributing a power of $z_2 + z_2^{-1} = 2\cos\theta_2$ (block-encoding). After normalization, the n th term contributes degree n in $\cos\theta_2$.

3. Frame rotations do not cancel when operating on the walk operator (as opposed to the Hamiltonian eigenspace). The n th Dyson term involves $2n$ frame rotations ($e^{\pm iH_R s_j}$ for each of the n factors), each expanded via Jacobi–Anger. Only the outermost pair of frame rotations ($e^{iH_R T}$ at the left and I at the right) contributes net phase, and intermediate frame rotations $e^{-iH_R s_j} e^{iH_R s_{j+1}}$ produce phases $e^{i\alpha_R(s_{j+1}-s_j)\cos\theta_1}$, which are expanded individually.

$V^{(n)}$ becomes a sum of terms, each involving a product of $n+1$ Jacobi–Anger expansions (for the $n+1$ intervals $[0, s_n], [s_n, s_{n-1}], \dots, [s_1, T]$). The convolution structure of the ordered integral ensures that the total z_1 -degree is at most d_R (the Jacobi–Anger truncation degree for the full interval $[0, T]$), not $(n+1)d_R$, because the Jacobi–Anger coefficients convolve multiplicatively in the Fourier domain:

$$\sum_{|m|\leq d_R} c_m^{(n)} z_1^m = \int_{T>s_1>\dots>s_n>0} \prod_{j=0}^n \left(\sum_{|k|\leq d_R^{(j)}} (-i)^{|k|} J_{|k|}(\alpha_R \Delta_j) z_1^k \right) ds, \quad (\text{D13})$$

where $\Delta_0 = s_n$, $\Delta_j = s_{n-j} - s_{n-j+1}$ for $1 \leq j \leq n-1$, and $\Delta_n = T - s_1$.

The convolution of $n+1$ Laurent polynomials of degrees $d_R^{(0)}, \dots, d_R^{(n)}$ has degree at most $\sum_j d_R^{(j)}$. $\sum_{j=0}^n \Delta_j = T$ for every integration point, so we can set $d_R^{(j)} = \lceil e\alpha_R \Delta_j / 2 + \log(3N(n+1)/\varepsilon) / (n+1) \rceil$ and obtain total degree $d_R = \lceil e\alpha_R T / 2 + \log(3N/\varepsilon) \rceil$ by the additivity of the Bessel bounds.

Total Jacobi–Anger error for the n th Dyson term is bounded by the sum of per-interval errors (since the truncation errors compose linearly in the interaction picture), and the allocation $\varepsilon_{\text{JA}}/(3N)$ per Dyson order ensures total Jacobi–Anger error at most $\varepsilon/3$ after summing over N orders.

The z_2 variable enters through the block-encoding U_I . On the eigenspace of H_I/β_I with eigenvalue $\cos\theta_2$, each query to U_I extracts one power of the signal variable. The n th Dyson order involves n applications of H_I , contributing degree n in the U_I -signal variable. After truncation at order N , the maximum z_2 -degree is $d_I = N$.

Corollary D.1 (Walk-operator implementation). *On the ancilla-zero subspace, the M -QSP circuit $G(\Theta, \mathbf{s})$ that makes d_R queries to W_R and d_I queries to U_I implements a bivariate Laurent polynomial $P(z_1, z_2)$ of bidegree (d_R, d_I) . The correspondence is:*

$$\begin{aligned} \text{Each query to } W_R &\longleftrightarrow \text{multiplication by } z_1^{\pm 1} \text{ (via Lemma D.1),} \\ \text{Each query to } U_I &\longleftrightarrow \text{multiplication by } z_2^{\pm 1} \text{ (via block-encoding signal),} \\ \text{Each rotation } R_k &\longleftrightarrow \text{scalar coefficient (signal-independent).} \end{aligned} \quad (\text{D14})$$

The target polynomial $P_\delta = (1-\delta) P_{\text{Dyson}}(z_1, z_2)/e^{\beta_I T}$ is valid for this circuit, with the bidegree and norm bounds established in Lemma B.2.

Appendix E: Recursive angle-finding: full specification

This appendix provides the complete pseudocode for Algorithm 1 (the recursive angle-finding procedure for bivariate M -QSP), including all edge cases, the FFT-based optimization variant, the warm-start strategy, and the complexity analysis.

1. Notation and conventions

- $d = d_R + d_I$: total degree (total number of oracle queries).
- $\mathbf{s} = (s(1), s(2), \dots, s(d)) \in \{R, I\}^d$: the Dyson schedule, specifying whether query k is to W_R (type R) or U_I (type I).
- $d_R^{(k)}, d_I^{(k)}$: the remaining number of R - and I -queries after step k . Initially $d_R^{(0)} = d_R, d_I^{(0)} = d_I$. At step k , $d_{s(k)}^{(k)} = d_{s(k)}^{(k-1)} - 1$ and $d_{\bar{s}(k)}^{(k)} = d_{\bar{s}(k)}^{(k-1)}$.
- $P^{(k)}(z_1, z_2)$: the residual polynomial at step k , of bidegree $(d_R^{(k)}, d_I^{(k)})$. Initially $P^{(0)} = P_\delta$.
- $a_j^{(k)}, b_j^{(k)}$: the leading and subleading Fourier coefficients of $P^{(k)}$ in the variable $z_{s(k+1)}$ (the variable corresponding to the next query).
- θ_k, ϕ_k : the rotation angles at step k , parameterizing $R_k = e^{i\phi_k Z/2} e^{-i\theta_k Y}$ on the ancilla qubit.

2. The CRC at each step

At step k , the circuit has the form $G^{(k)} = R_k A_{s(k+1)} G^{(k+1)}$, where $A_{s(k+1)}$ is the next signal operator query. The $(0, 0)$ -block of $G^{(k)}$ in the ancilla space implements $P^{(k)}$, and the CRC (Theorem VII.1) guarantees that the ratio

$$\frac{b_{d_s(k+1)}^{(k)}}{a_{d_s(k+1)}^{(k)}} = e^{-i\phi_k} \frac{\sin \theta_k}{\cos \theta_k} \quad (\text{E1})$$

is a scalar (independent of both signal operators' eigenvalues), where $a_{d_s(k+1)}^{(k)}$ is the leading coefficient of $P^{(k)}$ in $z_{s(k+1)}$ and $b_{d_s(k+1)}^{(k)}$ is the leading coefficient of the complementary polynomial $Q^{(k)}$.

The angle extraction is:

$$\theta_k = \arctan\left(\left|b_{d_s(k+1)}^{(k)} / a_{d_s(k+1)}^{(k)}\right|\right), \quad (\text{E2})$$

$$\phi_k = -\arg\left(b_{d_s(k+1)}^{(k)} / a_{d_s(k+1)}^{(k)}\right). \quad (\text{E3})$$

The residual polynomial is then:

$$P^{(k+1)}(z_1, z_2) = \frac{1}{\cos \theta_k} \left(P^{(k)} - e^{i\phi_k} \sin \theta_k \cdot z_{s(k+1)}^{d_s(k+1)} Q_{\text{red}}^{(k)} \right), \quad (\text{E4})$$

where $Q_{\text{red}}^{(k)}$ is the appropriately reduced complementary polynomial obtained from the SOS factorization. The bidegree of $P^{(k+1)}$ is $(d_R^{(k+1)}, d_I^{(k+1)})$, reduced by one in the $s(k+1)$ variable.

3. Algorithm 1: Recursive angle-finding

The auxiliary polynomial $\tilde{Q}_1^{(k)}$ in the degree-reduction step is defined by:

$$\tilde{Q}_1^{(k)}(z_1, z_2) = z_\sigma^{-d_\sigma} Q_1^{(k)}(z_1, z_2), \quad (\text{E5})$$

which is a Laurent polynomial of bidegree $(d_R^{(k)}, d_I^{(k)}) - \mathbf{e}_\sigma$ (degree reduced by one in the σ variable), since the leading coefficient in z_σ was factored out.

4. Algorithm 2: FFT-based optimization variant

The recursive algorithm's $\mathcal{O}((d_R + d_I) \cdot d_R \cdot d_I)$ cost may be reduced for large bidegrees by a gradient-based optimization in the Fourier domain.

Cost per iteration: $\mathcal{O}(d \cdot N_1 N_2) = \mathcal{O}((d_R + d_I) \cdot d_R \cdot d_I)$, the same as one pass of the recursive algorithm. The advantage is that the optimization can improve numerical accuracy beyond what the recursive algorithm achieves (which propagates rounding errors linearly through d steps).

5. Warm-start strategy

The recommended workflow combines both algorithms:

1. **Recursive initialization.** Run Algorithm 2 to obtain $\Theta^{(0)}$. This is exact in infinite numerical precision and provides a warm start in the correct basin of attraction. Cost: $\mathcal{O}((d_R + d_I) \cdot d_R \cdot d_I)$.
2. **Gradient refinement.** Run Algorithm 3 starting from $\Theta^{(0)}$ for a small number of iterations ($t_{\max} = \mathcal{O}(\log(1/\varepsilon_{\text{mach}}))$ typically suffices) to polish angles to machine precision.
Cost: $\mathcal{O}(t_{\max} \cdot (d_R + d_I) \cdot d_R \cdot d_I)$.

Algorithm 2. Recursive bivariate M-QSP angle-finding

Require: Target polynomial $P_\delta(z_1, z_2)$ of bidegree (d_R, d_I) with $\|P_\delta\|_{\mathbb{T}^2} < 1$; Dyson schedule $\mathbf{s} \in \{R, I\}^d$ with $d = d_R + d_I$;
SOS complement $\{Q_\ell\}_{\ell=1}^L$ satisfying $|P_\delta|^2 + \sum_\ell |Q_\ell|^2 = 1$ on \mathbb{T}^2 .
Ensure: Rotation angles $\{(\theta_k, \phi_k)\}_{k=0}^d$.

```

1:  $P^{(0)} \leftarrow P_\delta$ 
2:  $\{Q_\ell^{(0)}\}_\ell \leftarrow \{Q_\ell\}_\ell$ 
3:  $d_R^{(0)} \leftarrow d_R$ ;  $d_I^{(0)} \leftarrow d_I$ 
4: for  $k = d, d-1, \dots, 1$  do
5:    $\sigma \leftarrow s(k)$  {query type at step  $k$ :  $R$  or  $I$ }
6:    $d_\sigma \leftarrow d_\sigma^{(d-k)}$  {current degree in variable  $z_\sigma$ }
7:   // Extract leading coefficients
8:    $a \leftarrow [z_\sigma^{d_\sigma}] P^{(d-k)}$  {leading coefficient of  $P$  in  $z_\sigma$ ; a function of  $z_{\bar{\sigma}}$ }
9:    $b \leftarrow [z_\sigma^{d_\sigma}] Q_1^{(d-k)}$  {leading coefficient of first complementary polynomial}
10:  // Edge case 1: vanishing leading coefficient
11:  if  $\|a\|_\infty < \epsilon_{\text{mach}}$  then
12:     $\theta_k \leftarrow \pi/2$ ;  $\phi_k \leftarrow 0$  {pure reflection: all weight on  $Q$ }
13:    swap  $P^{(d-k)} \leftrightarrow Q_1^{(d-k)}$ 
14:    continue
15:  end if
16:  // Edge case 2: vanishing complementary leading coefficient
17:  if  $\|b\|_\infty < \epsilon_{\text{mach}}$  then
18:     $\theta_k \leftarrow 0$ ;  $\phi_k \leftarrow 0$  {pure transmission: all weight on  $P$ }
19:    continue
20:  end if
21:  // CRC: extract scalar ratio (Theorem VII.1)
22:   $r \leftarrow b/a$  {scalar by CRC; verify  $\|r - r(z_{\bar{\sigma}})\|_\infty < \epsilon_{\text{tol}}$ }
23:  if  $\max_{z_{\bar{\sigma}}} |r(z_{\bar{\sigma}}) - r(0)| > \epsilon_{\text{tol}}$  then
24:    raise CRC violation error
25:  end if
26:   $r_0 \leftarrow$  mean or median of  $r(z_{\bar{\sigma}})$  over sample points
27:  // Compute angles
28:   $\theta_k \leftarrow \arctan(|r_0|)$ 
29:   $\phi_k \leftarrow -\arg(r_0)$ 
30:  // Degree reduction
31:   $P^{(d-k+1)} \leftarrow \frac{P^{(d-k)} - e^{i\phi_k} \sin \theta_k \cdot z_\sigma^{d_\sigma} \tilde{Q}_1^{(d-k)}}{\cos \theta_k}$  { $\tilde{Q}_1$ : see Eq. (E5) below}
32:  Update each  $Q_\ell^{(d-k+1)}$  analogously
33:   $d_\sigma^{(d-k+1)} \leftarrow d_\sigma - 1$ ;  $d_{\bar{\sigma}}^{(d-k+1)} \leftarrow d_{\bar{\sigma}}^{(d-k)}$ 
34:  // Verification (optional)
35:  if verification enabled then
36:    Check  $\|P^{(d-k+1)}\|_{\mathbb{T}^2} < 1$ 
37:    Check bidegree of  $P^{(d-k+1)}$  is  $(d_R^{(d-k+1)}, d_I^{(d-k+1)})$ 
38:    Check  $|P^{(d-k+1)}|^2 + \sum_\ell |Q_\ell^{(d-k+1)}|^2 = 1$  on sample points
39:  end if
40: end for
41: // Final constant: step  $k = 0$ 
42:  $P^{(d)}$  is a scalar  $c_0 \in \mathbb{C}$  with  $|c_0| < 1$ 
43:  $\theta_0 \leftarrow \arcsin(|c_0|)$ ;  $\phi_0 \leftarrow \arg(c_0)$ 
44: return  $\{(\theta_k, \phi_k)\}_{k=0}^d$ 

```

Algorithm 3. FFT-based angle optimization

Require: Target polynomial P_δ (as 2D Fourier coefficient array of size $(2d_R + 1) \times (2d_I + 1)$); Dyson schedule \mathbf{s} ; initial angles $\Theta^{(0)} = \{(\theta_k^{(0)}, \phi_k^{(0)})\}$ (from Algorithm 2 or random initialization).
Ensure: Refined angles Θ^* .

```

1: for iteration  $t = 1, 2, \dots, t_{\max}$  do
2:   // Forward pass: compute circuit polynomial via 2D FFT
3:   Construct the circuit unitary  $G(\Theta^{(t-1)}, \mathbf{s})$  on a grid of  $(N_1, N_2)$  points  $(\theta_1^{(j)}, \theta_2^{(k)})$  with  $N_1 \geq 2d_R + 1, N_2 \geq 2d_I + 1$ 
4:   Extract  $P_{\text{circ}}(\theta_1^{(j)}, \theta_2^{(k)}) = \langle 0 | G(\Theta^{(t-1)}, \mathbf{s}) | 0 \rangle$  on each grid point { $\mathcal{O}(d \cdot N_1 N_2)$  operations}
5:   // Objective:  $L^2$  error on  $\mathbb{T}^2$ 
6:    $\mathcal{L}(\Theta) \leftarrow \frac{1}{N_1 N_2} \sum_{j,k} |P_{\text{circ}}(\theta_1^{(j)}, \theta_2^{(k)}) - P_\delta(\theta_1^{(j)}, \theta_2^{(k)})|^2$ 
7:   // Gradient via adjoint differentiation
8:   Compute  $\nabla_{\Theta} \mathcal{L}$  by back-propagation through the circuit product  $G = R_0 \prod_{j=1}^d A_{\mathbf{s}(j)} R_j$  { $\mathcal{O}(d \cdot N_1 N_2)$  per gradient}
9:   // Update
10:   $\Theta^{(t)} \leftarrow \Theta^{(t-1)} - \eta_t \nabla_{\Theta} \mathcal{L}$  {step size  $\eta_t$ ; use Adam or L-BFGS}
11: end for
12: return  $\Theta^{(t_{\max})}$ 

```

The warm start is important because the optimization landscape for M-QSP angle-finding is non-convex; the objective $\mathcal{L}(\Theta)$ generically has local minima. In the univariate case ($d_I = 0$), it is conjectured (but not proved) that all local minima are global [62]. In the bivariate case, we can locate no such conjecture. The recursive algorithm provides a starting point that is already a global optimum (in exact arithmetic), leaving gradient refinement to correct only finite-precision errors without risk of converging to a spurious minimum.

6. Complexity analysis

Proposition E.1 (Complexity of angle-finding). *Algorithm 2 computes all $d + 1 = d_R + d_I + 1$ rotation angles in*

$$\mathcal{O}((d_R + d_I) \cdot d_R \cdot d_I) \tag{E6}$$

arithmetic operations over \mathbb{C} , using $\mathcal{O}(d_R \cdot d_I)$ storage.

Proof. At each of the $d = d_R + d_I$ steps, the algorithm performs the following operations:

1. **Leading coefficient extraction.** The polynomial $P^{(k)}$ is stored as a 2D Fourier coefficient array of size at most $(2d_R^{(k)} + 1) \times (2d_I^{(k)} + 1)$. Extracting the leading coefficient in z_σ requires reading one row or column of the array: $\mathcal{O}(d_\sigma^{(k)})$ operations.
2. **CRC verification.** Checking that the ratio b/a is constant (to tolerance ϵ_{tol}) requires evaluating $b(z_{\bar{\sigma}})/a(z_{\bar{\sigma}})$ at $\mathcal{O}(d_\sigma^{(k)})$ points: $\mathcal{O}(d_\sigma^{(k)})$ operations.
3. **Degree reduction.** Computing $P^{(k+1)}$ from $P^{(k)}$ via Eq. (E4) requires subtracting a rank-one update (the product $z_\sigma^{d_\sigma} \tilde{Q}_1^{(k)}$) and dividing by $\cos \theta_k$. This modifies the coefficient array in-place: $\mathcal{O}(d_R^{(k)} \cdot d_I^{(k)})$ operations.
4. **Complementary polynomial update.** Each of the L complementary polynomials is updated similarly: $\mathcal{O}(L \cdot d_R^{(k)} \cdot d_I^{(k)})$ operations. Since $L \leq \min(d_R + 1, d_I + 1)$ and the complementary polynomials' degrees decrease with P , the total cost across all L polynomials is $\mathcal{O}(d_I \cdot d_R^{(k)} \cdot d_I^{(k)})$ per step.

The dominant cost is item (iv). Summing over all d steps:

$$C_{\text{total}} = \sum_{k=0}^{d-1} \mathcal{O}(d_I \cdot d_R^{(k)} \cdot d_I^{(k)}) \leq \mathcal{O}(d_I \cdot d_R \cdot d_I \cdot d) / d = \mathcal{O}((d_R + d_I) \cdot d_R \cdot d_I),$$

where the second line uses the fact that $d_R^{(k)}$ and $d_I^{(k)}$ decrease monotonically, so their product averaged over all steps is at most $d_R \cdot d_I/2$ (by the AM–GM inequality on the partial sums).

Storage: the coefficient arrays for P and the L complementary polynomials require $\mathcal{O}(L \cdot d_R \cdot d_I) = \mathcal{O}(d_I \cdot d_R \cdot d_I) = \mathcal{O}(d_R \cdot d_I^2)$ total. In practice, $d_I \leq d_R$ in most parameter regimes (since $\beta_I \leq \alpha_R$ for weakly dissipative systems), so storage is $\mathcal{O}(d_R \cdot d_I)$ per polynomial.

Remark E.1 (Numerical stability). The recursive algorithm propagates errors linearly: if the leading coefficient extraction at step k incurs error ϵ_k , the residual polynomial $P^{(k+1)}$ inherits error at most $\epsilon_k/|\cos \theta_k|$. The total accumulated error after d steps is bounded by

$$\epsilon_{\text{total}} \leq \sum_{k=0}^{d-1} \frac{\epsilon_k}{\prod_{j=k}^{d-1} |\cos \theta_j|}. \quad (\text{E7})$$

The condition number of the recursion is therefore $\kappa = \prod_{j=0}^{d-1} |\cos \theta_j|^{-1} = \prod_{j=0}^{d-1} \sec \theta_j$. For the Dyson polynomial, angles θ_j are small ($\theta_j = \mathcal{O}(1/d)$ on average, since the polynomial is close to the identity for small ε), giving $\kappa = \mathcal{O}(\exp(\sum_j \theta_j^2)) = \mathcal{O}(d_R + d_I)$ (polynomial, not exponential).

In the worst case (when some θ_j approaches $\pi/2$, meaning the polynomial has a near-zero leading coefficient), the condition number can grow. δ -regularization ($P_\delta = (1 - \delta)P$) prevents this, ensuring $|P_\delta| \leq 1 - \delta$ on \mathbb{T}^2 , guaranteeing no θ_j reaches $\pi/2$ during the recursion (Definition VI.2). The resulting condition number is $\kappa \leq \mathcal{O}(1/\delta) = \mathcal{O}(\beta_I T/\varepsilon)$.

Appendix F: Case Analysis for Example VI.1

We verify that $H = 4 - 2 \cos \theta_1 - 2 \cos \theta_2$ has no representation $|Q|^2$ for $Q(z_1, z_2) = a + bz_1 + cz_2 + dz_1z_2$.

Expanding $|Q(e^{i\theta_1}, e^{i\theta_2})|^2$ and matching Fourier coefficients gives the system:

$$\begin{aligned} |a|^2 + |b|^2 + |c|^2 + |d|^2 &= 4, \\ \bar{a}b + \bar{c}d &= -1, \\ \bar{a}c + \bar{b}d &= -1, \\ \bar{a}d &= 0, \\ \bar{b}c &= 0. \end{aligned} \quad (\text{F1})$$

We see $a = 0$ or $d = 0$, and $b = 0$ or $c = 0$.

Case 1 ($d = 0, c = 0$): $\bar{a}b = -1$, but $0 = -1$. Contradiction.

Case 2 ($d = 0, b = 0$): $0 = -1$. Contradiction.

Case 3 ($a = 0, c = 0$): $\bar{b}d = -1$, but $0 = -1$. Contradiction.

Case 4 ($a = 0, b = 0$): $0 = -1$. Contradiction.

No solution exists.

Appendix G: Notation and Convention

Symbol	Definition
$H_{\text{eff}} = H_R + iH_I$	Effective non-Hermitian Hamiltonian, $H_R = H_R^\dagger$, $H_I \succeq 0$
α_R, β_I	$\alpha_R := \ H_R\ _{\text{op}}$, $\beta_I := \ H_I\ _{\text{op}}$
W_R	Walk operator encoding H_R/α_R on $\mathcal{H}_s \otimes \mathcal{H}_{a_R}$
U_I	Walk operator encoding H_I/β_I on $\mathcal{H}_s \otimes \mathcal{H}_{a_I}$
$V(T)$	Interaction-picture propagator: $e^{iH_R T} e^{-iH_{\text{eff}} T}$
$\tilde{H}_I(s)$	$e^{iH_R s} H_I e^{-iH_R s}$ (interaction-picture Hamiltonian)
$\mathcal{H}_a, \mathcal{H}_s$	QSP ancilla and system Hilbert spaces
$\mathbf{s} \in \{R, I\}^{d_R+d_I}$	Binary schedule of oracle queries
(d_R, d_I)	Bidegree of bivariate Laurent polynomial
Poly_{d_R, d_I}^+	Non-negative Laurent polynomials of bidegree $\leq (d_R, d_I)$ on \mathbb{T}^2
$\mathbb{T}^2 = \mathbb{T} \times \mathbb{T}$	Bitorus (product of two unit circles)
$z_1 = e^{i\theta_1}, z_2 = e^{i\theta_2}$	Coordinates on \mathbb{T}^2
ε	Target operator-norm approximation error

Appendix H: Bivariate Spectral Factorization

This appendix establishes the sum-of-squares (SOS) decomposition used in the complementary polynomial construction of Sec. VI. For $H \in \mathcal{T}_{d_1, d_2}$ with $H > 0$ on \mathbb{T}^2 and $H = 1 - |P|^2$ for some $P \in \mathcal{P}_{d_1, d_2}^+$, we show:

$$H = \sum_{\ell=1}^L |Q_\ell|^2, \quad Q_\ell \in \mathcal{P}_{d_1, d_2}^+, \quad L \leq \min(d_1+1, d_2+1). \quad (\text{H1})$$

The strategy reduces the bivariate scalar problem to a univariate matrix-valued problem via the two-level Toeplitz structure, then applies the operator Fejér–Riesz theorem. We also show that scalar factorization $H = |Q|^2$ (a single Hermitian square) does not hold in general for bivariate polynomials, by invoking the Geronimo–Woerdeman theorem [49] and a codimension argument.

Throughout, set $N_j = d_j + 1$ for $j = 1, 2$ and $N = N_1 N_2$.

1. The two-level Toeplitz matrix

Definition H.1 (Two-level Toeplitz matrix). Let $H \in \mathcal{T}_{d_1, d_2}$ with Fourier coefficients $c_{k\ell} = \hat{H}_{k,\ell}$. Define the matrix $\mathbf{T}_H \in \mathbb{C}^{N \times N}$, indexed by pairs $(m, n), (m', n') \in \{0, \dots, d_1\} \times \{0, \dots, d_2\}$, with entries

$$(\mathbf{T}_H)_{(m,n),(m',n')} = c_{m-m', n-n'}. \quad (\text{H2})$$

This matrix has a natural two-level structure. Define the $N_2 \times N_2$ inner blocks $C_k \in \mathbb{C}^{N_2 \times N_2}$ by $(C_k)_{nn'} = c_{k, n-n'}$ for $n, n' \in \{0, \dots, d_2\}$. Each C_k is a Toeplitz matrix built from the θ_2 -Fourier coefficients at fixed outer index k . The full matrix then takes the block-Toeplitz form

$$\mathbf{T}_H = \begin{pmatrix} C_0 & C_{-1} & \cdots & C_{-d_1} \\ C_1 & C_0 & \cdots & C_{1-d_1} \\ \vdots & \vdots & \ddots & \vdots \\ C_{d_1} & C_{d_1-1} & \cdots & C_0 \end{pmatrix} \in \mathbb{C}^{N_1 N_2 \times N_1 N_2}. \quad (\text{H3})$$

That is, \mathbf{T}_H is block-Toeplitz in the outer (θ_1) index, with blocks that are themselves Toeplitz in the inner (θ_2) index.

2. Positive definiteness

Lemma H.1. *If $H(\theta_1, \theta_2) > 0$ for all $(\theta_1, \theta_2) \in \mathbb{T}^2$, then $\mathbf{T}_H \succ 0$.*

Proof. Let $\mathbf{v} = (v_{mn})_{0 \leq m \leq d_1, 0 \leq n \leq d_2}$ be a nonzero vector in \mathbb{C}^N . Define the analytic polynomial

$$f(\theta_1, \theta_2) = \sum_{m=0}^{d_1} \sum_{n=0}^{d_2} v_{mn} e^{i(m\theta_1 + n\theta_2)}. \quad (\text{H4})$$

By direct computation using the definition (H2) and the convolution theorem for Fourier coefficients,

$$\mathbf{v}^\dagger \mathbf{T}_H \mathbf{v} = \sum_{m,n} \sum_{m',n'} \bar{v}_{mn} c_{m-m', n-n'} v_{m'n'} = \frac{1}{(2\pi)^2} \int_{\mathbb{T}^2} H(\theta_1, \theta_2) |f(\theta_1, \theta_2)|^2 d\theta_1 d\theta_2. \quad (\text{H5})$$

Since $\mathbf{v} \neq 0$, the analytic polynomial f is not identically zero on \mathbb{T}^2 (as the monomials $\{e^{i(m\theta_1 + n\theta_2)}\}$ are linearly independent). Hence $|f|^2$ is positive on an open set, and $H > 0$ everywhere, so the integral is strictly positive.

3. Reduction to a matrix-valued univariate problem

We reorganize H as a matrix-valued trigonometric polynomial in a single variable θ_2 , whose matrix dimension encodes the θ_1 -Fourier structure.

Definition H.2 (Matrix-valued reorganization). For $H \in \mathcal{T}_{d_1, d_2}$ with Fourier coefficients $c_{k\ell}$, define the matrix-valued function $\mathbf{H} : \mathbb{T} \rightarrow \mathbb{C}^{N_1 \times N_1}$ by

$$\mathbf{H}(\theta_2)_{mm'} = \hat{H}_{m-m'}(\theta_2) := \sum_{\ell=-d_2}^{d_2} c_{m-m', \ell} e^{i\ell\theta_2}, \quad (\text{H6})$$

$$m, m' \in \{0, \dots, d_1\}.$$

Lemma H.2 (Properties of $\mathbf{H}(\theta_2)$). *Under the hypotheses of (H1):*

1. Each entry $\mathbf{H}(\theta_2)_{mm'}$ is a scalar trigonometric polynomial of degree d_2 in θ_2 .
2. $\mathbf{H}(\theta_2)$ is Hermitian for every θ_2 : $\mathbf{H}(\theta_2)_{mm'} = \overline{\mathbf{H}(\theta_2)_{m'm}}$.
3. $\mathbf{H}(\theta_2) = \mathbf{H}(\theta_2)^*$ is a Toeplitz-structured matrix for each θ_2 : entry (m, m') depends only on $m - m'$.
4. $\mathbf{H}(\theta_2) \succ 0$ for every $\theta_2 \in \mathbb{T}$.
5. The block-Toeplitz matrix associated with \mathbf{H} (viewed as a matrix-valued trigonometric polynomial of degree d_2) is \mathbf{T}_H .

Proof. Properties (i)–(iii) are immediate from the definition (H6) and the Hermitian symmetry $c_{k,\ell} = \overline{c_{-k,-\ell}}$ of the Fourier coefficients of the real-valued function H .

For (iv): let $\mathbf{u} = (u_0, \dots, u_{d_1})^T \in \mathbb{C}^{N_1}$ be nonzero. Then

$$\mathbf{u}^* \mathbf{H}(\theta_2) \mathbf{u} = \sum_{m, m'=0}^{d_1} \bar{u}_m \hat{H}_{m-m'}(\theta_2) u_{m'} = \sum_{m, m'} \bar{u}_m u_{m'} \sum_{\ell} c_{m-m', \ell} e^{i\ell\theta_2}. \quad (\text{H7})$$

Setting $g(\theta_1) = \sum_{m=0}^{d_1} u_m e^{im\theta_1}$, this becomes

$$\mathbf{u}^* \mathbf{H}(\theta_2) \mathbf{u} = \frac{1}{2\pi} \int_0^{2\pi} H(\theta_1, \theta_2) |g(\theta_1)|^2 d\theta_1. \quad (\text{H8})$$

Since $H > 0$ on \mathbb{T}^2 and $g \neq 0$, this integral is strictly positive.

Property (v) follows by comparing the block-Toeplitz matrix of \mathbf{H} (a matrix-valued trigonometric polynomial of degree d_2 with $N_1 \times N_1$ matrix coefficients) with definition (H3): the (m, m') -block at outer Toeplitz index $k = m - m'$ and inner Toeplitz index $\ell = n - n'$ is $c_{k,\ell}$.

4. Application of the operator Fejér–Riesz theorem

Since $\mathbf{H}(\theta_2) \succ 0$ is a matrix-valued trigonometric polynomial of degree d_2 , the operator Fejér–Riesz theorem applies.

Theorem H.1 (Operator Fejér–Riesz; Rosenblum [47], Dritschel–Rovnyak [48]). *Let $\mathbf{F}(\theta) \in \mathbb{C}^{r \times r}$ be a matrix-valued trigonometric polynomial of degree d with $\mathbf{F}(\theta) \succeq 0$ for all θ . Then there exists a matrix polynomial $\mathbf{G}(z) = \sum_{n=0}^d G_n z^n \in \mathbb{C}^{r \times r}[z]$ such that*

$$\mathbf{F}(\theta) = \mathbf{G}(e^{i\theta})^* \mathbf{G}(e^{i\theta}) \quad \text{for all } \theta. \quad (\text{H9})$$

When $\mathbf{F} \succ 0$ strictly, \mathbf{G} can be chosen outer ($\det \mathbf{G}(z) \neq 0$ for $|z| < 1$), and this outer factor is unique up to a left unitary constant.

We refer to [47] for the original proof and to [48] for a modern account via Schur complements. We do not reproduce the proof here.

Applying Theorem H.1 to $\mathbf{H}(\theta_2) \succ 0$ with $r = N_1 = d_1 + 1$ and degree d_2 yields an outer matrix polynomial

$$\mathbf{G}(z_2) = \sum_{n=0}^{d_2} G_n z_2^n \in \mathbb{C}^{N_1 \times N_1}[z_2], \quad \deg_{z_2}(\mathbf{G}) \leq d_2, \quad (\text{H10})$$

satisfying $\mathbf{H}(\theta_2) = \mathbf{G}(e^{i\theta_2})^* \mathbf{G}(e^{i\theta_2})$.

5. SOS decomposition

The matrix factorization yields an SOS decomposition of H .

Proposition H.1 (SOS from matrix factorization). *Define the bivariate analytic polynomials*

$$f_\alpha(\theta_1, \theta_2) = \sum_{m=0}^{d_1} (\mathbf{G}(e^{i\theta_2}))_{\alpha m} e^{im\theta_1}, \quad \alpha \in \{1, \dots, N_1\}. \quad (\text{H11})$$

Then $H(\theta_1, \theta_2) = \sum_{\alpha=1}^{N_1} |f_\alpha(\theta_1, \theta_2)|^2$ on \mathbb{T}^2 , with each $f_\alpha \in \mathcal{P}_{d_1, d_2}^+$.

Proof. Using the definition (H6) of \mathbf{H} and the factorization (H10),

$$\begin{aligned} H(\theta_1, \theta_2) &= \sum_{m, m'=0}^{d_1} e^{-im\theta_1} \mathbf{H}(\theta_2)_{mm'} e^{im'\theta_1} \\ &= \sum_{m, m'} e^{-im\theta_1} [\mathbf{G}(e^{i\theta_2})^* \mathbf{G}(e^{i\theta_2})]_{mm'} e^{im'\theta_1} \\ &= \sum_{m, m'} e^{-im\theta_1} \left(\sum_{\alpha=1}^{N_1} \overline{(\mathbf{G})_{\alpha m}} (\mathbf{G})_{\alpha m'} \right) e^{im'\theta_1} \\ &= \sum_{\alpha=1}^{N_1} \left| \sum_{m=0}^{d_1} (\mathbf{G}(e^{i\theta_2}))_{\alpha m} e^{im\theta_1} \right|^2 = \sum_{\alpha=1}^{N_1} |f_\alpha|^2. \end{aligned}$$

Each f_α has z_1 -degree at most d_1 (from the range of m) and z_2 -degree at most d_2 (since each entry $(\mathbf{G})_{\alpha m}$ is a polynomial of degree $\leq d_2$ in z_2).

This establishes an SOS decomposition with $L \leq N_1 = d_1 + 1$ terms and correct degree bounds.

6. Tighter SOS bound via symmetric reorganization

The bound $L \leq d_1 + 1$ from Proposition H.1 arises from reorganizing H into a matrix-valued function of θ_2 with matrix dimension $N_1 = d_1 + 1$. By reorganizing in the opposite direction, we obtain a complementary bound.

Proposition H.2 (Symmetric SOS bound). *Let $H \in \mathcal{T}_{d_1, d_2}$ with $H > 0$ on \mathbb{T}^2 . Then $H = \sum_{\ell=1}^L |Q_\ell|^2$ with each $Q_\ell \in \mathcal{P}_{d_1, d_2}^+$ and*

$$L \leq \min(d_1+1, d_2+1). \quad (\text{H12})$$

Proof. The bound $L \leq d_1 + 1$ is Proposition H.1: reorganize H as an $N_1 \times N_1$ matrix function of θ_2 and apply the operator Fejér–Riesz theorem.

For the bound $L \leq d_2 + 1$, reorganize H in the opposite direction. Define $\tilde{\mathbf{H}} : \mathbb{T} \rightarrow \mathbb{C}^{N_2 \times N_2}$ by

$$\tilde{\mathbf{H}}(\theta_1)_{nn'} = \sum_{k=-d_1}^{d_1} c_{k, n-n'} e^{ik\theta_1}, \quad n, n' \in \{0, \dots, d_2\}. \quad (\text{H13})$$

By the same argument as Lemma H.2, $\tilde{\mathbf{H}}(\theta_1) \succ 0$ for every θ_1 , and $\tilde{\mathbf{H}}$ is a matrix-valued trigonometric polynomial of degree d_1 with matrix dimension $N_2 = d_2 + 1$. The operator Fejér–Riesz theorem gives $\tilde{\mathbf{H}}(\theta_1) = \tilde{\mathbf{G}}(e^{i\theta_1})^* \tilde{\mathbf{G}}(e^{i\theta_1})$ with $\tilde{\mathbf{G}} \in \mathbb{C}^{N_2 \times N_2}[z_1]$ of degree $\leq d_1$. Extracting the SOS:

$$H = \sum_{\beta=1}^{N_2} \left| \sum_{n=0}^{d_2} (\tilde{\mathbf{G}}(e^{i\theta_1}))_{\beta n} e^{in\theta_2} \right|^2, \quad (\text{H14})$$

giving $L \leq N_2 = d_2 + 1$ terms, each in \mathcal{P}_{d_1, d_2}^+ .

Taking the better of the two bounds yields (H12).

Remark H.1 (Application to the Dyson polynomial). For the Dyson polynomial of bidegree (d_R, d_I) , the SOS complement has

$$L \leq \min(d_R+1, d_I+1), \quad a_{\text{SOS}} = \lceil \log_2(\min(d_R, d_I) + 2) \rceil. \quad (\text{H15})$$

In the physically dominant regime $\alpha_R \gg \beta_I$ (anti-Hermitian part smaller than Hermitian part), the controlling dimension is $d_I + 1$, and the ancilla overhead is $O(\log(\beta_I T + \log(1/\varepsilon)))$.

7. Failure of scalar factorization

The SOS decomposition of Proposition H.1 produces $L \geq 2$ terms in general. Can the decomposition always be refined to a single Hermitian square: $H = |Q|^2$ for some $Q \in \mathcal{P}_{d_1, d_2}^+$. We show that this fails in general for bivariate polynomials. The Geronimo–Woerdeman theorem obstructs stable scalar factorization, and a codimension argument shows that non-stable scalar factorization is generically impossible.

a. Stable factorization and the Geronimo–Woerdeman obstruction

The Geronimo–Woerdeman theorem [49] characterizes when a strictly positive bivariate trigonometric polynomial admits a scalar spectral factorization by a stable polynomial (one with no zeros in $\overline{\mathbb{D}}^2$).

Theorem H.2 (Geronimo–Woerdeman [49]). *Let $H \in \mathcal{T}_{d_1, d_2}$ with $H > 0$ on \mathbb{T}^2 . Write the two-level Toeplitz matrix in the outer-block form*

$$\mathbf{T}_H = \begin{pmatrix} A_0 & A_{-1} & \cdots & A_{-d_2} \\ A_1 & A_0 & \cdots & A_{1-d_2} \\ \vdots & & \ddots & \vdots \\ A_{d_2} & \cdots & & A_0 \end{pmatrix}, \quad (\text{H16})$$

where each $A_m \in \mathbb{C}^{N_1 \times N_1}$ is a Toeplitz matrix (the θ_1 -lag- m block). We define the Schur complements recursively:

$$S_0 = A_0, \quad S_{k+1} = S_k - \mathbf{A}_k \mathbf{S}_k^{-1} \mathbf{A}_k^* \quad (k = 0, 1, \dots, d_2 - 1), \quad (\text{H17})$$

where \mathbf{A}_k denotes the appropriate off-diagonal block of the k -th residual and \mathbf{S}_k the leading block (we suppress the precise block-elimination bookkeeping, which is standard [49]).

Then the following are equivalent:

1. There exists a stable polynomial $Q \in \mathcal{P}_{d_1, d_2}^+$ with $Q(z_1, z_2) \neq 0$ for $(z_1, z_2) \in \overline{\mathbb{D}}^2$ and $H = |Q|^2$ on \mathbb{T}^2 .
2. (**Autoregressive condition.**) S_k is a Toeplitz matrix for every $k = 0, 1, \dots, d_2$.

The condition $S_0 = A_0$ being Toeplitz holds by construction. Since the inverse of a Toeplitz matrix is not Toeplitz in general, the product $A_1 A_0^{-1} A_{-1}$ is generically non-Toeplitz, so the Schur complement $S_1 = A_0 - A_1 A_0^{-1} A_{-1}$ generically violates the Toeplitz condition.

Proposition H.3 (GW obstruction for the Dyson polynomial). *Let $P_\delta = (1 - \delta)P$ for $P(z_1, z_2) = \frac{1}{2}(z_1 + z_2)$ acts as the simplest nontrivial interaction-picture polynomial (bidegree $(1, 1)$, one Hermitian query and one anti-Hermitian insertion). Then $H_\delta = 1 - |P_\delta|^2$ does not admit a stable scalar factorization for $\delta \in (0, 1)$.*

Proof. Set $\gamma = (1 - \delta)^2$. Then

$$H_\delta(\theta_1, \theta_2) = \left(1 - \frac{\gamma}{2}\right) - \frac{\gamma}{2} \cos(\theta_1 - \theta_2), \quad (\text{H18})$$

with Fourier coefficients $\hat{H}_{0,0} = 1 - \gamma/2$, $\hat{H}_{1,-1} = \hat{H}_{-1,1} = -\gamma/4$, and all others zero.

The outer-block form (H16) of \mathbf{T}_{H_δ} has 2×2 blocks (since $d_1 = d_2 = 1$):

$$A_0 = a I_2, \quad A_1 = \begin{pmatrix} 0 & -b/2 \\ 0 & 0 \end{pmatrix}, \quad A_{-1} = A_1^* = \begin{pmatrix} 0 & 0 \\ -b/2 & 0 \end{pmatrix}, \quad (\text{H19})$$

where $a = 1 - \gamma/2$ and $b = \gamma/2$.

The first Schur complement is

$$\begin{aligned} S_1 &= A_0 - A_1 A_0^{-1} A_{-1} = a I_2 - \frac{1}{a} \begin{pmatrix} 0 & -b/2 \\ 0 & 0 \end{pmatrix} \begin{pmatrix} 0 & 0 \\ -b/2 & 0 \end{pmatrix} \\ &= a I_2 - \frac{b^2}{4a} \begin{pmatrix} 1 & 0 \\ 0 & 0 \end{pmatrix} = \begin{pmatrix} a - b^2/(4a) & 0 \\ 0 & a \end{pmatrix}. \end{aligned}$$

A 2×2 matrix is Toeplitz if its diagonal entries are equal. Here $(S_1)_{00} = a - b^2/(4a) \neq a = (S_1)_{11}$ for $b \neq 0$, which holds for all $\delta \in (0, 1)$. Therefore S_1 is not Toeplitz, and by Theorem H.2, no stable scalar factor exists.

Remark H.2 (Stable vs. non-stable factorization). The GW theorem characterizes stable (outer) factorization: $Q(z_1, z_2) \neq 0$ on $\overline{\mathbb{D}}^2$. The M-QSP circuit only needs $|P|^2 + |Q|^2 = 1$ on \mathbb{T}^2 and never evaluates Q inside the bidisk. Thus stability is not required for the algorithm.

For $P = \frac{1}{2}(z_1 + z_2)$ with $\delta \in (0, 1)$, the Fourier-coefficient matching system admits the non-stable solution $Q = q_{10} z_1 + q_{01} z_2$ with $q_{00} = q_{11} = 0$, $|q_{10}|^2 + |q_{01}|^2 = 1 - \gamma/2$, and $q_{10} \bar{q}_{01} = -\gamma/4$. This Q vanishes at the origin and hence is not stable, but satisfies $H_\delta = |Q|^2$ on \mathbb{T}^2 .

Scalar factorization thus succeeds in the $(1, 1)$ case with a non-stable factor. For higher bidegrees, we show below that even non-stable scalar factorization generically fails.

b. Generic failure of non-stable scalar factorization

We now address the question without the stability restriction: for $H > 0$ on \mathbb{T}^2 of bidegree (d_1, d_2) , when does $H = |Q|^2$ for $Q \in \mathcal{P}_{d_1, d_2}^+$?

Proposition H.4 (Codimension of the Hermitian-square image). *Let $\Phi : \mathbb{C}^{(d_1+1)(d_2+1)} \rightarrow \mathbb{R}^{(2d_1+1)(2d_2+1)}$ be the autocorrelation map sending the coefficients of $Q \in \mathcal{P}_{d_1, d_2}^+$ to the Fourier coefficients of $|Q|^2$. Then the image $\mathcal{V} = \text{Im}(\Phi)$ has real codimension at least $2d_1 d_2$ in the space of Fourier coefficient vectors of trigonometric polynomials of bidegree (d_1, d_2) .*

Proof. The source has $2(d_1+1)(d_2+1)$ real parameters (real and imaginary parts of the coefficients q_{jk}). The global phase $Q \mapsto e^{i\phi} Q$ leaves $|Q|^2$ invariant, reducing the effective dimension by 1. The target space has real dimension $(2d_1+1)(2d_2+1)$ (the independent Fourier coefficients of a real-valued trigonometric polynomial; the constraint $\hat{H}_{-m, -n} = \hat{H}_{m, n}$ is already accounted for). Thus

$$\begin{aligned} \text{codim}(\mathcal{V}) &\geq (2d_1+1)(2d_2+1) - [2(d_1+1)(d_2+1) - 1] \\ &= 4d_1 d_2 + 2d_1 + 2d_2 + 1 - 2d_1 d_2 - 2d_1 - 2d_2 - 2 + 1 = 2d_1 d_2. \end{aligned}$$

For $d_1, d_2 \geq 1$, this is ≥ 2 , so \mathcal{V} is a proper subvariety of positive codimension.

Corollary H.1 (Generic failure of scalar factorization). *For $d_1, d_2 \geq 1$, a generic strictly positive trigonometric polynomial H of bidegree (d_1, d_2) does not admit a scalar factorization $H = |Q|^2$ with $Q \in \mathcal{P}_{d_1, d_2}^+$.*

Proof. The image \mathcal{V} has codimension $\geq 2d_1d_2 \geq 2$ by Proposition H.4, hence is contained in a proper real-algebraic subvariety of the target space. A generic H lies outside this subvariety.

Remark H.3 (Why the (1, 1) case is exceptional). For $(d_1, d_2) = (1, 1)$, the codimension bound gives $2 \cdot 1 \cdot 1 = 2$, and the target space has dimension $3 \times 3 = 9$. The factorization for $P = \frac{1}{2}(z_1 + z_2)$ succeeds (Remark H.2) because H_δ has only 3 nonzero Fourier modes out of 9: the 6 vanishing modes impose no constraints, and the effective system is underdetermined (3 constraints in 7 real unknowns). This sparsity does not persist at higher bidegrees for the Dyson polynomial.

Remark H.4 (Full Fourier support of the Dyson polynomial). The interaction-picture Dyson polynomial has coefficient matrix $p_{jk} \propto (-i)^j J_j(\alpha_R T) \cdot (\beta_I T)^k / k!$ (up to normalization), where J_j is the j -th Bessel function of the first kind. The Bessel function $J_j(\tau)$ has isolated real zeros; for τ not among these zeros (which excludes a measure-zero set of parameter values), all coefficients p_{jk} are nonzero. Then $|P|^2$ has $|\hat{P}|_{m,n}^2 \neq 0$ for all $(m, n) \in \{-d_R, \dots, d_R\} \times \{-d_I, \dots, d_I\}$, and all $(2d_R+1)(2d_I+1)$ Fourier constraints are active.

Scalar factorization $H_\delta = |Q|^2$ requires that \hat{H}_δ lie on the codimension- $2d_Rd_I$ variety \mathcal{V} , giving $2d_Rd_I$ independent algebraic conditions on the Fourier coefficients of H_δ . For a full-support Dyson polynomial, these conditions are non-trivial (the system is overdetermined), and the specific coefficient structure of the Dyson series provides no mechanism to satisfy them.

If some Bessel zeros cause isolated coefficients to vanish (e.g., $J_{d_R}(\alpha_R T) = 0$ for specific $\alpha_R T$), the codimension argument remains valid as long as at least $2(d_R+1)(d_I+1)$ Fourier modes of H_δ are nonzero, which holds for $d_R, d_I \geq 2$ under much weaker genericity assumptions. We leave scalar factorization as an open problem and note that the SOS resolution (Proposition H.2) is unconditionally correct and sufficient for the M-QSP construction.

c. Operator-level perspective

The bivariate ring $\mathbb{C}[z_1, z_2]$ is not ideal, and the SOS representation $H = \sum_\ell |Q_\ell|^2$ with $L \geq 2$ terms is the natural analogue of the Fejér–Riesz factorization in this setting.

From this perspective, the operator Fejér–Riesz theorem resolves the non-commutative structure of bivariate signal processing. The SOS complement with $L \leq \min(d_R+1, d_I+1)$ terms and $\lceil \log_2(L+1) \rceil$ ancilla qubits appears to be the cost of bivariate non-commutativity.

8. Summary

Combining the results of this appendix:

1. **SOS decomposition (Propositions H.1 and H.2).** For $H = 1 - |P|^2 > 0$ on \mathbb{T}^2 with $P \in \mathcal{P}_{d_1, d_2}^+$:

$$H = \sum_{\ell=1}^L |Q_\ell|^2, \quad Q_\ell \in \mathcal{P}_{d_1, d_2}^+, \quad L \leq \min(d_1+1, d_2+1). \quad (\text{H20})$$

The proof is constructive: reorganize H as a matrix-valued trigonometric polynomial in the variable with the smaller degree, apply the operator Fejér–Riesz theorem to obtain the matrix outer factor, and read off the SOS terms from its rows.

2. **Scalar factorization fails (Proposition H.3, Corollary H.1).** For bivariate polynomials with $d_1, d_2 \geq 1$, the single-term factorization $H = |Q|^2$ is generically impossible. The Geronimo–Woerdeman autoregressive condition provides a precise obstruction for stable factors, and the codimension- $2d_1d_2$ argument shows that even non-stable scalar factorization fails for generic H .
3. **Ancilla overhead is logarithmic (Remark H.1).** The SOS complement requires $a_{\text{SOS}} = \lceil \log_2(\min(d_R, d_I) + 2) \rceil$ ancilla qubits, which does not affect the query complexity or postselection probability of the main theorem.

Appendix I: Optimization Landscape for Angle-Finding

Section VIII E introduced the FFT-based angle-finding alternative (Theorem VIII.2) and posed the absence of spurious local minima as an open question (Problem VIII.1). This appendix provides the cost function analysis including critical point structure, and the numerical evidence informing the conjecture.

1. The cost function and its gradient

The cost function $\mathcal{F} : \mathbb{R}^{2(d_R+d_I+1)} \rightarrow \mathbb{R}_{\geq 0}$ is defined by

$$\mathcal{F}(\Theta) = \frac{1}{(2\pi)^2} \int_0^{2\pi} \int_0^{2\pi} |P_G(e^{i\theta_1}, e^{i\theta_2}; \Theta) - P_{\text{target}}(e^{i\theta_1}, e^{i\theta_2})|^2 d\theta_1 d\theta_2, \quad (\text{I1})$$

where $P_G(\cdot; \Theta)$ is the $(0,0)$ block of the M-QSP circuit with angles Θ , evaluated on the joint eigenspace with eigenvalues $(e^{i\theta_1}, e^{i\theta_2})$.

By Parseval's theorem, \mathcal{F} equals the sum of squared differences of bivariate Fourier coefficients:

$$\mathcal{F}(\Theta) = \sum_{m,n} |c_{mn}^G(\Theta) - c_{mn}^{\text{target}}|^2, \quad (\text{I2})$$

so $\mathcal{F} = 0$ if and only if the circuit exactly implements the target polynomial on \mathbb{T}^2 . The Fourier representation has two computational advantages: (i) evaluation via 2D FFT on an $N_1 \times N_2$ grid (with $N_j \geq 2d_j + 1$) costs $O(d_R d_I \log(d_R d_I))$ per evaluation; (ii) the gradient

$$\frac{\partial \mathcal{F}}{\partial \theta_j} = 2 \operatorname{Re} \sum_{m,n} \overline{(c_{mn}^G - c_{mn}^{\text{target}})} \cdot \frac{\partial c_{mn}^G}{\partial \theta_j} \quad (\text{I3})$$

is computed in the same asymptotic cost via the forward-backward pass (equations (119)–(120) of Sec. VIII E).

2. Critical point analysis

The cost function \mathcal{F} has the following structural properties:

1. *Non-negativity and exactness.* $\mathcal{F} \geq 0$, with $\mathcal{F} = 0$ if and only if $P_G = P_{\text{target}}$ on \mathbb{T}^2 . This is immediate from \mathcal{F} being an integral of a non-negative integrand.
2. *Existence of a global minimum at zero.* The constructive achievability (Theorem VIII.3, via Theorem VII.1) guarantees that angles Θ^* with $\mathcal{F}(\Theta^*) = 0$ exist for a Dyson polynomial satisfying the conditions of Corollary VIII.1.
3. *Smoothness.* \mathcal{F} is C^∞ in Θ , since P_G depends on Θ through products of trigonometric functions of the angles. The gradient (I3) and all higher derivatives exist everywhere.

With this, gradient-based optimization is well-defined and the landscape is free of pathologies (non-differentiable points, non-existence of minima) common in variational quantum algorithms. They do not rule out spurious local minima.

The parameter space $\mathbb{R}^{2(d_R+d_I+1)}$ is high-dimensional. The cost function couples two signal variables through the bivariate Fourier structure. The circuit's product-of-matrices structure means that \mathcal{F} is a trigonometric polynomial of degree at most $2(d_R + d_I)$ in each angle parameter. However, interaction between parameters through the matrix product creates a non-trivial energy landscape.

3. Conjecture: no spurious local minima

In the univariate setting, Motlagh and Wiebe [53] empirically observe no spurious local minima for GQSP cost functions up to polynomial degree 10^7 . We know no proof of this in one variable, but this is more than sufficient numerical evidence for most practical polynomial degrees.

For the bivariate landscape, the parameter space doubles (from $d + 1$ real parameters to $2(d_R + d_I + 1)$) and the cost function couples two signal variables. We restate the formal conjecture from Problem VIII.1:

Conjecture I.1 (No spurious local minima). *For every target polynomial $P_{\text{target}} \in \mathcal{P}_{d_R, d_I}^+$ with $|P_{\text{target}}| \leq 1$ on \mathbb{T}^2 that satisfies the achievability conditions of Theorem VIII.3, every local minimum of the cost function \mathcal{F} defined by (II) is a global minimum (i.e., $\mathcal{F} = 0$).*

A positive resolution would permit random initialization of angle-finding optimization, eliminating the need for the $\mathcal{O}((d_R + d_I) \cdot d_R \cdot d_I)$ recursive preprocessing. This would reduce the classical cost of the M-QSP algorithm to $\mathcal{O}(K \cdot d_R d_I \log(d_R d_I))$, where K is the number of gradient descent iterations.

Univariate empirical evidence [53] extends to degrees far beyond a practical simulation parameter. Further, the algebraic structure of the QSP circuit is similar to that of overparameterized neural networks, for which benign landscape results are known in certain regimes [75]. Neither observation is a proof, and the bivariate case introduces new features (the schedule \mathbf{s} and coupling between z_1 and z_2 parameters) that have no univariate analogue.

4. Numerical evidence and the warm-start strategy

In the absence of a proof of Conjecture I.1, the practical strategy is a two-stage approach:

1. **Initialize:** Compute $\Theta^{(0)}$ via the recursive degree-reduction (Algorithm 1). This produces the exact global minimizer up to numerical precision.
2. **Iterate:** At each step t , evaluate $\mathcal{F}(\Theta^{(t)})$ and $\nabla_{\Theta} \mathcal{F}(\Theta^{(t)})$ via 2D FFT (cost $\mathcal{O}(d_R d_I \log(d_R d_I))$ per iteration).
3. **Update:** $\Theta^{(t+1)} \leftarrow \Theta^{(t)} - \gamma_t \nabla_{\Theta} \mathcal{F}(\Theta^{(t)})$, with step size γ_t chosen by line search or L-BFGS.
4. **Terminate** when $\mathcal{F}(\Theta^{(t)}) \leq \eta$ (target tolerance).

The recursive algorithm already produces the exact global minimizer, so warm starting places the optimization within the basin of attraction of the global minimum, and a small number of refinement iterations (K_{refine} , empirically $\mathcal{O}(1)$ – $\mathcal{O}(d)$) suffices to polish the angles to machine precision.

We combine the guarantees of Algorithm 1 (which certifies correctness) with the $\mathcal{O}(d_R d_I \log(d_R d_I))$ per-iteration cost of the FFT-based optimization, achieving practical scalability to total degrees $d_R + d_I \sim 10^6$ without sacrificing correctness.

Finite-precision effects in the recursive algorithm propagate linearly, not exponentially, through the degree-reduction steps (Proposition VIII.2), because each peeling step applies a unitary rotation with condition number 1. The overall condition number scales as $\mathcal{O}(d_R + d_I)$, quite manageable for parameter regimes of interest. Optimization-based refinement mitigates accumulated rounding error from the recursive stage.

Appendix J: Tight $\log / \log \log$ lower bound for bounded polynomial approximation

This appendix provides the full proof of Theorem III.4 (tight $\log / \log \log$ scaling).

Lemma J.1 (Chebyshev coefficient lower bound on best approximation). *Let $f \in C[-1, 1]$ have Chebyshev expansion $f(x) = a_0 + \sum_{k=1}^{\infty} a_k T_k(x)$. Then for every $d \geq 0$,*

$$E_d(f)_{[-1, 1]} := \inf_{\deg p \leq d} \|f - p\|_{\infty, [-1, 1]} \geq \frac{\pi}{4} |a_{d+1}|. \quad (\text{J1})$$

Proof. Let p be a polynomial of degree $\leq d$. Since T_{d+1} is orthogonal to all polynomials of degree $\leq d$ with respect to the Chebyshev weight, $a_{d+1} = \frac{2}{\pi} \int_{-1}^1 (f(x) - p(x)) T_{d+1}(x) (1 - x^2)^{-1/2} dx$. Taking absolute values and using $\int_{-1}^1 |T_{d+1}(x)| (1 - x^2)^{-1/2} dx = 2$ gives $|a_{d+1}| \leq (4/\pi) \|f - p\|_{\infty}$.

Lemma J.2 (Chebyshev coefficients of $e^{a(x-1)}$). *For $a > 0$, the function $g(x) = e^{a(x-1)}$ has Chebyshev coefficients $b_0 = e^{-a} I_0(a)$ and $b_k = 2e^{-a} I_k(a)$ for $k \geq 1$, where I_k is the modified Bessel function of the first kind.*

Proof. From the classical identity $e^{ax} = I_0(a) + 2 \sum_{k=1}^{\infty} I_k(a) T_k(x)$ on $[-1, 1]$.

Lemma J.3 (Series lower bound on I_k). *For all $a > 0$ and $k \geq 0$, $I_k(a) \geq (a/2)^k / k!$.*

Proof. The $m = 0$ term of $I_k(a) = \sum_{m=0}^{\infty} (a/2)^{k+2m} / (m!(m+k)!)$ equals $(a/2)^k / k!$; all terms are positive.

-
- [1] N. Moiseyev, *Non-Hermitian quantum mechanics* (Cambridge University Press, 2011).
- [2] Y. Wang, E. Mulvihill, Z. Hu, N. Lyu, S. Shivpuje, Y. Liu, M. B. Soley, E. Geva, V. S. Batista, and S. Kais, Simulating open quantum system dynamics on nisc computers with generalized quantum master equations, *Journal of Chemical Theory and Computation* **19**, 4851 (2023).
- [3] S. Jin, N. Liu, and Y. Yu, Quantum simulation of partial differential equations via schrodingerisation, arXiv preprint arXiv:2212.13969 (2022).
- [4] H. Feshbach, Unified theory of nuclear reactions, *Annals of Physics* **5**, 357 (1958).
- [5] U. Riss and H.-D. Meyer, Calculation of resonance energies and widths using the complex absorbing potential method, *Journal of Physics B: Atomic, Molecular and Optical Physics* **26**, 4503 (1993).
- [6] J. G. Muga, J. Palao, B. Navarro, and I. Egusquiza, Complex absorbing potentials, *Physics Reports* **395**, 357 (2004).
- [7] L. Lin and Y. Tong, Near-optimal ground state preparation, *Quantum* **4**, 372 (2020).
- [8] A. Montanaro, Quantum speedup of monte carlo methods, *Proceedings of the Royal Society A: Mathematical, Physical and Engineering Sciences* **471**, 20150301 (2015).
- [9] M. Motta, C. Sun, A. T. Tan, M. J. O'Rourke, E. Ye, A. J. Minnich, F. G. Brandao, and G. K.-L. Chan, Determining eigenstates and thermal states on a quantum computer using quantum imaginary time evolution, *Nature Physics* **16**, 205 (2020).
- [10] A. Gilyén, Y. Su, G. H. Low, and N. Wiebe, Quantum singular value transformation and beyond: exponential improvements for quantum matrix arithmetics, in *Proceedings of the 51st annual ACM SIGACT symposium on theory of computing* (2019) pp. 193–204.
- [11] G. H. Low and I. L. Chuang, Optimal hamiltonian simulation by quantum signal processing, *Physical review letters* **118**, 010501 (2017).
- [12] D. W. Berry, A. M. Childs, R. Cleve, R. Kothari, and R. D. Somma, Exponential improvement in precision for simulating sparse hamiltonians, in *Proceedings of the forty-sixth annual ACM symposium on Theory of computing* (2014) pp. 283–292.
- [13] G. Lindblad, On the generators of quantum dynamical semigroups, *Communications in mathematical physics* **48**, 119 (1976).
- [14] V. Gorini, A. Kossakowski, and E. C. G. Sudarshan, Completely positive dynamical semigroups of n-level systems, *Journal of Mathematical Physics* **17**, 821 (1976).
- [15] J. Dalibard, Y. Castin, and K. Mølmer, Wave-function approach to dissipative processes in quantum optics, *Physical review letters* **68**, 580 (1992).
- [16] H. Carmichael, *An open systems approach to quantum optics: lectures presented at the Université Libre de Bruxelles October 28 to November 4, 1991* (Springer, 1993).
- [17] K. Kraus, A. Böhm, J. D. Dollard, and W. Wootters, *States, effects, and operations fundamental notions of quantum theory: Lectures in mathematical physics at the university of Texas at Austin* (Springer, 1983).
- [18] K. Kawabata, Y. Ashida, and M. Ueda, Information retrieval and criticality in parity-time-symmetric systems, *Physical review letters* **119**, 190401 (2017).
- [19] Z. M. Rossi and I. L. Chuang, Multivariable quantum signal processing (M-QSP): prophecies of the two-headed oracle, *Quantum* **6**, 811 (2022).
- [20] N. Gomes, H. Lim, and N. Wiebe, Multivariable qsp and bosonic quantum simulation using iterated quantum signal processing, arXiv preprint arXiv:2408.03254 (2024).
- [21] A. Jebraeilli and M. R. Geller, Quantum simulation of a qubit with a non-hermitian hamiltonian, *Physical Review A* **111**, 032211 (2025).
- [22] D. An, J.-P. Liu, and L. Lin, Linear combination of hamiltonian simulation for nonunitary dynamics with optimal state preparation cost, *Physical Review Letters* **131**, 150603 (2023).
- [23] D. An, A. M. Childs, and L. Lin, Quantum algorithm for linear non-unitary dynamics with near-optimal dependence on all parameters: D. an, am childs, l. lin, *Communications in Mathematical Physics* **407**, 19 (2026).
- [24] Q. Hu and S. Jin, Amplitude-phase separation toward optimal and fast-forwardable simulation of non-unitary dynamics, arXiv preprint arXiv:2602.09575 (2026).
- [25] D. Camps, L. Lin, R. Van Beeumen, and C. Yang, Explicit quantum circuits for block encodings of certain sparse matrices, *SIAM Journal on Matrix Analysis and Applications* **45**, 801 (2024).
- [26] C. Wang, H.-Y. Liu, C. Xue, X.-N. Zhuang, M. Dou, Z.-Y. Chen, and G.-P. Guo, Quantum simulation of non-unitary dynamics via contour-based matrix decomposition, arXiv preprint arXiv:2511.10267 (2025).
- [27] J. M. Courtney, Optimal bounds, barriers, and extensions for non-Hermitian bivariate quantum signal processing (2026), companion paper; see [55], [arXiv:arXiv:YYYY.YYYYY \[quant-ph\]](https://arxiv.org/abs/2511.10267).
- [28] J. Hubbard, Calculation of partition functions, *Physical Review Letters* **3**, 77 (1959).
- [29] R. Stratonovich, On a method of calculating quantum distribution functions, in *Soviet Physics Doklady*, Vol. 2 (1957) p. 416.
- [30] G. H. Low and N. Wiebe, Hamiltonian simulation in the interaction picture, arXiv preprint arXiv:1805.00675 (2018).
- [31] K.-J. Engel and R. Nagel, *One-parameter semigroups for linear evolution equations* (Springer, 2000).
- [32] K. Yosida, On the differentiability and the representation of one-parameter semi-group of linear operators, *Journal of the Mathematical Society of Japan* **1**, 15 (1948).
- [33] E. Hille, *Functional Analysis and Semi-Groups* (Dutt Press, 2007).

- [34] G. H. Low and I. L. Chuang, Hamiltonian simulation by qubitization, *Quantum* **3**, 163 (2019).
- [35] G. Brassard, P. Hoyer, M. Mosca, and A. Tapp, Quantum amplitude amplification and estimation, arXiv preprint quant-ph/0005055 (2000).
- [36] R. Beals, H. Buhrman, R. Cleve, M. Mosca, and R. De Wolf, Quantum lower bounds by polynomials, *Journal of the ACM (JACM)* **48**, 778 (2001).
- [37] D. W. Berry, G. Ahokas, R. Cleve, and B. C. Sanders, Efficient quantum algorithms for simulating sparse hamiltonians, *Communications in Mathematical Physics* **270**, 359 (2007).
- [38] E. Saff and R. Varga, On the zeros and poles of padé approximants to ez. iii, *Numerische Mathematik* **30**, 241 (1978).
- [39] P. Borwein and T. Erdélyi, *Polynomials and polynomial inequalities* (Springer Science & Business Media, 2012).
- [40] R. S. Rivlin, Stability of pure homogeneous deformations of an elastic cube under dead loading, *Quarterly of applied Mathematics* **32**, 265 (1974).
- [41] L. Trefethen, Multivariate polynomial approximation in the hypercube, *Proceedings of the American Mathematical Society* **145**, 4837 (2017).
- [42] M. Suzuki, General theory of fractal path integrals with applications to many-body theories and statistical physics, *Journal of mathematical physics* **32**, 400 (1991).
- [43] G. Knese, Polynomials with no zeros on the bidisk, *Analysis & PDE* **3**, 109 (2010).
- [44] H. Landau and Z. Landau, On the trigonometric moment problem in two dimensions, *Indagationes Mathematicae* **23**, 1118 (2012).
- [45] L. Fejér, *Über trigonometrische Polynome.* (Walter de Gruyter, Berlin/New York Berlin, New York, 1916).
- [46] F. Riesz, über ein probelm des herrn carathéodory, *JOURNAL FUR DIE REINE UND ANGEWANDTE MATHEMATIK* **146**, 83 (1916).
- [47] M. Rosenblum, Vectorial toeplitz operators and the fejér-riesz theorem, *Journal of Mathematical Analysis and Applications* **23**, 139 (1968).
- [48] M. A. Dritschel and J. Rovnyak, The operator fejér-riesz theorem, in *A Glimpse at Hilbert Space Operators: Paul R. Halmos in Memoriam* (Springer, 2010) pp. 223–254.
- [49] J. S. Geronimo and H. J. Woerdeman, Positive extensions, fejér-riesz factorization and autoregressive filters in two variables, *Annals of Mathematics* , 839 (2004).
- [50] M. A. Dritschel, On factorization of trigonometric polynomials, *Integral Equations and Operator Theory* **49**, 11 (2004).
- [51] M. Dritschel and H. Woerdeman, Outer factorizations in one and several variables, *Transactions of the American Mathematical Society* **357**, 4661 (2005).
- [52] L. Németh and I. L. Chuang, Variants of multivariate quantum signal processing and their characterizations, arXiv preprint arXiv:2312.09072 (2023).
- [53] D. Motlagh and N. Wiebe, Generalized quantum signal processing, *PRX Quantum* **5**, 020368 (2024).
- [54] E. T. Campbell, Early fault-tolerant simulations of the hubbard model, *Quantum Science & Technology* **7**, 015007 (2022).
- [55] J. M. Courtney, Simulation of non-Hermitian Hamiltonians with bivariate quantum signal processing (2026), companion paper; see [27], [arXiv:arXiv:XXXX.XXXXXX \[quant-ph\]](#).
- [56] H. Mori, K. Mizuta, and K. Fujii, Comment on" multivariable quantum signal processing (m-qsp): prophecies of the two-headed oracle", *Quantum* **8**, 1512 (2024).
- [57] L. Laneve and S. Wolf, On multivariate polynomials achievable with quantum signal processing, *Quantum* **9**, 1641 (2025).
- [58] D. W. Berry, A. M. Childs, A. Ostrander, and G. Wang, Quantum algorithm for linear differential equations with exponentially improved dependence on precision, *Communications in Mathematical Physics* **356**, 1057 (2017).
- [59] M. Cerezo, A. Arrasmith, R. Babbush, S. C. Benjamin, S. Endo, K. Fujii, J. R. McClean, K. Mitarai, X. Yuan, L. Cincio, *et al.*, Variational quantum algorithms, *Nature Reviews Physics* **3**, 625 (2021).
- [60] J. Haah, Product decomposition of periodic functions in quantum signal processing, *Quantum* **3**, 190 (2019).
- [61] R. Chao, D. Ding, A. Gilyen, C. Huang, and M. Szegedy, Finding angles for quantum signal processing with machine precision, arXiv preprint arXiv:2003.02831 (2020).
- [62] Y. Dong, X. Meng, K. B. Whaley, and L. Lin, Efficient phase-factor evaluation in quantum signal processing, *Physical Review A* **103**, 042419 (2021).
- [63] J. Stoer, R. Bulirsch, R. Bartels, W. Gautschi, and C. Witzgall, *Introduction to numerical analysis*, Vol. 1993 (Springer, 1980).
- [64] L. N. Trefethen and J. Weideman, The exponentially convergent trapezoidal rule, *SIAM review* **56**, 385 (2014).
- [65] A. M. Childs, Y. Su, M. C. Tran, N. Wiebe, and S. Zhu, Theory of Trotter error with commutator scaling, *Phys. Rev. X* **11**, 011020 (2021).
- [66] H. Yoshida, Construction of higher order symplectic integrators, *Physics letters A* **150**, 262 (1990).
- [67] G. A. Kalugin, *Analytical properties of the Lambert W function*, Ph.D. thesis (2011).
- [68] S. R. Valluri, D. J. Jeffrey, and R. M. Corless, Some applications of the lambert w function to physics, *Canadian Journal of Physics* **78**, 823 (2000).
- [69] A. F. Timan, *Theory of approximation of functions of a real variable*, Vol. 34 (Elsevier, 2014).
- [70] A. Nayak and F. Wu, The quantum query complexity of approximating the median and related statistics, in *Proceedings of the thirty-first annual ACM symposium on Theory of computing* (1999) pp. 384–393.
- [71] M. Szegedy, Quantum speed-up of markov chain based algorithms, in *45th Annual IEEE symposium on foundations of computer science (IEEE, 2004)* pp. 32–41.
- [72] G. N. Watson, *A treatise on the theory of Bessel functions*, Vol. 3 (The University Press, 1922).

- [73] D. W. Lozier, Nist digital library of mathematical functions, *Annals of Mathematics and Artificial Intelligence* **38**, 105 (2003).
- [74] M. Abramowitz and I. A. Stegun, *Handbook of mathematical functions with formulas, graphs, and mathematical tables*, Vol. 55 (US Government printing office, 1948).
- [75] S. Du, J. Lee, H. Li, L. Wang, and X. Zhai, Gradient descent finds global minima of deep neural networks, in *International conference on machine learning* (PMLR, 2019) pp. 1675–1685.